

Ninevah University
College of Electronic Engineering
Electronic Department



**SIMULATING THE IMPACT OF THE PHYSICAL PARAMETERS
ON ELECTRICAL CHARACTERISTICS OF TUNNEL DIODE**

**A Thesis in
Electronic Engineering**

**Supervised by
Prof. Dr. Qais Thanon Najm
And
Asst. Prof. Dr. Ahmed Mohammed Salama**

**Simulating the impact of the Physical Parameters
On electrical characteristics of tunnel diode**

**A Thesis Submitted by
Rafal Emad Abdalqadir**

To

**The Council of the College of Electronics Engineering
Ninevah University**

As a Partial Fulfillment of the Requirements

For the Degree of Master of Science

In

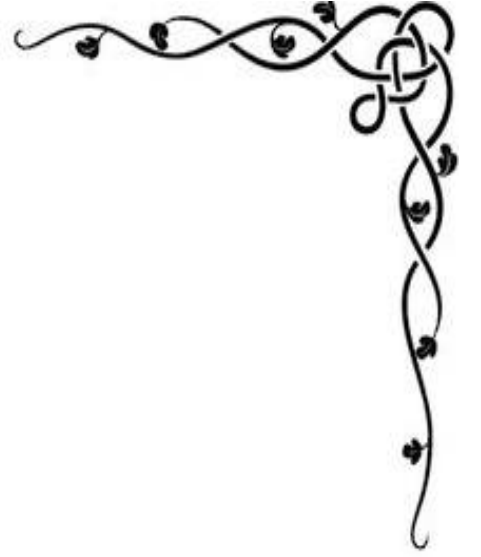
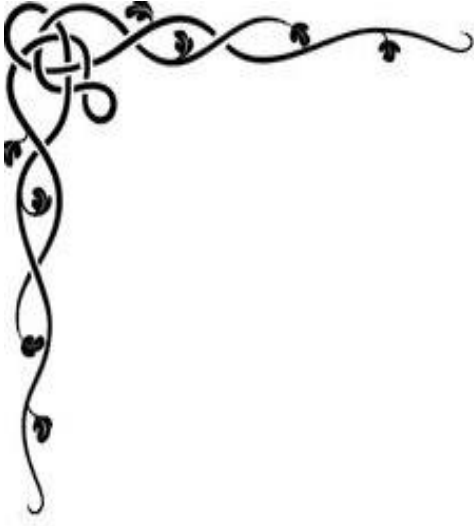
Electronic Engineering

Supervised by

Prof. Dr. Qais Thanon Najm

And

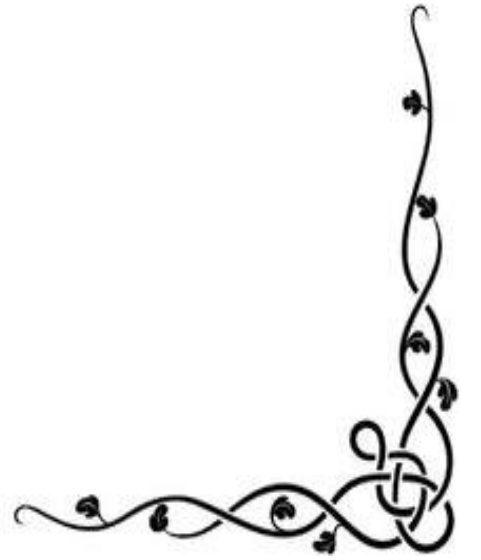
Asst. Prof. Dr. Ahmed Mohammed Salama



بِسْمِ اللَّهِ الرَّحْمَنِ الرَّحِيمِ

﴿ رَبِّ أَوْزِعْنِي أَنْ أَشْكُرَ نِعْمَتَكَ الَّتِي أَنْعَمْتَ عَلَيَّ وَعَلَىٰ وَالِدَيَّ وَأَنْ أَعْمَلَ
صَالِحًا تَرْضَاهُ وَأَدْخِلْنِي بِرَحْمَتِكَ فِي عِبَادِكَ الصَّالِحِينَ ﴾

صدق الله العظيم



سورة النمل الاية (19)



Acknowledgments



Allah Almighty said in his holy book: "Whoever gives thanks, he gives thanks to himself".

First of all, I must express my thanks and gratitude to Almighty God, who enabled me to reach this scientific stage and complete my dissertation. I would also like to thank my first supervisor, Prof. Dr. Qais Thanon Najm, for his patience and giving him a lot of time, as it was for his guidance and valuable advice in directing this scientific thesis in the form in which it appeared. I am grateful to him for his support and continuous encouragement for me to become a successful researcher. I learned a lot from him. I would also like to express my thanks and gratitude to my second supervisor, Asst. Prof. Dr. Ahmed Mohammed Salama, for his help and valuable advice throughout the research period. This research would not have been possible without their help and insightful advice. I would like to take this opportunity to express my thanks and gratitude to Dena Namir for her moral support to me throughout the search. I am grateful to her. I am indebted to my beloved parents, and my dear sisters. For their, endless support, help, and encouragement during my journey at the Master's, I'm so lucky in them.

ABSTRACT

The main objective of this thesis is to investigate the impact of some of the physical characteristics, such as barrier heights, electron affinity, and other parametric studies such as the thickness of the potential barrier (thickness of insulators) and materials types, on the electrical characteristics of the tunnel diode. These parameters are simulated using Silvaco TCAD software. Al/Al₂O₃/Al and Al/Al₂O₃/Au MIM diodes have been simulated to study the impact of using similar and dissimilar electrodes on the current-voltage (I-V) curve of MIM diode. The results revealed that the symmetric diode does not behave as a tunnel diode. Its result indicates that this structure works as an open circuit. The asymmetric diode has a very asymmetrical I-V curve and also has large FOM, where Figures of merit characterize the performance of a specific device or system. The influence of the barrier heights for dissimilar electrodes has been simulated using scenarios; firstly by varying the barrier height from the anode side and the other by varying the barrier height from the cathode side. Simulation results revealed that the change in the work function (ϕ) of the anode does not produce much difference in the tunnel current. Secondly, the impact of the barrier height variation from the cathode side has been studied. The results revealed that the current-voltage curve depends strongly on the work function of the metals, where the structure has a large difference between left and right work functions that produce a large forward current with lower turn-on voltage. In the third part of the present work, the impact of the barrier height variation with a fixed barrier difference has been investigated, using different metals on both sides. Although these structures produce a fixed work functions difference, but the result reveals that the I-V responses of the diodes are qualitatively related to the barrier height. The influence of insulator thickness has been studied on the performance of the MIM diode. The simulation results show that decreasing the thickness of the insulator leads to an increase in the tunnel

phenomenon. Since electron affinity is an important physical parameter of the materials, the current study involved its impact on the electrical characteristics of a MIM diode. When using a set of different insulators, with different electron affinity. The results show a higher asymmetrical current voltage for the insulator (Al_2O_3). Subsequently, the equivalent circuit of the MIM tunnel diode is represented in ADS software based on the results of the Silvaco to study the scattering parameter (S_{11}) at higher frequencies. The obtained results reveal a low value for S_{11} (-28 dB) for the structure that has less insulator thickness. This result indicates that junction capacitance has a high effect on S-Parameter (S_{11}).



LIST OF CONTENTS



	Subject	Page No
	Abstract	
	List of Contents	
	List of Tables	
	List of Figures	
	CHAPTER ONE INTRODUCTION AND LITERATURE REVIEW	
1.1	INTRODUCTION	2
1.2	LITERATURE REVIEW	4
1.3	AIM OF THE WORK	9
1.4	ORGANIZATION OF THE THESIS	9
	CHAPTER TWO PRINCIPLES OF QUANTUM MECHANICAL TUNNELING AND MIM TUNNELING DIODE	
2.1	INTRODUCTION	11
2.1.1	PN JUNCTION AND SCHOTTKY BARRIER DIODE	11
2.2	QUANTUM MECHANICAL TUNNELING	13
2.3	METAL-INSULATOR-METAL(MIM DIODE)	17
2.4	DIELECTRIC FILM CONDUCTION MECHANISMS	20
2.4.1	ELECTRODE-LIMITED CONDUCTION MECHANISM	21
2.4.1.1	THERMIONIC EMISSION	22
2.4.1.2	TUNNELING THROUGH FOWLER-NORDHIEM	22
2.4.1.3	DIRECT TUNNELING	23
2.4.1.4	THERMIONIC-FIELD EMISSION	24
2.4.2	BULK-LIMITED CONDUCTION MECHANISM	25
2.4.2.1	POOLE-FRENKLE EMISSION	26
2.4.2.2	HOPPING CONDUCTION	26
2.4.2.3	OHMIC CONDUCTION	26
2.4.2.4	SPACE-CHARGE LIMITED CONDUCTION	27
2.4.2.5	IONIC CONDUCTION	27
2.4.2.6	GRAIN-BOUNDARY LIMITED CONDUCTION	27
2.5	CONDUCTION MECHANISM OF MIM DIODE	27
2.6	CHARATERISTICS OF MIM DIODE	29

2.6.1	ASYMMETRY	30
2.6.2	NONLINEARITY	30
2.6.3	RESPONSIVITY	30
2.6.4	RESISTIVITY	31
2.7	ELECTRICAL MODELING OF MIM DIODE	31
	CHAPTER THREE SIMULATION SOFTWARE	
3.1	INTRODUCTION	35
3.2	ATLAS INPUTS AND OUTPUTS	35
3.3	DECK BUILD	36
3.4	STRUCTURE SPECIFICATION	37
3.4.1	MESH	37
3.4.2	REGION	38
3.4.3	ELECTRODES	39
3.4.4	QUANTUM TUNNELING MESH	40
3.5	MATERIAL MODELS SPECATIONS	41
3.5.1	MATERIAL	41
3.5.2	MODELS	41
3.5.3	CONTACT	41
3.6	NUMERICAL METHOD SELECTION	42
3.7	SOLUTION SPECIFICATION	42
3.7.1	LOG	42
3.7.2	SOLVE	42
3.7.3	SAVE	43
3.8	RESULTS ANALYSIS	43
3.9	INTRODUCTION TO THE ADS SOFTWARE	44
3.9.1	MIM DIODE REPRESENTATION IN ADS	44
	CHAPTER FOUR SIMULATION RESULTS AND DISCUSSION	
4.1	INTRODUCTION	47
4.2	INFLUENCE OF USING SYMMETRIC AND ASYMMETRIC ELECTRODES	47
4.3	INFLUENCE THE BARRIER HEIGHTS ON THE PERFORMANCE OF MIM FOR DISSIMILAR ELECTRODES	53
4.3.1	IMPACT THE BARRIER HEIGHTS VARIATION FROM THE ANODE SIDE	53

4.3.2	IMPACT THE BARRIER HEIGHTS VARIATION FROM THE CATHODE SIDE	59
4.3.3	IMPACT THE BARRIER HEIGHTS VARIATION WITH FIXED BARRIER DIFFERENCE	66
4.4	INFLUENCE OF INSULATOR THICKNESS ON THE PERFORMANCE OF MIM DIODE	70
4.5	IMPACT THE INSULATOR ELECTRON AFFINITY ON THE PERFORMANCE	74
4.6	RF CHARACTERIZATION	79
4.6.1	MIM DIODE CHARACTERIZATION	79
	CHAPTER FIVE CONCLUSIONS AND FUTURE WORKS	
5.1	CONCLUSIONS	89
5.2	SUGGESTIONS FOR FUTURE WORKS	91



LIST OF FIGURES



Subject	Page No
(2.1) PN junction diode at zero voltage bias	12
(2.2) Schematic of schottky diode	13
(2.3) Tunneling of the electron	14
(2.4) Tunneling of electron waves across a potential barrier	15
(2.5) Energy band schematic of MIM diode	19
(2.6) Dielectric films conduction mechanisms	21
(2.7) Schottky emission energy band diagram	22
(2.8) Schematic of Fowler-Nordheim tunneling energy bands	23
(2.9) Direct tunneling energy band diagram	24
(2.10) Thermionic-Field emission in MIS	25
(2.11) Poole-Frenkle emission energy band diagram in MIS structure	26
(2.12) Energy band diagram of an asymmetric metal in MIM diode at zero, forward, and reverse bias	28
(2.13) (a) Conventional Diode Characteristics Curve (b) MIM Diode Characteristics Curve	29
(2.14) Equivalent circuit of MIM diode	31
(3.1) Atlas inputs and outputs	36
(3.2) Atlas command groups	36
(3.3) Mesh creation using Atlas syntax	37
(3.4) Tunnel junction region	38
(3.5) Electrodes of MIM diode	39
(3.6) Quantum tunneling mesh of MIM diode	40
(3.7) Equivalent circuit of MIM diode in ADS software	45
(4.1) Proposed structures of the MIM diode with symmetric and asymmetric electrodes	48
(4.2) I-V characteristics curve of symmetric and asymmetric MIM diode	50
(4.3) a) Asymmetry, b) Nonlinearity, c) Resistivity, and d) Responsivity of proposed MIM diode	52
(4.4) Energy band diagram of proposed MIM diode	54
(4.5) I-V characteristics curve for fixed cathode metal MIM diode	56
(4.6) a) Asymmetry, b) Nonlinearity, c) Resistivity, and d) Responsivity for fixed cathode metal MIM diode	58
(4.7) Energy band diagram for fixed anode metal MIM diode	60

(4.8) I-V characteristics curve for fixed anode metal MIM diode	61
(4.9) a)Asymmetry, b)Nonlinearity, c)Resistivity, and d)Responsivity for fixed anode metal MIM diode	63
(4.10) a)Asymmetry, b)Nonlinearity, c)Resistivity, and d)Responsivity as a function of increasing work functions difference($\varphi_c-\varphi_A$)	65
(4.11) Energy band diagram for constant barrier potential MIM diode	67
(4.12) I-V characteristics curve for constant barrier potential MIM diode	67
(4.13) a)Asymmetry, b)Nonlinearity, c) Resistivity, and d)Responsivity for constant barrier potential MIM diode	69
(4.14) Energy band diagram of MIM diode with different thicknesses of insulator	71
(4.15) I-V characteristics curve with various thickness for MIM diode	71
(4.16) a)Asymmetry, b)Nonlinearity, c)Resistivity , and d)Responsivity for various thicknesses MIM diode	73
(4.17) Barrier heights of MIM diode with different insulators	75
(4.18) I-V characteristics curve with different insulators for MIM diode	76
(4.19) a)Asymmetry, b)Nonlinearity,c)Resistivity , and d)Responsivity for different insulators MIM diode	78
(4.20) Equivalent circuit of MIM diode	81
(4.21) I-V characteristics curve of MIM diode have different insulators	81
(4.22) Equivalent circuit model of proposed MIM diode in ADS	83
(4.23) S-Parameters of proposed MIM diode in ADS	84
(4.24) I-V curve of MIM diode with variable thickness of insulators	84



LIST OF TABLES



Subject	Page No
Table (4.1) The structures of symmetric and asymmetric MIM diode	49
Table (4.2) Parameters extracted at zero bias of MIM diode	51
Table (4.3) The structures of MIM diode with fixed cathode metal	55
Table (4.4) Parameters extracted at zero bias of MIM diode	57
Table (4.5) The structures of MIM diode with fixed anode metal	60
Table (4.6) Parameters extracted at zero bias of MIM diode	62
Table (4.7) The structures of MIM diode with constant barrier potential	67
Table (4.8) The structures of MIM diode with different insulators	75
Table (4.9) Theoretical and simulation parameters extracted at zero bias of MIM diode	84
Table (4.10) Theoretical and simulation parameters extracted at zero bias	87



LIST OF ABBREVIATIONS



ABBREVIATIONS	DESCRIPTION
MIM	Metal-Insulator-Metal
Al	Aluminum
Al ₂ O ₃	Aluminum Oxide
Au	Gold
I-V	Current-Voltage
FOM	Figures of Merit
SiO ₂	Silicon dioxide
MI ² M	Metal-Insulator-Insulator-Metal
MI ³ M	Metal-Insulator-Insulator-Insulator-Metal
ZrO ₂	Zirconium dioxide
HfO ₂	Hafnium oxide
ADS	Advanced design system
DC	Direct Current
AC	Alternating Current
THz	Terahertz
Nm	Nanometer
QW-ASPAT	Quantum Well-Asymmetric spacer tunnel
TOV	Turn-on voltage
NDR	Negative Differential Resistance
M	Metal
SE	Schottky-Emission
MIS	Metal-Insulator-Semiconductor
F-N	Fowler-Nordheim
FNT	Fowler-Nordheim tunneling
P-F	Poole-Frenkle
I _F	Forward Current
I _R	Reverse Current
2D	Two Dimension
QT	Quantum Tunneling
MDS	Microwave design system
S-Parameter	Scattering parameter

Cd	Cadmium
Co	Carbon monoxide
Pt	Platinum
Ba	Barium
Ta	Tantalum
La	Lithium
Zn	Zinc
Ni	Nickel
Cu	Copper
Ir	Iron
Zr	Zirconium
3D	Three Dimension
RF	Radio Frequency
A/W	Ampere per watt

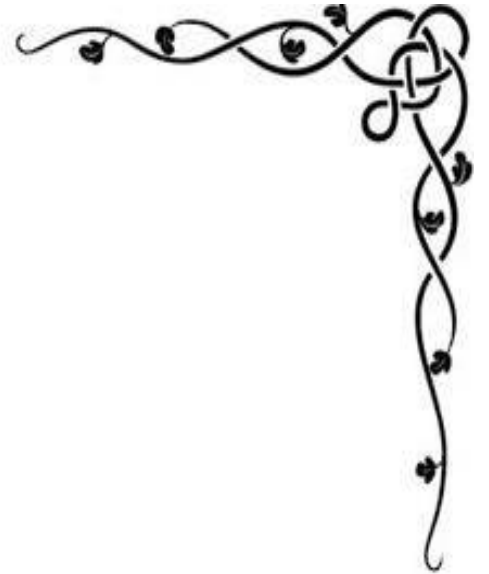


LIST OF SYMBOLS

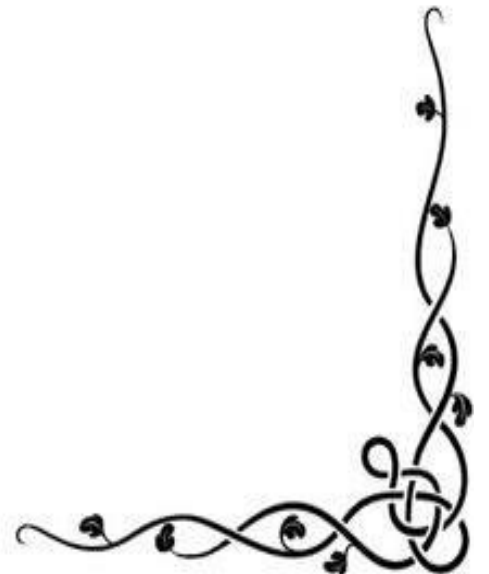
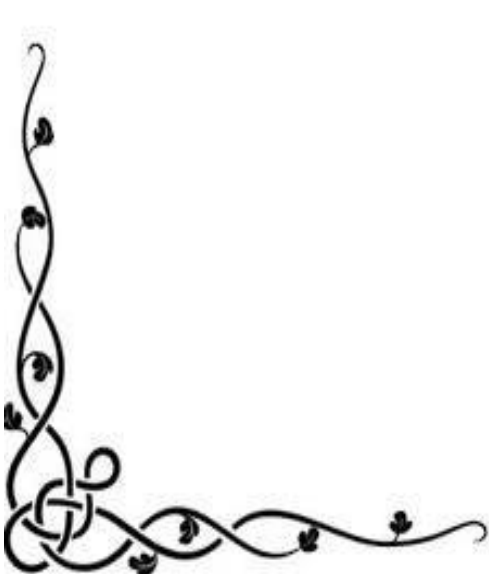


SYMBOL	DESCRIPTION
m	Electron mass
r	Position vector
$V_{(r)}$	Potential Energy
E	Total Energy of electron
\hbar	Reduced Plank's constant
$\Psi_{(r)}$	Wave function vector
m^*	Effective mass
A	Amplitude of the signal
K	Wave vector/ Propagation constant
J	Current Density
Q	Electron charge
$T_{(EX)}$	Tunneling probability
F	Fermi distribution function
V	Applied bias
T	Temperature
K	Boltzmann constant
E_f	Fermi level
ϕ	Barrier Height
φ	Work function
χ	Electron Affinity
T	Dielectric's thickness
$q\varphi_B$	Barrier Energy level
$q\varphi_T$	Trap Energy level
I	Current
V	Voltage
C_j	Junction Capacitance
R_j	Junction Resistance
R_s	Series Resistance
f_c	Cutoff frequency
A	Constant area

d	Thickness of insulator
ϵ_r	Relative dielectric constant
ϵ_0	Vacuum permittivity
D	Transmission probability
L	Length
P	Resistivity
EG	Band-gap
ϕ_c	Constant Barrier Height
φ_c	Cathode work function
φ_A	Anode work function
$\Delta\varphi_m$	Difference work function in metals
$\Delta\varphi$	Difference work function
dt	Change in dielectric thickness
E_V	Top edge of the valence band
E_c	Bottom edge of the conduction band



Chapter One
Introduction and Literature Review



CHAPTER ONE

Introduction and Literature Review

1.1 Introduction

Finding new energy sources that are efficient, safe, and affordable is required due to the periodic demand for energy. Although fossil fuels are frequently employed because of their effectiveness, they are very expensive and unfriendly to the environment. Solar cells are one of the major energy sources; however, because of the restricted band gaps of semiconductors and their high cost, they are not as efficient as fossil fuels. However, considering that the Earth receives 1000 W/m^2 of sunlight at sea level on clear days, the sun continues to be a considerable source of energy [1]. Because of the sun's abundant energy, researchers have developed novel methods for converting solar energy to electricity. A rectifying antenna, commonly known as a rectenna, is one of the energy harvesting tools that turns solar radiation directly into electricity. The antenna, rectifier system, and DC pass filter make up the rectenna. After receiving electromagnetic radiation from the antenna, the rectifier directs the current in one direction. To enable DC power output, the current is then converted to a direct current (DC) by the DC pass filter. The visible and infrared spectrums are where the sun's radiation is strongest. The rectifier in the antenna must react very quickly to rectify the current at these high-frequency ranges (THz). Due to their quick response, tunnel diodes are a type of diode that can correct the current at high frequencies. A MIM diode (Metal-Insulator-Metal) is a nano-electronic device that consists of an ultrathin insulator layer sandwiched between two metal contacts. MIM diodes have shown promise in a variety of high-frequency applications such as infrared detection [2]. Solar energy harvesting and wireless power transmission [3] are two examples. Focus has been placed on MIM diodes because of the rising demand for high-speed electronics with compact physical footprints.

Due to their rapid quantum tunneling conduction process, MIM diodes are useful; it has terahertz (THz) frequency applications capability. The MIM diode's primary function in any system is to correct a high-frequency (THz) AC signal to DC. A strong current at forward biases compared to a low "near-zero" current at reverse biases is required by the ideal diode current-voltage (IV) characteristic. The Figures of Merit (FOM) are three measures that have been found to describe a diode's rectification performance [4]. A diode that achieves the highest FOM is capable of effective rectification. The FOM quantifies the nonlinearity of the IV response of a diode. The ratio of forward current to reverse current is referred to asymmetry, and values greater than one denote rectification. Nonlinearity is the degree of sharpness in the turn on a specific area of the IV curve. Lastly, responsiveness measures the amount of DC produced per unit of AC power. Selected metals, insulator materials, and insulator thickness have an important impact on the MIM Diode's properties. To achieve the tunneling current as the basic mode of transport in a MIM diode, the thickness of the insulator should be less than 10nm [5]. MIM diodes come in two varieties: symmetric and asymmetric. The insulator barrier's heights on both sides are affected by whether the metals on the two sides are similar [6] or dissimilar [7], and this feature is accomplished by utilizing different metals. The barrier heights are defined as the difference between the work function of the metal and the insulator's electron affinity at metal-insulator interfaces. There are two different potential barrier values between first metal and the insulator, as well as between second metal and the insulator if just one insulator is employed. These two interfaces have an impact on the breakdown and turn-on voltages depending on the work functions of the metals [8].

1.2 Literature Review

- During the first century of the 1960s, MIM diodes have been studied by NASA [9]. In 1982 NASA coming up with the idea of capturing solar energy using a MIM diode [10]. Between the antenna and the diode, there was a coupling efficiency issue [11].
- According to Gustafon [12], efficiency is constrained by difficulties in the fabrication process. Yet, according to Landsberg [13], sounds have a 93% limit on coupling efficiency.
- Subsequently, a study by Bareib et al [14] stated that MIM nano-diodes with a 93nm diameter can perform properly up to 219 THz. Due to the femto second rapid transport mechanism of quantum tunneling, MIM diodes can function at the THz range [15]. As a result of that, MIM tunnel diodes starting was fabricated and widely used in high-frequency applications.
- S. Krishnan et al in 2007 [16] fabricated an asymmetric planar thin film. Tunnel diodes made of metal-insulator-metal at room temperature with NiO as an insulator layer sandwiched between Ni and Au, Cr metals as cathode and anode respectively. They found that the contact area and dielectric thickness play a vital role in improving the detector's current where an increase in the detector current from 1.5 nA to 0.8 mA was obtained by tailoring these parameters. These outcomes support the conduction mechanism via tunneling and are consistent with theoretical assumptions. The nonlinearity and asymmetry of this structure suggest that it is helpful in the infrared spectrum. The authors demonstrated how the current-voltage (I-V) characteristics of tunnel diodes are asymmetric as a result of the construction and layout asymmetry, which enhances the performance of the diode.

- k. Choi et al in 2010 [17] studied the tunneling phenomena for Metal-Insulator-Metal by using similar and dissimilar electrodes (polysilicon-SiO₂-Ti, Au) and (Ni-NiO-Ni). The results of fabricated illustrated that asymmetric electrodes have sensitivity and I-V curvature reach 71% and 350% respectively, while symmetric diode reaches 15% and 39%.
- P. Periasamy et al in 2011 [18] succeeded in fabricating the MIM diode with an ultrathin layer of Nb₂O₅ as an insulator layer and used the same metal on the cathode (Nb) with different eight metals on the anode (Hf, Nb, Ti, Cu, Ag, Cr, Au, and pt), to study the effect of $\Delta\phi$ on the performance of the device, via an approach to novel bent wire point-contact. Quantitative analysis of the eight devices clearly shows that the rectifier properties (f_{ASYM} and f_{NL}) are influenced by $\Delta\phi$.
- Aydinoglu in 2013 [19] fabricated MIM diodes made of (Pt/Al₂O₃/Al) and (Cr/Al₂O₃/Cr) to show how the materials affected the current-voltage (I-V) curve. It is demonstrated that when compared to the (Cr/Al₂O₃/Cr) MIM diode, the (Pt/Al₂O₃/Al) MIM diode exhibits a large asymmetrical I-V curve. This asymmetry in the materials leads to enhancing the performance of the MIM diode. A recent investigation to ascertain the impact of metals on rectification performance was reported by many authors. The study shows that it is sufficient to choose the metals such that their work functions differently to achieve desired rectification characteristics (high asymmetry and nonlinearity).
- Simultaneously, in the same year according to a study done by S.Grover and G.Moddel in 2013 [20] two processes for enhancing the effectiveness of multi-insulator diodes were investigated. Single and multi-insulator metal diodes could be created using either of these mechanisms. To determine the appropriate choice of insulators and barrier thicknesses, two double-insulator (MIIM) diodes based on these mechanisms are simulated and their characteristics are compared with MIM diodes. The simulations demonstrated that double-insulator diodes

had a higher responsivity than single-insulator diodes. Since single-insulator diodes have a restricted responsive range, double-insulator devices can achieve both required qualities.

- Aparajita Singh et al, in 2014 [21] fabricated MIM diode with single-insulator layer (Ni-NiO_x-Cr) and MIIM diode double-insulator (Ni-NiO_x-ZnO-Cr) tunnel diodes. They observed enhanced asymmetry in the case of bilayer at low voltage. Also, the sensitivity of the device improved in the case of the added second insulator layer. These results proved that the second insulator increased from the transport through the tunneling.
- Shilpi Shrivastava et al, in 2018 [22] a thorough investigation into MIM diodes was carried out, highlighting improvements in the design and production of diodes. Fabricated (Al/AlO_x/Gr) MIM diode, exhibited highly asymmetric current-voltage characteristics with large current density and a good degree of nonlinearity. An asymmetry exceeding 2500 and the corresponding current density up to 1 A/cm² were obtained at a voltage bias of 1 V. The peak nonlinearity was 3.8. The (Al/AlO_x/Gr) MIM diode with Grafine element has a great deal of promise for its possible usage in rectification in recta phones because these performance metrics are extremely desirable for rectification operations.
- Su Jin Heo et al, in 2018[23] examined the characteristics of basic, flat MIM diodes that use a tunneling mechanism by fabricating vertical metal cylinder array structures for high rectifying effects. The flat MIM diodes fabricated have single and double insulators. They show that the MIIM diode using double insulator layers has enhancement in asymmetrical I-V characteristics and illustrated more Nonlinearity and Asymmetry. They proved that the MIIM diode can have high rectification useful for THz applications.

- Daisuke Matsuura et al, in 2019 [24] suggested a novel tunnel diode double insulator made of (Pt-TiO₂-TiO_{1.4}-Ti) with an oxygen-non-stoichiometry-controlled homo interface structure (MO_x/ MO_{xy}). A current density of MIIM diode 4.6×10^6 A/m² was achieved which is 400 times greater than that of a (Pt-TiO₂-Ti) MIM diode. It is shown that the MIIM diode may achieve a current density of 10⁸ and an asymmetry of 0.9 by adjusting the insulator layer's thickness. This led to an increase in the optical rectenna efficiency by 10,000.
- S.B. Tekin et al, in the year 2021 [25]fabricated tunnel-barrier rectifiers that included a single insulator layer(Al₂O₃) in (Au-Al₂O₃-Ti), and a triple insulator layer composed of(Ta₂O₅-Nb₂O₅-Al₂O₃) to study the current-voltage characteristics also figures of merit(f_{Asym} and f_{NL})for the structure(Au-Al₂O₃-Ti) diode responsivity reached to 0.6 A/W at zero bias, whereas the MI3M demonstrated asymmetry reach 6 at low voltage 0.1v and responsivity reach 4.3 A/W at 0.35v. This enhancement is a result of using triple insulators on these structures to make them useful in optical applications.
- Abdullah Alodhayb et al, in 2021 [26] proved that using an extra barrier at the interfaces of the oxide lead to enhancing both Asymmetry and Nonlinearity properties. After comparing the simulation results of the MIM and MIIM diodes, the MIIM diode has higher dynamic resistance than a MIM diode for the same overlap area and thickness. Also the Nonlinearity and Asymmetry are more pronounced in the MIIM diode. MIIM diodes have indicated an ability superior to MIM diodes in terms of rectification capability.

- Sana Abrar, and Muhammad Bilal et al in 2022 [27] fabricated a Metal-Insulator-Insulator-Metal (MIIM) diode with a double bilayer of insulators (SnO_2 , NiO) with symmetric electrodes (Cr), via e-beam evaporation. Results show smooth dense and uniform coating was obtained with a small thickness of insulators. The Nonlinearity and Sensitivity reach 2.6 and 9.0 v^{-1} , respectively, at 1.5 v. They showed that this nanostructured ($\text{Cr}/\text{SnO}_2/\text{NiO}/\text{Cr}$) diode is useful for future rectification devices.
- Fatima M. AbdelHamied et al in 2022 [28] constructed and studied a rectangular spiral nano-antenna (NA) design coupled rectifier diode, using a double layer of insulators between asymmetric metals that have different work functions to enhance the performance rectifying diode. They achieved higher results in a MIIM diode compared with MIM, where resistance $43.6 \text{ k}\Omega$, Responsivity 7.73 A/W , and Asymmetry 45, all at zero bias in a MIM, while a MIIM diode achieved higher Responsivity and Asymmetry reached 18.9 A/W and 100 respectively.
- Shamil. H et al in 2023 [29] built, analyzed, and compared innovative well-barrier QW-ASPAT diodes with the traditional Quantum-well ASPAT devices (QW-GaAs and QW-InGaAs) and ASPAT diodes. The results of the simulation show that the KV is enhanced for GaAs devices from 13 v^{-1} to 32.5 v^{-1} and for $\text{In}_{0.53}\text{Ga}_{0.47}\text{As}$ devices 33 v^{-1} . Results for this enhancement proved that this proposed QW-ASPAT tunneling diodes can be used in the high-frequency applications.
- After reviewing the previous literature. We noted that the majority of the MIM diode works are fabricated. In this thesis, we simulated the MIM diode to study the effect of physical parameters and their impact on electrical characteristics. The results were discussed in chapter four.

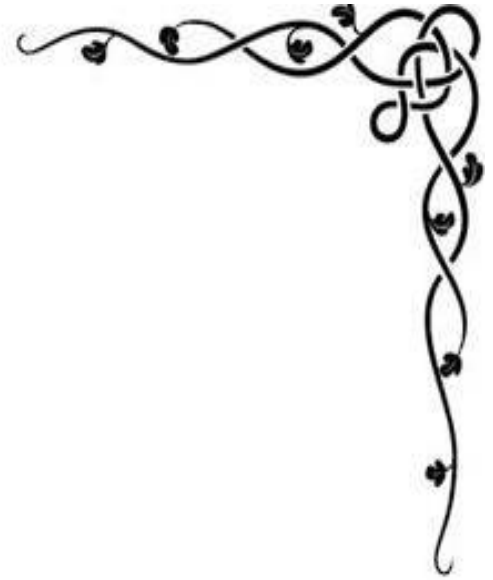
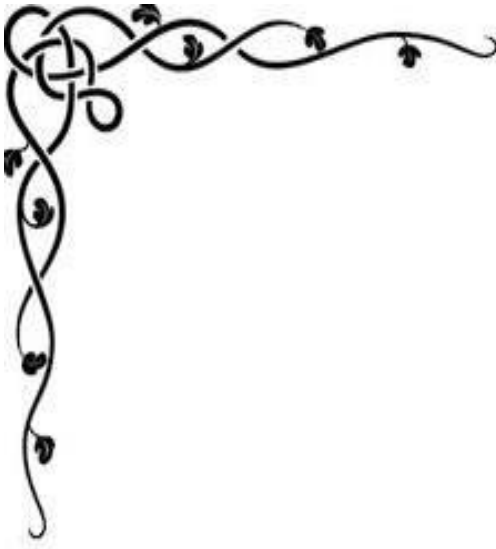
1.3 AIM OF THE WORK

The current work focuses on investigating the physical characteristics, such as the barrier heights, the thickness of the dielectric films, and tunnel diode materials and their impact on the electrical characteristics of the tunnel diode. These can be reached to these results by using small barrier heights that increase the forward current at a lower turn-on voltage (TOV). The thinner dielectric films increase the probability of quantum mechanical tunneling. Also increasing the difference in the work functions between metals gives a higher FOM for the MIM tunnel diode.

1.4 ORGANIZATION OF THE THESIS

There are five chapters in the thesis. The following is a summary of the chapter's outline:

- Chapter one includes a general introduction for MIM tunnel diodes and literature review.
- In chapter two, the principles of quantum mechanical tunneling of MIM diodes are covered.
- Chapter three describes the methodology of simulation MIM diode in Silvaco software.
- In chapter four, the simulation results and discussion of MIM diode are stated.
- Finally, in chapter five, the conclusion and suggestions for future works are presented.



CHAPTER TWO

PRINCIPLES OF QUANTUM MECHANICAL TUNNELING AND MIM TUNNELING DIODE



CHAPTER TWO

Principles of Quantum Mechanical Tunneling And MIM Tunneling Diodes

2.1 Introduction

Semiconductor electronic devices have emerged as a crucial building block in the development and application of intelligent systems that operate at high speeds and high frequencies in the modern technological era. Development of nano-semiconductor technology is a direct result of intense work being put forth simultaneously in many other fields. The groundbreaking Esaki and Tsu's work, who investigated novel quantum structures while engineering band gap devices by stacking layers of various semiconductors, is largely responsible for the advancements in this era [30, 31]. As a result, in the 1980s, the development of super lattice semiconductors and the notable impacts of resonant transport and quantum wells over thin barriers began to flourish [32]. The fundamental physics of electrons in semiconductor hetero-structures was established at that time. This laid the groundwork for the crucial quantum confinement principle for semiconductor technologies. This was swiftly followed by the appearance of new notions and structures that were carefully investigated.

2.1.1 PN junction and Schottky barrier diode

PN junctions are commonly utilized in diode, transistor, and solid-state circuits. A PN-junction diode is formed when a p-type semiconductor is fused to an n-type semiconductor creating a potential barrier voltage across the diode junction. So in the middle, the neutral equilibrium state breaks down. There are depletion regions or space charge regions that only have ions and do not have charge carriers (holes and electrons). The junction shows the rectification characteristics from the depletion region. Rectification is blocking the current at reverse bias and flow the current

across the depletion region at forward bias. A common application for PN junction diodes is to convert alternating current (AC) to direct current (DC). However, because of the wide depletion area, this mechanism is not appropriate for high-speed rectification [33,34].

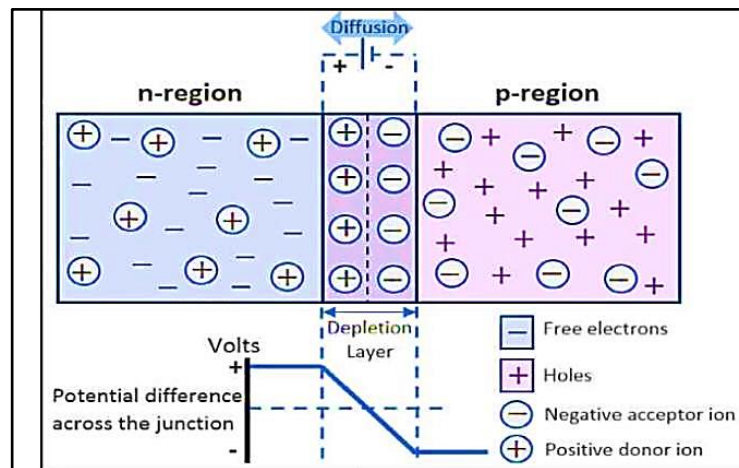


Figure (2.1) PN Junction Diode at Zero Voltage bias [35]

A metal-semiconductor contact is known as a Schottky barrier diode. Due to the Schottky diode lack of accumulation effect, the current flow is due to the majority of carriers rather than the minority carriers. Therefore, the reverse recovery period of the Schottky diode is very fast. It is thus appropriate for high-speed switching. Low noise generation and lower forward resistance are two additional benefits of the Schottky diode [36]. The forward current operates at a modest voltage as a result. Schottky diodes can also be used as integrators and detectors for microwave receivers. But the maximum operating frequency for Schottky diodes is 5 THz [37]. As a result, a new strategy for use with greater frequencies is required.

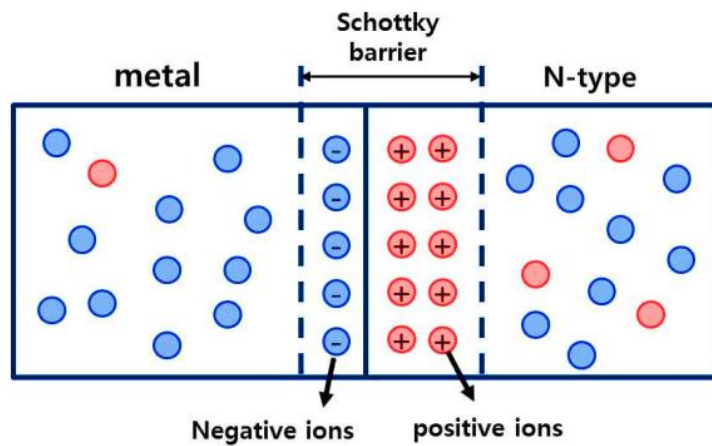


Figure (2.2) Schematic of Schottky diode [38]

2.2 Quantum Mechanical Tunneling

In the late 19th century, quantum mechanical tunneling was discovered [39,40]. It was a logical progression from research on radioactivity disintegration. A quantum mechanical phenomenon known as quantum tunneling allows for the passage of electrons due to a barrier that is suitably thin in comparison to the wavelength of an electron [41]. Figure (2.3) a) illustrate the classical perspective, where Figure (2.3) b) shows a perspective of quantum mechanics of electron tunneling [40]. Typical electron morphology that effectively crosses a barrier is depicted in Figure (2.3) a) an electron must possess enough energy across the barrier in classical physics. Otherwise, it will ricochet back from the barrier. On the other hand, quantum mechanical tunneling, as shown in Figure (2.3) b) enables the possibility of an electron navigating a barrier. The thickness of the barrier and the probability of electrons tunneling are depicted by the yellow line in Figure (2.3) b). When the electron is viewed as a wave, it

might appear to be quite big with the thickness of the barrier. It is incredibly unlikely that the particle will be visible on the other side of a substantial barrier. Therefore, a thinner barrier considerably increases the probability that an electron will pass through it [40].

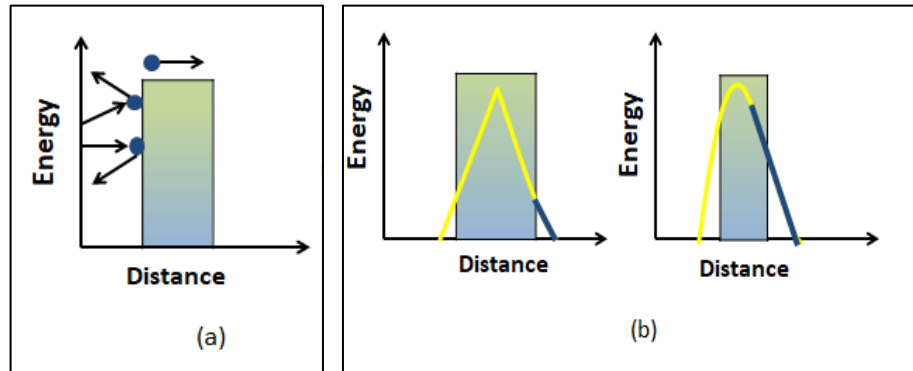


Figure (2.3) Tunneling of electron (a) Classical mechanical (b) Quantum mechanical [40]

Wave function-based treatment methods for electrons moving through semiconductors have been around for a while. As a result, the Schrödinger equation, the basic physical equation (2.1), is used to describe the behavior of quantum mechanics in semiconductor technology. The result of an electron scattering when it encounters a discontinuity, such as a flaw in a crystal or the boundary between two semiconductors, is explained by this equation (2.1) using wave functions [40].

$$E\Psi_{(r)} = -\frac{\hbar^2}{2m}\nabla^2\Psi_{(r)} + V_{(r)}\Psi_{(r)} \quad (2.1)$$

The mass of an electron is denoted by m , r stands for the position vector, the potential energy at position r is denoted by $V_{(r)}$, and the total energy of the electron is denoted by E , and \hbar is the reduced Planck's constant is denoted by $\hbar = \frac{h}{2\pi}$. To demonstrate the phenomenon in one dimension,

Figure (2.4) shows the possible structure of this phenomenon. The passage of an electron must be taken into account in three distinct areas.

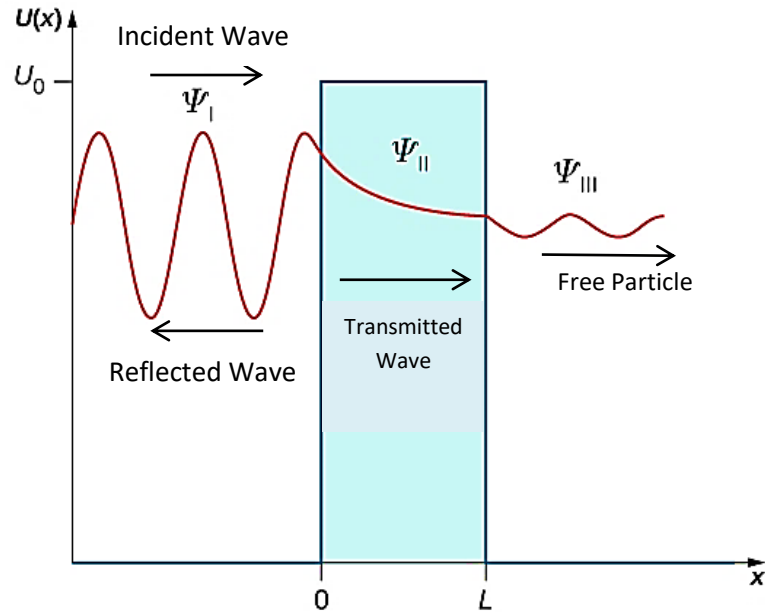


Figure (2.4) Tunneling of electron waves across a potential barrier [42]

Figure (2.4) illustrates how quantum particle could tunnel through a potential barrier. In region I, an incident wave packet (known as an incident particle) and a reflected wave packet (known as a reflected particle) coexist where $x < 0$. In region II a part of the incident wave that has not been reflected and a damping will happen for amplitude at $x=0$ moves as a transmitted wave in constant potential and enters region III at $x=L$. A wave packet (transmitted particle) in region III for $x > L$ travels as a free particle in the potential free zone after the tunneling through the potential barrier [42]. When the height (U_0) and the length (L) regions reach infinite, this reduces the probability of tunneling

By applying equation (2.1) to the electron wave behavior in Figure (2.4), we get:

$$-\frac{\hbar^2}{2m^*} \frac{d^2\Psi_{I(x)}}{dx^2} + V(x)\Psi_{I(x)} = E\Psi_{I(x)} \quad X < 0 \text{ Region I} \quad (2.2)$$

$$-\frac{\hbar^2}{2m^*} \frac{d^2\Psi_{II(x)}}{dx^2} + V\Psi_{II(x)} = E\Psi_{II(x)} \quad 0 < X < L \text{ Region II} \quad (2.3)$$

$$-\frac{\hbar^2}{2m^*} \frac{d^2\Psi_{III(x)}}{dx^2} + E\Psi_{III(x)} \quad X > L \text{ Region III} \quad (2.4)$$

Equations solving (2.2) - (2.4)

$$\Psi_{I(x)} = A_1 e^{iK_1 x} + B_1 e^{-iK_1 x} \quad \text{where } K_1 = \frac{\sqrt{2m(E)}}{\hbar} \quad (2.5)$$

$$\Psi_{II(x)} = A_2 e^{K_2 x} + B_2 e^{-K_2 x} \quad \text{where } K_2 = \frac{\sqrt{2m(V-E)}}{\hbar} \quad (2.6)$$

$$\Psi_{III(x)} = A_3 e^{iK_3 x} \quad \text{where } K_3 = K_1 = \frac{\sqrt{2m(E)}}{\hbar} \quad (2.7)$$

A_1 , A_2 , and A_3 stand for the amplitudes of the incident, reflected, and transmitted waves; respectively k is a wave vector. The incident wave's amplitude is B_1 , whereas the reflected wave's amplitude is B_2 .

Applying the boundary conditions at $x=0$ and $x=L$ to equations (2.5) - (2.7) and matching the first derivatives at the boundary results in the relationships shown below [43]:

$$A_1 + B_1 = A_2 + B_2 \quad (2.8)$$

$$iK_1 A_1 - iK_1 B_1 = K_2 A_2 + K_2 B_2 \quad (2.9)$$

$$A_2 e^{K_2 L} + B_2 e^{-K_2 L} = A_3 e^{iK_3 L} \quad (2.10)$$

$$K_2 A_2 e^{K_2 L} - K_2 B_2 e^{-K_2 L} = iK_3 A_3 e^{iK_3 L} \quad (2.11)$$

Solving for all the equations above gives the transmission probability

$$T = \left| \frac{A_3}{A_1} \right|^2 = \frac{1}{1 + \left(\frac{k_1^2 + k_2^2}{2k_1 k_2} \right) \sinh 2(k_2 d)} \quad (2.12)$$

The tunneling probability concepts are derived from equation (2.12), which states that the electron has a finite probability (T) of tunneling through the potential barrier.

2.3 Metal-Insulator-Metal tunnel diode

The metal-insulator-metal (MIM) diodes structurally consist of a thin insulator layer placed between two identical or differing metal electrodes. With a narrow barrier, the probability of electron tunneling increases. The fact that tunneling occurs at a lower working voltage (low threshold voltage) than it does for Schottky barrier diodes and p-n junction diodes demonstrates that MIM tunnel diodes are better suited for high-speed operation. There are many essential requirements that must be taken into consideration while designing MIM diodes for them to work effectively [44]. These requirements are: 1) for the tunneling effect to occur, the insulator layer needs to be very thin a few nanometers. 2) The (I-V) characteristics' behavior ought to be asymmetric. This can be achieved by utilizing different metals with significant changes in their work functions on either side of the insulator layer. 3) Low resistance to effectively match the diode and antenna's impedance. MIM can be used in radiation detectors and combine optical and infrared photons [45]. A conventional point-contact diode was used to construct the first MIM tunnel diode. A cat-whisker diode was the name given to the MIM diode. The Cat-whisker diode was a tungsten wire that, by squeezing a metal plate created a tunnel junction. Due to certain dust that formed barrier layers that accumulated on the surface or some naturally occurring oxide layers, this type of diode proved to be challenging to manufacture. Cat-whisker diodes have been developed and utilized in communications for more than 20 years for high-frequency rectification, despite these obstacles. Thin-film transistor liquid

crystal displays (TFT-LCD) systems have also utilized MIM diodes as switching components and for image display [46]. In a MIM diode, free electrons at metal 1 (M_1) can tunnel to metal 2 (M_2) when the insulator layer is several nanometers thick. In the same way, free electrons at M_2 can tunnel to M_1 . Currents flow from M_2 to M_1 and from M_1 to M_2 , respectively, as a result of tunneling from M_1 to M_2 and from M_2 to M_1 . Equations (2.13) and (2.14) are used to get the two current densities (J) [47].

$$J_{2 \rightarrow 1} = \frac{4\pi m_2 q}{h^3} \int_0^\infty T(E_x) \left[\int_{E_x}^\infty f_2(E) dE \right] dE_x \quad (2.13)$$

$$J_{1 \rightarrow 2} = \frac{4\pi m_1 q}{h^3} \int_0^\infty T(E_x) \left[\int_{E_x}^\infty f_1(E) dE \right] dE_x \quad (2.14)$$

Where m is the electron's mass, q is charge of the electron, Planck's constant is h , and the probability of tunneling is $T(E_x) = \exp\left\{-\frac{2}{h} \sum_{j=1}^N \int_{x_j}^{x_{j+1}} \sqrt{2m_j[E_x - U_j]} dx\right\}$ [48], and f_1 and f_2 are the Fermi distribution functions that are depicted in the following equations:

$$f_1(E) = \frac{1}{\exp\left(\frac{E - E_f}{kT}\right) + 1} \quad (2.15 a)$$

$$f_2(E) = \frac{1}{\exp\left(\frac{E - E_f + qV_{\text{bias}}}{kT}\right) + 1} \quad (2.15 b)$$

Where V denotes applied bias, T denotes temperature, k denotes Boltzmann constant, and E_f denotes the Fermi level of the metal. The tunneling probability and Fermi distribution functions are the only factors that can change the current density, according to equations (2.13) and (2.14). Tunneling is more likely to occur in a MIM diode when the insulator layer thickness is decreased. The barrier height value (ϕ), which represents the

potential difference between the two materials, alters the Fermi distribution functions. The difference between the work function (ϕ) of the metal and the electron affinity (χ) of the insulator at the metal-insulator contacts yields the barrier height value. As a result, with MIM diodes, the kind of material and insulator thickness is crucial. Figure (2.5) shows the energy band diagrams of MIM tunnel diodes made of the different metals with zero bias, and with a negative bias.

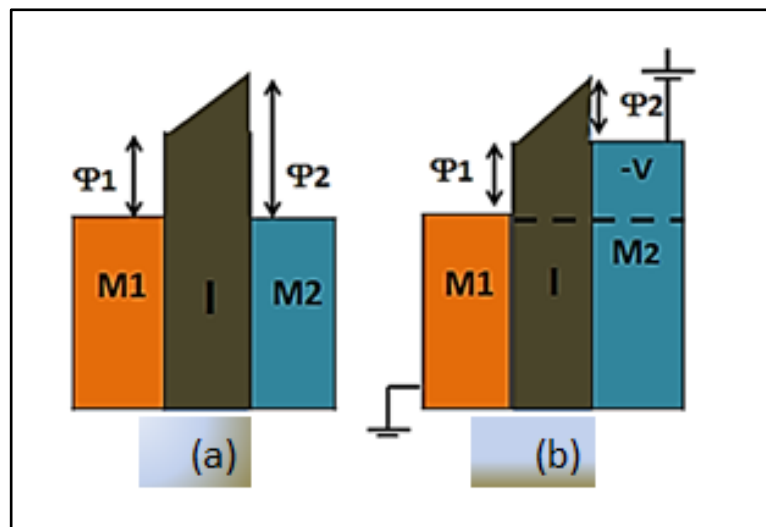


Figure (2.5) Energy bands schematic of a MIM diode when (a) different metals under zero bias (b) metal 2 is exposed to a negative voltage [49]

The current density in positive direction becomes greater when M2 has higher work function value than M1 (Figure 2.5(b)). In this case the energy band diagram of the insulator in this instance has a triangular form. This triangle form sharpens Figure 2.5(b) when a negative bias is applied to metal2, and the tunneling distance decreases as the energy increases. This increases the probability of tunneling at certain energy levels. As a result, in the case of Figure 2.5(b), the positive current density is substantially higher than the negative current density. Comparing (Figure 2.5 (a)) with (Figure 2.5 (b)), because metal 2 has more energy in (Figure 2.5(b)) this led the positive current density is higher in it.

2.4 Dielectric Film Conduction Mechanisms:

For dielectric materials to be used effectively, the dielectric films' conduction processes are crucial. In dielectric films, there are two kinds of conduction mechanisms: electrode-limited and bulk-limited conduction mechanisms. The electrode-dielectric interface's electrical characteristics are crucial to the electrode-limited conduction mechanism. The effective mass of conduction carriers in dielectric films and the barrier height at the electrode-dielectric interface can be determined using this kind of conduction mechanism. The bulk-limited conduction mechanism is determined by the electrical characteristics of the dielectric. This type of conduction is interested by the density of states in the conduction band, the dielectric relaxation time, the trap level, the trap spacing, and the trap density; the carrier drift mobility. The traps can all be determined from analyses of bulk-limited conduction mechanisms in the dielectric films. This dissertation discusses analytical methods for electrode-limited conduction mechanisms in dielectric films. The success of integrated circuits depends heavily on the investigation of various dielectric film conduction mechanisms. To quantify the conduction flow through the dielectric film, we should set up an example gadget for testing of some type. In general, sample testing employs two distinct types of device structures. The MIM capacitor or MIM diode is one such structure, which consists of metal-insulator-metal. The possibility of asymmetry in the electrical properties between the top and bottom electrodes is a concern in MIM capacitors constructed from various metals. Metal-dielectric interface barriers are different for different metals because they typically have different work functions. The barrier height of the metal-dielectric interface and the effective mass of the conduction carriers are the primary parameters in this type of measurement. Measurement of the temperature-dependent conduction currents may provide us with a useful technique to understand the makeup of the conduction currents because numerous

conduction processes depend on the temperature in different ways [50-59]. The classification of conduction modes in dielectric films is shown in Figure (2.6).

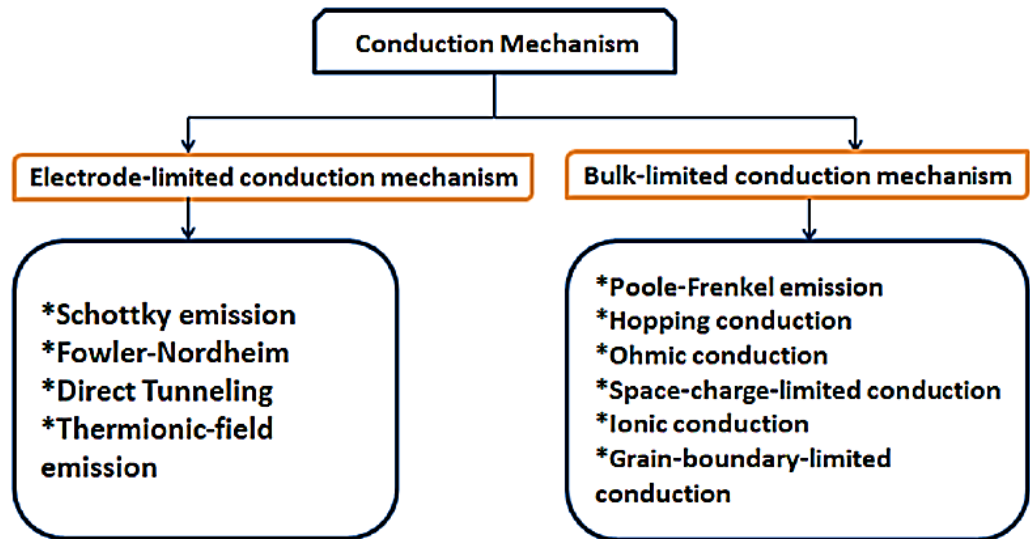


Figure (2.6) Dielectric films conduction mechanisms [60]

2.4.1 Electrode-limited conduction mechanisms

The electrical properties of the electrode-dielectric contact affect the mechanisms of electrode-limited conduction. For this kind of conduction process, the barrier height at the electrode-dielectric interface is essential. Fowler-Nordheim emission, direct emission, Schottky or thermionic emission, and thermionic-field outflow are among the anode-restricted conduction components. Although the burrowing current is virtually temperature independent, the current caused by thermionic outflow is severely temperature dependent. The effective mass of the conduction carriers in dielectric films, in addition to the barrier height at the electrode-dielectric interface, is a key element of the electrode-limited conduction mechanism [60].

2.4.1.1 Thermionic Emission:

If the metal's electrons can get enough energy from thermal activation, the energy barrier at the metal-dielectric interface can be overcome by them and move to the dielectric by Schottky emission. Figure (2.7) displays the MIS energy band diagram, when the metal electrode is under a negative bias for the dielectric and semiconductor substrate. At the metal-dielectric interface, the image force can reduce the height of the energy barrier. The lowering of barriers caused by the image force is known as the Schottky effect. The term "thermionic emission" refers to this particular sort of conduction process caused by electron emission from the metal to the dielectric.

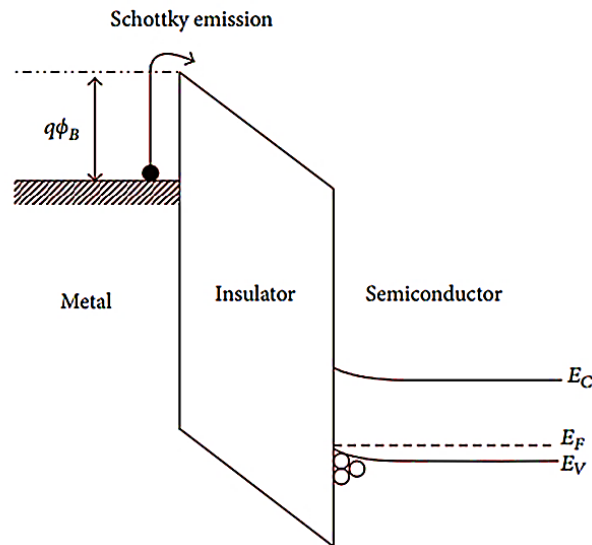


Figure (2.7) Schottky emission energy band diagram [60]

2.4.1.2 Tunneling through Fowler-Nordheim:

The electrons will be reflected when their energy is less than the potential barrier, according to classical physics. However, when the barrier is thin enough, quantum mechanics predicts that the electron wave function will pass through it. Consequently, the likelihood of electrons existing at the opposite side of the potential is not zero due to the tunneling impact. Figure (2.8) shows a schematic representation of the energy band diagram for Fowler-Nordheim (F-N) tunneling. When the applied electric field is

sufficiently strong, the electron wave function can pass past the triangular potential barrier and into the dielectric's conduction band, resulting in F-N tunneling equation (2.16) describe this relation [60].

$$I \propto \exp(\phi_B)^{\frac{3}{2}} / \phi_B \quad (2.16)$$

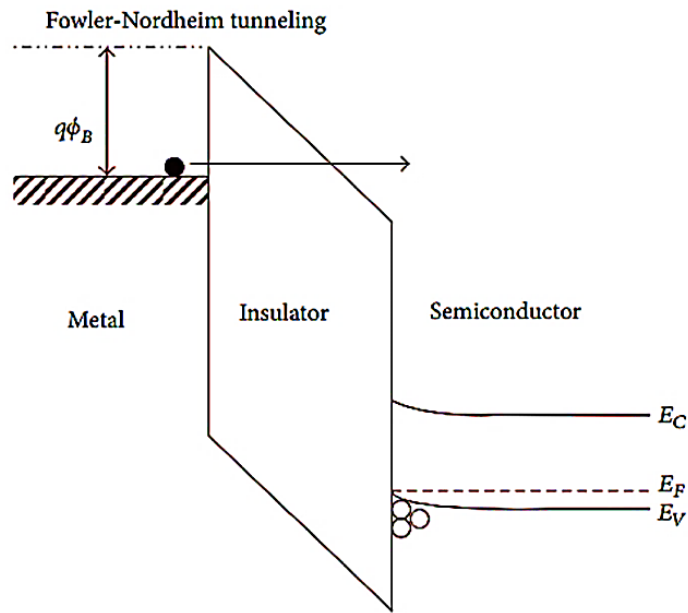


Figure (2.8) Schematic of Fowler-Nordheim Tunneling energy bands [60]

2.4.1.3 Direct Tunneling:

In SiO₂ films, there are two key approaches for conducting gate currents. The gate current is caused by F-N tunneling if the triangle barrier can be seen by the electrons due to a high enough voltage across the SiO₂. The gate current, on the other hand, is caused by directed tunneling if there is a small voltage applied across SiO₂ and the electrons can see the entire oxide layer. For the SiO₂-Si contact, the driving oxide voltage varies between the two mechanisms at about 3.1V. F-N tunneling predominates for SiO₂ thicknesses of 4-5 nm and above, while directed tunneling takes over for SiO₂ thicknesses of less than about 3.5 nm. Figure (2.9) depicts the

schematic energy band diagram for direct tunneling. The direct tunneling current is expressed as based on Lee and Hu's discoveries on a polysilicon-SiO₂-silicon structure as follows [61]:

$$J = \frac{q^2}{8\pi\hbar\epsilon\phi_B} c(V_G, V, t, \phi_B) \times \exp\left\{\frac{8\pi\sqrt{2m^*}(q\phi_B)^{3/2}}{3\hbar q|E|}\right\} \cdot \left|1 - \left(1 - \frac{|V|}{\phi_B}\right)^{3/2}\right| \quad (2.17)$$

Where t is the dielectric's thickness, V is the voltage applied across it, the barrier height is denoted by ϕ_B , and q is the charge of an electron.

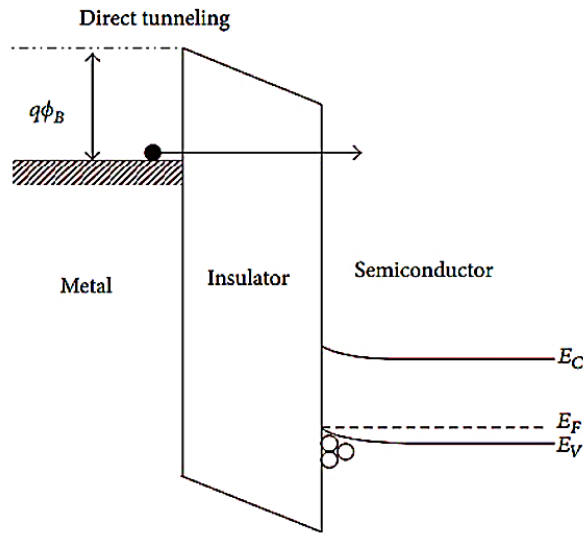


Figure (2.9) direct tunneling energy band diagram [60]

2.4.1.4 Thermionic-Field Emission:

Thermionic-field emission happens transitionally between field emission and Schottky emission. The tunneling electrons should have the energy between the Fermi level of the metal and the conduction band edge of the dielectric. Figure (2.10) a) depicts the thermionic-field emission schematic energy band diagram. Figure (2.10) b) depicts the distinction between field emission, thermionic-field emission. The thermionic-field emission current density can roughly be expressed as (2.18) [60]:

$$J = \frac{q^2 \sqrt{m} (KT)^{\frac{1}{2}} E}{8h^2 \pi^{\frac{5}{2}}} \exp\left(-\frac{q\phi_B}{KT}\right) \exp\left[\frac{h^2 q^2 E^2}{24m(KT)^3}\right] \quad (2.18)$$

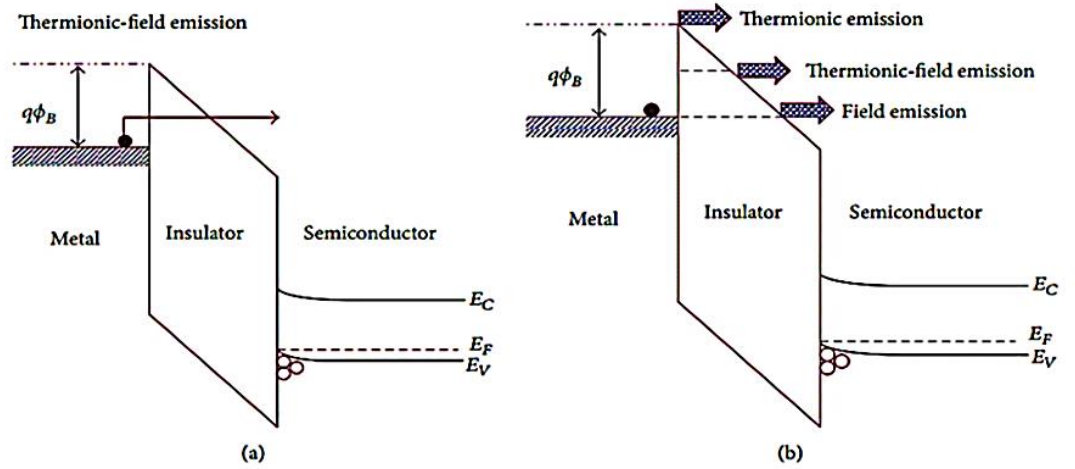


Figure (2.10) (a) Thermionic -field emission in a system of metal, insulators, and semiconductors is shown schematically in the energy band diagram. (b) A comparison of thermionic-field emission, thermionic emission, and field emission [60].

2.4.2 Bulk-Limited Conduction Mechanisms

The bulk-limited conduction mechanisms depend on the electrical characteristics of the dielectric itself. The trap energy level in the insulator layers is the most crucial parameter in this kind of conduction mechanism. Poole-Frenkel emission, hopping conduction, ohmic conduction, space-charge-limited conduction, ionic conduction, and grain-boundary-limited conduction are types of the bulk-limited conduction mechanisms. Some crucial electrical characteristics of the dielectric films, such as the trap energy level, the trap spacing, the trap density, the electronic drift mobility, the dielectric relaxation time, and the density of states in the conduction band, can be determined based on the bulk-limited conduction mechanisms [60].

2.4.2.1 Poole-Frenkel Emission

Similar to Schottky emission, Poole-Frenkel(PF) emission is caused by the thermal excitation of electrons that may emit from traps into the dielectric's conduction band. As a result, P-F emission is also known as internal Schottky emission.

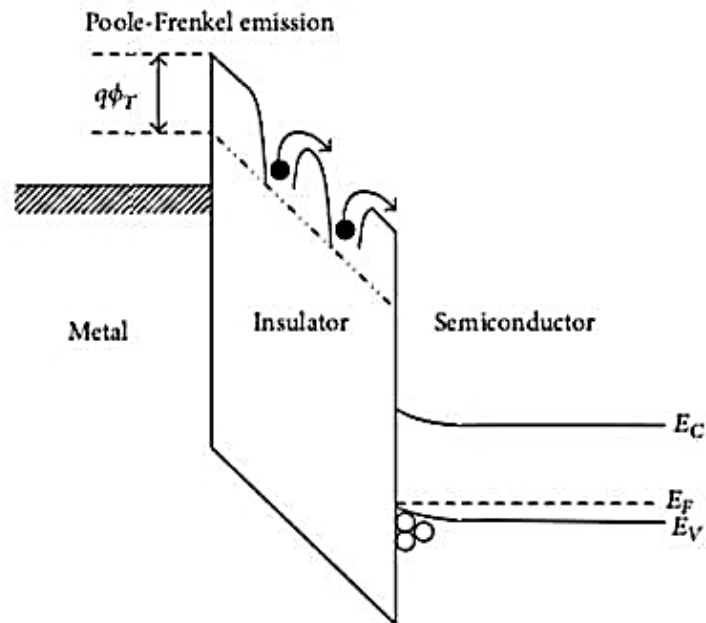


Figure (2.11) Poole-Frenkel emission energy band diagram in MIS structure [60]

2.4.2.2 Hopping Conduction

The tunneling effect caused by trapped electrons "hopping" from one trap site to another in dielectric films is what causes the hopping conduction.

2.4.2.3 Ohmic Conduction

Ohmic conduction happens by the motion of mobile electrons in the conduction band and holes in the valence band. This conduction mechanism, can represent the relation between the electrical field and the current density as a linear relation.

2.4.2.4 Space-Charge-Limited Conduction

If an electron-injecting contact is applied to the insulator, electrons will move from the metal into the insulator's conduction band and create a space charge resembling that of a vacuum diode. A space charge is an accumulation of charges in a specific region.

2.4.2.5 Ionic Conduction

Ions move as a result of an applied electric field, which causes ionic conduction. Lattice flaws in the dielectric layers could be the cause of the ions' motion. The ions may cross a potential barrier from one defect site to another due to the effect of the external electric field on the defect energy level.

2.4.2.6 Grain-Boundary-Limited Conduction

The resistivity of the grain boundaries in a polycrystalline dielectric material may be significantly higher than that of the grains. Therefore, the electrical characteristics of the grain boundaries might be used to limit the conduction current. Grain-boundary-limited conduction is the term used to describe this conduction mechanism.

2.5 Conduction mechanism of MIM diode:

The simple structure of MIM diode comprised a thin insulator film between two different metal plates. Figure (2.12) depicts the MIM diode's operation theory. The electron affinity of the insulators χ and the work functions of metals are ϕ_1 and ϕ_2 . The insulator's barrier thickness is dt . The asymmetric diodes shown here are made of different metals, but symmetric diodes can be made of the same metal for each electrode.

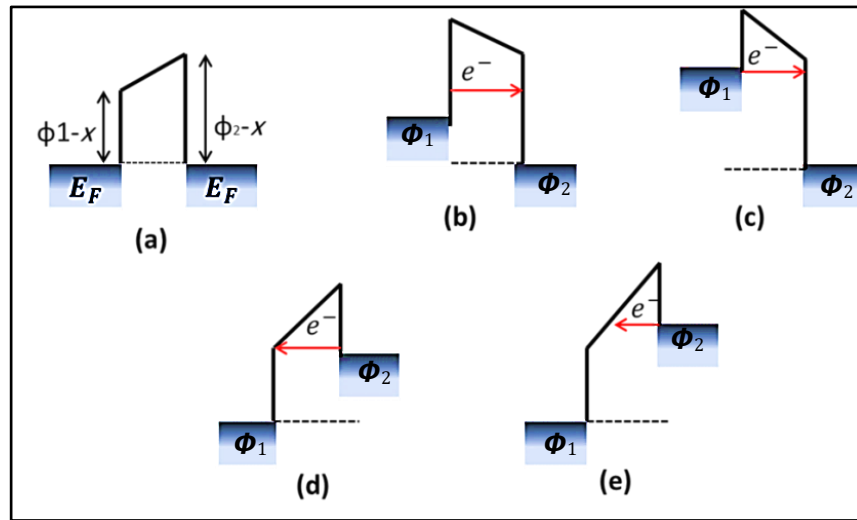


Figure (2.12) Energy band diagram of an asymmetric metal MIM diode at zero, forward, and reverse bias [62]

As shown in Figure (2.12) a) the metals' Fermi level is aligned at zero bias. A built-in field is created when the insulator's energy band is bent. Figure (2.12) b) illustrated that the direct tunneling can be confirmed if a metal is subjected to negative bias (also known as metal 1 subjected to reverse bias). The effective distance of the tunneling barrier can be expressed as dt , the thickness of the dielectric film. In Figure (2.12) c) there will be a greater disparity between the Fermi level of the two metals if a larger reverse bias is used. Additionally, The effective thickness dt is less than the thickness of the dielectric material. Fowler-Nordheim(FN) tunneling begins in this instance. When a metal 1 subjected forward bias, the band shift occurs as shown in Figure (2.12) d); this make FN tunneling principle occurs at low voltage. When a greater forward bias is used, the probability of FN tunneling increases because the effective thickness dt decreases as shown in figure (2.12) e) [63].

2.6 Characteristics of the MIM Diode

The IV curves represent the relationship between the electric current and the corresponding voltage in the circuit. The (I-V) curve of an ideal diode should have a high breakdown voltage and a turn-on voltage near zero volts. The (I-V) curve of a MIM diode is different on the I-V curve in the conventional diode. The turn-on voltage of MIM diodes with extremely low threshold voltages should be near to zero volts as shown in figure (2.13). The curve of I-V characteristics shows the details about the behavior of MIM tunnel diode. Main parameters extracted from this curve are asymmetry, nonlinearity, responsivity, and resistivity. These parameters affected by many factors such as changing the barrier heights and other factors such as the thicknesses of the dielectric films, change the electron affinity for insulators and the material types for electrodes. Each of these parameters will be discussed in the following section.

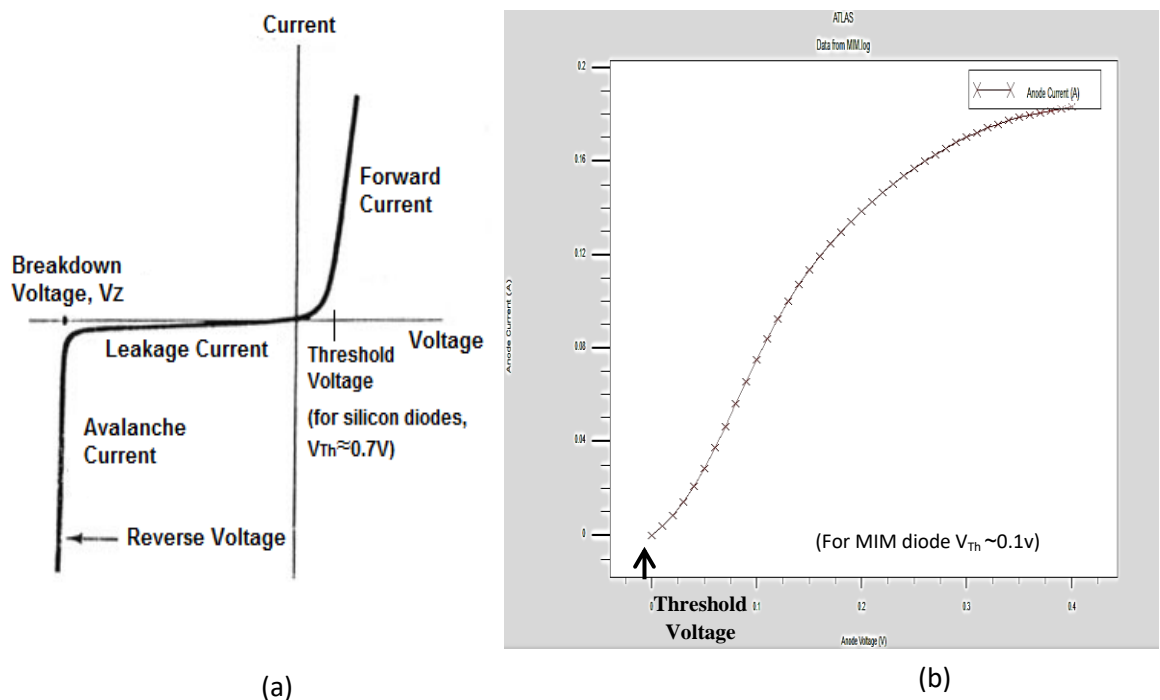


Figure (2.13) (a) Conventional Diode Characteristics Curve (b) MIM Diode Characteristics Curve

2.6.1 Asymmetry

The asymmetry is a factor to show the ratio of the forward current to reverse current. It is a simple measure of how well a diode can perform in a rectenna. The semi classical responsivity also depends on how asymmetric the (I-V) curve is around a particular bias point. To get efficient rectification, a diode's asymmetry value ought to be higher than 1.

$$\eta = \left| \frac{I_F}{I_R} \right| \quad (2.19)$$

At a specific voltage I_F stands for forward current and I_R for reverse current.

2.6.2 Nonlinearity

The nonlinearity is defined as the degree of the sharp turn-on voltage. We can investigate higher current densities by high nonlinear diodes at smaller voltage. The nonlinearity is calculated by equation (2.20) [64].

$$\text{Nonlinearity} = \frac{dI}{dV} \bigg/ \frac{I}{V} \quad (2.20)$$

2.6.3 Responsivity

The responsivity of a diode is a scale of how efficiently the diode can rectify. It is the curvature divided by the slope along any point on the (I-V) curve. The responsivity is calculated by equation (2.21):

$$\text{Responsivity} = \frac{dI^2}{dV^2} \bigg/ \frac{dI}{dV} \quad (2.21)$$

2.6.4 Resistivity

Classically, resistance or differential resistance (r_d) is obtained by differentiating the dark $I(V)$ curve. A low r_d is typically needed to impedance-match the diode to the antenna. This last feature makes it superior in high speed devices. The resistivity is calculated by the equation (2.22)

$$\text{Resistivity} = \frac{dV}{dI} \quad (2.22)$$

2.7 Electrical Modeling of MIM Diode

Figure (2.14) shows that the equivalent circuit of MIM diode is composed of junction resistor (R_j) and junction capacitance (C_j) are connected parallel. Both are connected in series with internal or series resistor (R_s).

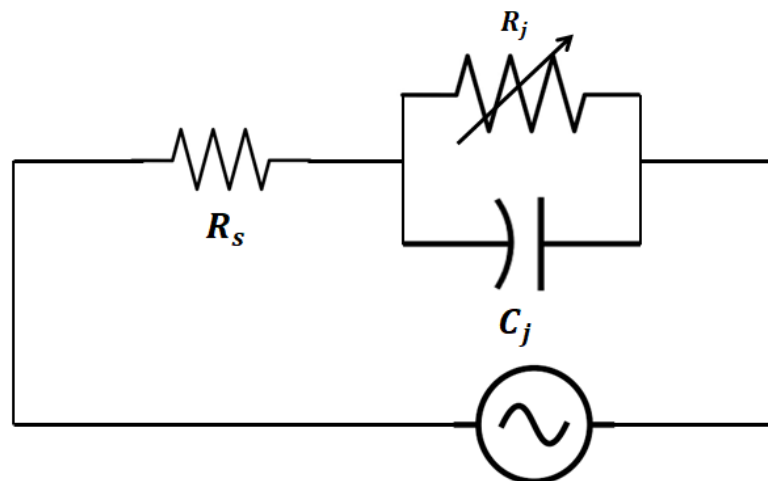


Figure (2.14) equivalent circuit of a MIM diode [65]

The equation (2.23) indicates the cut-off frequency:

$$f_c = \frac{1}{2\pi C_j R_j} \quad (2.23)$$

Where R_j is the overall resistance, C_j is the diode's capacitance, and f_c is the diode's cut-off frequency. One of the key elements for high-speed operation is the cut-off frequency, which represents the diode's maximum operating frequency. According to the equation above, C_j and R_j should be modest to raise the cut-off frequency of the MIM diode.

$$C_j = \frac{\epsilon_0 \epsilon_r A}{d} \quad (2.24)$$

This equation expresses the capacitance, where A is the contact area, d is the thickness of the insulator, ϵ_r is the relative dielectric constant, and ϵ_0 is the vacuum permittivity. According to the equation above, the contact area and insulator layer thicknesses, which may be changed by reducing the contact area A or increasing the thickness d , have a significant impact on the capacitance. Transmission probability (D) represented by equation (2.25)

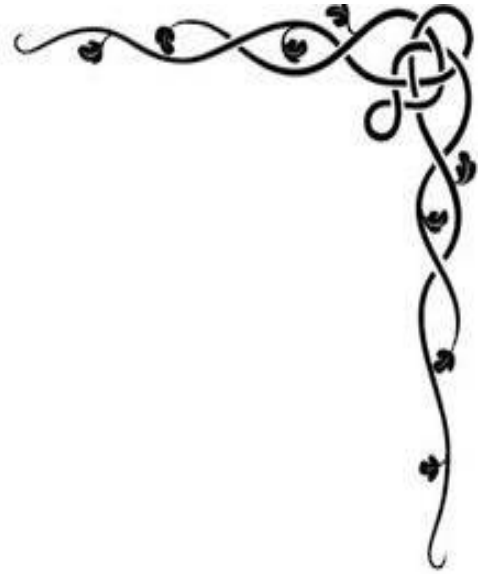
$$D = e^{-2d\sqrt{\frac{2m(V-E)}{h^2}}} \quad (2.25)$$

However, If the insulator layer's thickness is extended to 5 nm or higher and the diode's I-V curve becomes nonlinear, as indicated by the tunneling probability equation above, the chance of tunneling decreases significantly. Here, D stands for transmission probability, d for insulator layer thickness, m for electron mass, V for barrier height, and E for electron energy. This equation states that the thin insulator layer is what causes the high transmission probability. Therefore, the contact area A should be reduced to get a lower capacitance. Resistance has an impact on high-speed functioning as well; therefore it must be taken into account.

$$R_d = \rho \frac{L}{A} \quad (2.26)$$

L stands for length, A is contact area, the resistivity of material is $\rho = \frac{RA}{L}$.

We can create a small capacitance by lowering the contact area. However, the resistance shows that the high resistance is caused by the small contact area.



CHAPTER THREE
SIMULATION SOFTWARE



CHAPTER THREE

SIMULATION SOFTWARE

3.1 Introduction

The SILVACO TCAD software is a simulation package for semiconductor devices, which enables the simulation of the electrical characteristics of a specific structure. A semiconductor device's accuracy in simulation by the ATLAS is a very important feature for industry and research applications. The ATLAS simulation tool was created specifically for modeling in 2D and 3D based on the physics of semiconductor components, which include their electrical, thermal, and optical properties. After specifying size and dimension, ATLAS offers a library of materials that are preconfigured for creating any semiconductor device [66].

3.2 ATLAS Inputs and Outputs

The sorts of data that go into and out of ATLAS are depicted in Figure (3.1). Two input files are used by most ATLAS simulations. A text file serving as the first input file gives instructions for ATLAS to follow. A structure file that describes the structure that will be simulated is the second input file. Three different file types are produced by ATLAS. The run-time output is the first form of output file and it shows the simulation's progress along with any errors or warnings that may have occurred. The second type of output file is the log file, which contains all terminal voltages and currents from the device examination. The solution file, which contains values' 2D and 3D data, is the third type of output file.

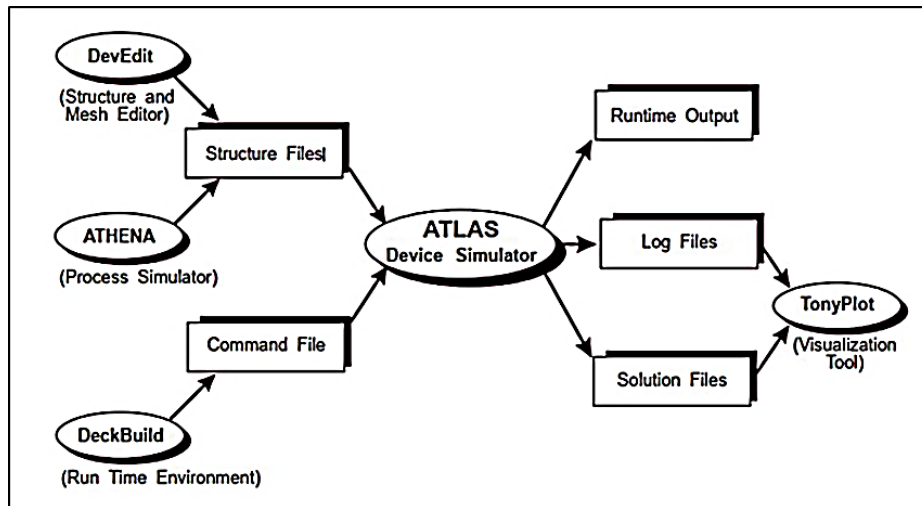


Figure (3.1) Atlas Inputs and Outputs [67]

3.3 Deck Build

The ".in" extension designates DeckBuild, the run-time environment used to enter a command file or deck. The user must first launch the ATLAS simulator using the following command to execute ATLAS in the DeckBuild environment:

<go atlas>

Other simulation tools like ATHENA and DevEdit may be utilized with DeckBuild, but ATLAS is the most suitable environment setting for this thesis. The main groupings of statements are shown in Figure (3.2). The disordering of this statements sequence will cause a program termination or produce erroneous results.

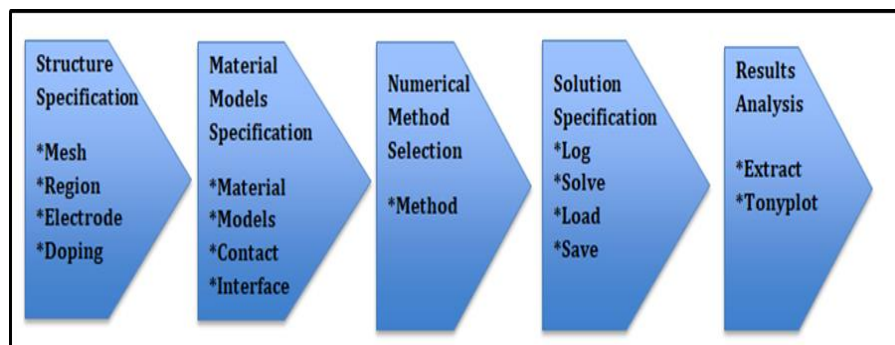


Figure (3.2) ATLAS Command Groups, each of which contains a primary statement

3.4 STRUCTURE SPECIFICATION

3.4.1 Mesh

The mesh declaration specifies the structure of an inverted 2D or 3D Cartesian grid. The x-axis is positive from left to right, the y-axis is negative from top to bottom, and the z-axis is positive from the plane of the x-y axis into the workspace. The y-axis is inverted because the manufacturing coordinates are often given as depth below the surface. The sharpness and precision at a particular place are adjusted using the spacing, and all coordinates are supplied in microns. Based on the user-input parameters, ATLAS generates a series of intersections to create the mesh. Figure (3.3) displays the parameters entered in ATLAS along with the mesh of a tunnel junction [68].

The first statement is defined as follows:

```
Mesh width=<Value>
```

This is followed by a series of x. mesh and y. mesh statements:

```
x. mesh    location=<value>    spacing=<value>
```

```
y. mesh    location=<value>    spacing=<value>
```

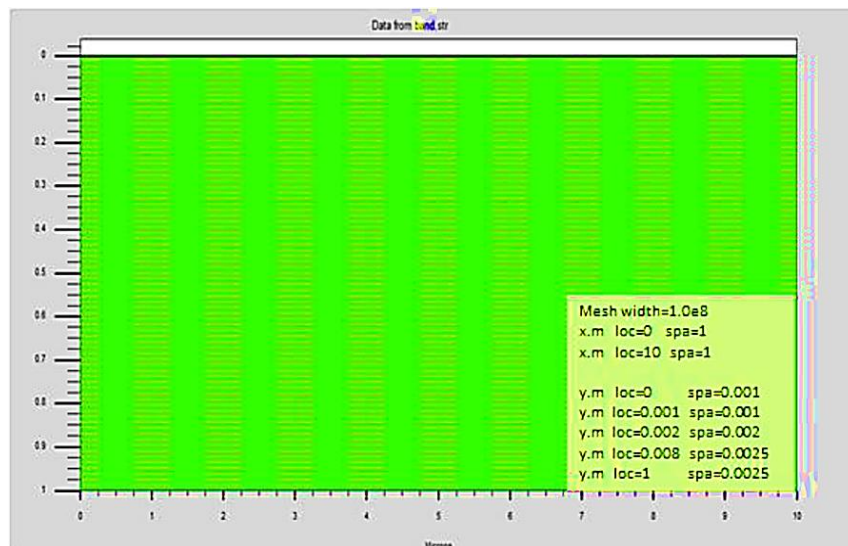


Figure (3.3) Mesh Creation using ATLAS Syntax

3.4.2 Region

The region statement establishes the primary material characteristics that may subsequently be identified by a region number and are utilized to divide the initial mesh statement into discrete blocks. A structure must allocate a region to every mesh area, in addition to the need that the regions are ordered from lowest to highest. Region 5 cannot be defined before Region 4. The region lines and Deck Build instructions in Figure (3.4) together describe the tunnel junction.

These Regions are defined as the following statements:

```
Region number=<integer> <material_ type> <position  
parameters>
```

```
Region num=1 material=Al2O3 x. min=0.0 y. min=0.0  
x. max=10 y.max=0.002 thick=0.002
```

```
Region num=2 material=silicon x. min=0.0 y. min=0.002  
x. max=10 y.max=1.0 thick=0.998
```

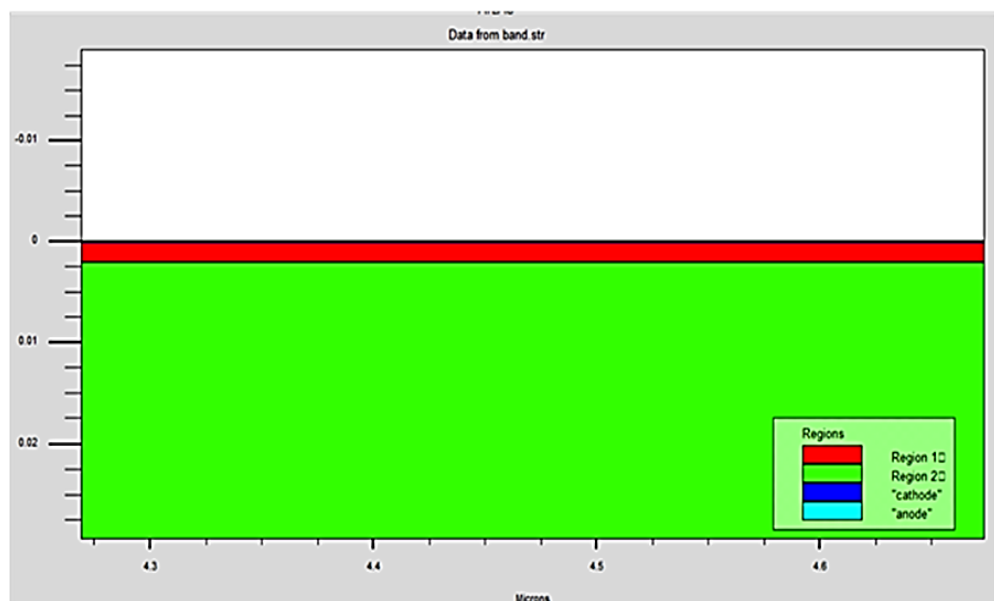


Figure (3.4) Tunnel Junction Region

3.4.3 Electrodes

Even though the Silvaco program allows for the specification of up to 50 electrodes, in this MIM diode configuration only the anode and cathode are needed [69]. These electrodes are defined as the following statements:

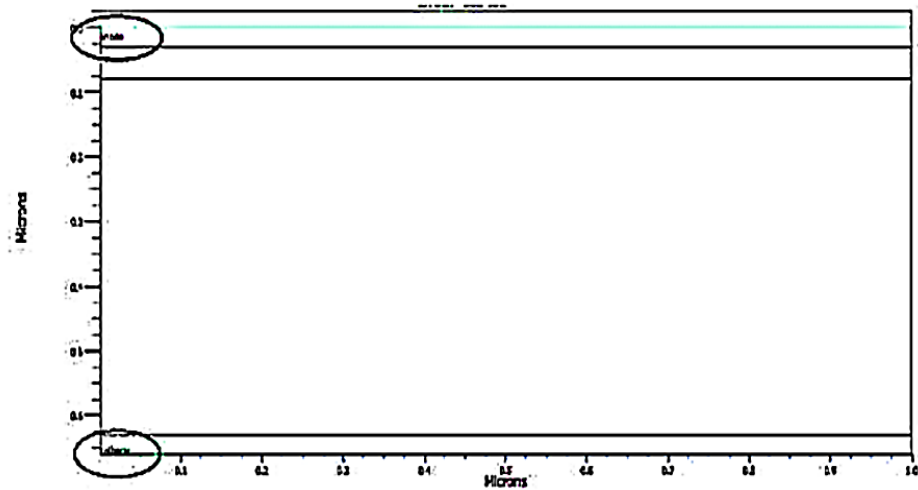


Figure (3.5) Electrodes of MIM diode

```
electrode name=cathode material=Al top
electrode name=anode material=Au bottom
```

3.4.4 QUANTUM TUNNELING MESH

The resolution of the junction is required to determine a hypothetical barrier's quantum tunneling by defining the **qtx.mesh** and **qty.mesh** commands, ATLAS achieves this. Additionally, a separate parameter must be used in the model's statement to specify the tunneling direction. The superior precise **qty.mesh** and the input parameters used to reach this level of precision are shown in Figure (3.6). Although the fact that the **qtx.mesh** has been specified, the slices are only very finely tuned in the y direction because this is where tunneling occurs. The old triangular mesh is placed over the new rectangular mesh, and the tunneling current will evaluate and take into account both mesh assertions. The **qty.mesh** spacing is specified like the other ATLAS spacing parameters.

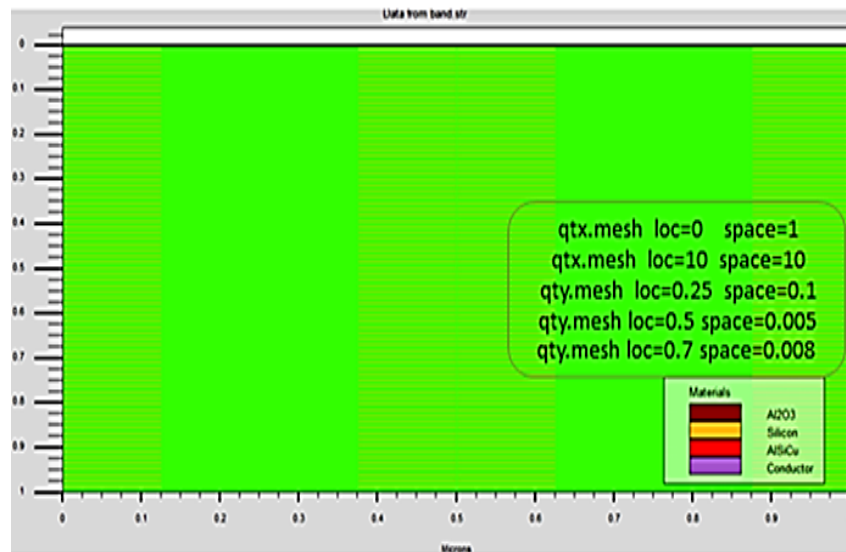


Figure (3.6) Quantum tunneling Mesh of MIM

3.5 MATERIAL MODELS SPECIFICATIONS

3.5.1 Material

When the structure of the devices has been fully completed, the statement of the material utilized to create the device must be described. The material statement permits the identification of several factors essential parameters, such as the type of the material and its characteristics (EG and Electron affinity).

The material is defined as the following statement:

```
Material material=Al2O3 EG300=8.7 affinity=1.35
```

Where (EG300) is the room temperature band-gap, χ : electron affinity of the insulator.

3.5.2 Models

The model's statement sets flags for ATLAS to signal the inclusion of several mathematical models, physical mechanisms, and other global characteristics like substrate temperature, which is crucial for the accurate modeling of a specific phenomenon [66]. The following is a list of the sample thesis and its criteria:

```
Models print conmob fldmob consrh qtnlsc.el qtnl.derivs
```

Where, conmob: standard-concentration dependent mobility model,
Consrh: Concentration Dependent, fldmob: Parallel Electric Field
Dependence, qtnsc.el: self-consistent of the quantum electron tunneling,
qtnl.derivs: non local derivatives into the system matrix to achieve a
converged solution.

3.5.3 Contact

Contact sets the features of the electrode. The statement of contact is as follows:

```
Contact number=<value> work function=<value>
```

The statement of contact in this thesis is:

```
Contact name=cathode work function=4.06
```

3.6 Numerical Method Selection:

Problems of semiconductor devices can be solved numerically using a variety of techniques. The METHOD statements of the input file contain numerical methods such as Gummel, Newton, and Block. The Gummel method solves for every unknown and retaining all other variables constant. The Newton method solves all unknowns concurrently. The Block method solves some of the equations by the Gummel method and solves others by using the Newton method [66].

This statement is defined as the following:

```
Method newton clim.dd=1e8 dvmax=0.1
```

climit or clim.dd specify minimal values of concentrations. dvmax: controls the maximum update of potential per iteration of Newton's method.

3.7 Solution Specification

Atlas simulations employ the log/solve/save instructions to produce data files.

3.7.1 Log

Using the log statement, all terminal characteristics generated by a solution statement can be stored in a file.

3.7.2 Solve

The bias points that should be used to generate output are specified in the solution statement. Depending on the desired stimulus, there are numerous ways to specify the bias points, including step, initial.

3.7.3 Save

All node point data is saved into an output file using the save statement.

Below is an example of how the log/solve/save commands are frequently used for the tunnel junction under study.

```
Solve init
```

```
Solve prev
```

```
log outfile=MIM.log j. hole j. electron j. tun
```

```
solve name=anode Vanode=-0.4 Vstep=0.01 Vfinal=0.5
```

```
solve name=anode Vanode=0.2 Vstep=0.05 Vfinal=0.4
```

3.8 Results Analysis

The data can be extracted and displayed graphically by Tonyplot, in addition devices parameters could be extracted.

```
Output band. param val. band con. band
```

```
Save outf=band. str
```

```
tonyplot band. str
```

```
tonyplot MIM.log -set MIM. Set
```

3.9 Introduction to the Advanced Design System (ADS) Software

The Path Wave Design branch of Keysight Technologies creates the Advanced Design System (ADS), a software program for electronic design automation. Its initial release surfaced in 1985 named-Microwave Design System (MDS). It was introduced in 2016 with improvement in its speed, performance and design flexibility. It gives designers of RF electronic products including mobile phones, pagers, wireless networks, satellite communication, radar systems, and high-speed data links access to an integrated design environment [70]. Keysight ADS support all design process, schematic capture, layout, design rule checking, frequency-domain and time-domain circuit, and electromagnetic field simulation.

3.9.1 MIM Diode Representation in ADS

Figure (3.7) illustrates the equivalent circuit of MIM diode. The MIM equivalent circuit is consisting of voltage dependent and independent components. $R_j(V_j)$ represents the voltage dependent nonlinear junction resistance of the diode, R_s denotes the series resistance, and C_j denotes the diode shunt junction capacitance. ADS topology was used to measured s-parameter data from the equivalent circuit model for data extracted from the Silvaco software.

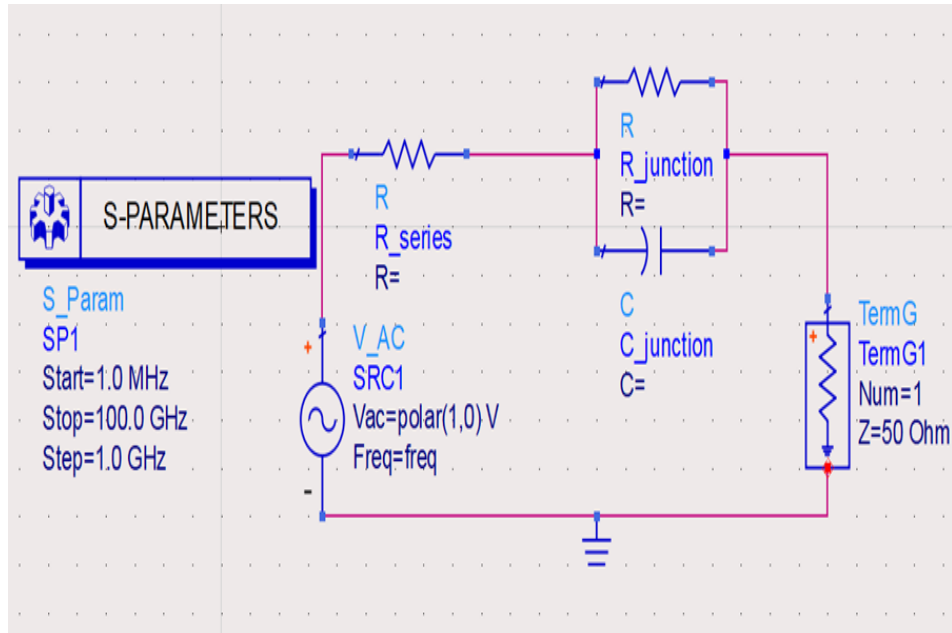


Figure (3.7) equivalent circuit of MIM diode in ADS software



CHAPTER FOUR
SIMULATION RESULTS AND DISCUSSION



CHAPTER FOUR

Simulation Results and Discussion

4.1 Introduction

According to classical mechanics, if a particle's energy is lower than the potential barrier, it cannot pass through it. A particle in quantum mechanics has a probability of tunneling through the potential barrier. This chance is known as the tunneling probability. The operation of MIM diodes can be explained in terms of quantum physics. The probability of tunneling is determined by the thickness of the insulators and the work functions of the metals [71]. As we mentioned previously in Chapter 2, the current is greatly reliant on the tunneling probability. In this dissertation, the parameters that should be taken into consideration before simulating a MIM diode and their influence on the performance are studied, such as the material type of the electrodes, the thickness of the insulator layer, considering the effects of altering barrier heights through the disparity between the work function (ϕ)eV of metals and the insulator's electron affinity(χ) eV, ($\Delta\phi=\phi - \chi$). In this chapter, we studied the impact of physical parameters by using different structures, such as the use of metals with different working functions to achieve variation in barrier heights, the effect of using different thicknesses of insulators, and the use of different insulators to study the effect of band gap variation.

4.2 Influence of Using Symmetric and Asymmetric Electrodes:

The MIM diode is simulated with different structures at standard conditions. The first structure involved setting a fixed material where Aluminum is used as a metal on both sides as (cathode and anode) with work function (4.26 eV) for the MIM structure. Aluminum oxide (Al_2O_3) with an electron affinity of 1.35 eV is used as an insulator layer [72]. The thickness of this layer is fixed at 2 nm. To achieve the electrodes dissimilarity in the second structure used the metal aluminum with a work

function of (4.02eV) as the reference cathode on the left side of MIM structure, while the gold is used as the reference anode on the right side of MIM structure with the same thickness of insulator also the same type of insulator used in the first structure. These two structures (Al-Al₂O₃-Al and Al-Al₂O₃-Au) have been fabricated by Su Jin Heo (2018) [73] and their results are compared with simulation results carried out by Silvaco in this thesis. Table (4.1) summarized the parameters of these structures.

Table (4.1) The Structures of Symmetric and Asymmetric MIM diode [74,75]:

<i>Structures</i>	φ_C eV	φ_A eV	EA eV	Plane _C	Plane _A
Al-Al ₂ O ₃ -Al	4.26	4.26	1.35	111	111
Al-Al ₂ O ₃ -Au	4.02	5.31	1.35	110	111

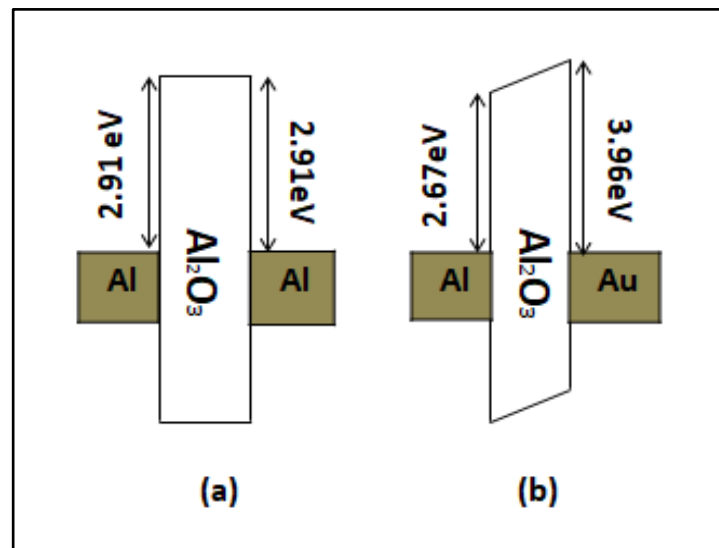


Figure (4.1) proposed Structures of the MIM diode with (a) Symmetric electrodes, (b) Asymmetric electrodes

Simulated I-V characteristics are plotted in the voltage range -0.4V to 0.4V. The crucial parameters extracted from the IV simulated data, such as asymmetry (f_{Asym}), nonlinearity (f_{NL}), responsivity (f_{Res}), and resistivity. In order to check the impact of each of these parameters on the overall performance, it is suggested to adopt a figure of merit (FOM) formula as

represented in equation (4.1). These parameters are extracted from I-V curve for studying the impact of the barrier height by using similar and dissimilar electrodes on the MIM diode performance. Figure (4.2) shows a set of I-V for the structures that are summarized in Table (4.1), where it seems that the I-V curve strongly depends on the work function difference of the metals of the MIM structure, since the structures that have a difference between the left and right work functions produce a large forward current with lower turn-on voltage (TOV). The value (TOV) represents the forward voltage of a semiconductor diode. It acts as the required voltage across the diode before it starts to conduct current in the forward direction. It can be noticed in Figure (4.2) that the asymmetric structure produces a large forward current, to introduce a forward bias. The tunneling distance decreases as the energy increases. According to the FN tunneling mechanism, the barrier is thinner, allowing electrons to more readily pass through the triangular barrier and produce the tunneling effect. Conversely, the reversed biased current increases for symmetric structure, with low forward current. This result indicated that symmetric MIM diode behaves as an open circuit not as a rectifier diode. These results agree with the results represented by the researcher Su Jin Heo (2018)[73], which clearly show that the rectification increases when using asymmetric electrodes at MIM diode design.

$$\text{FOM Factor} = \frac{f_{(\text{ASYM})} * f_{(\text{NL})} * f_{(\text{Res})}}{f_{(\text{Resistivity})}} \quad (4.1)$$

Table (4.2) Parameters Extracted at Zero Bias of MIM diodes:

Parameters	Symmetric Electrodes	Asymmetric Electrodes
Asymmetry ($\eta = \frac{I_F}{I_R}$)	0.9	8.7
Nonlinearity ($\frac{dI/dV}{I/V}$)	0.9	1.3
R_D [$M\Omega$]	20	2.3
Responsivity [A/W]	5.5	10.5
Figures of Merit(FOM)	0.22275	47.502

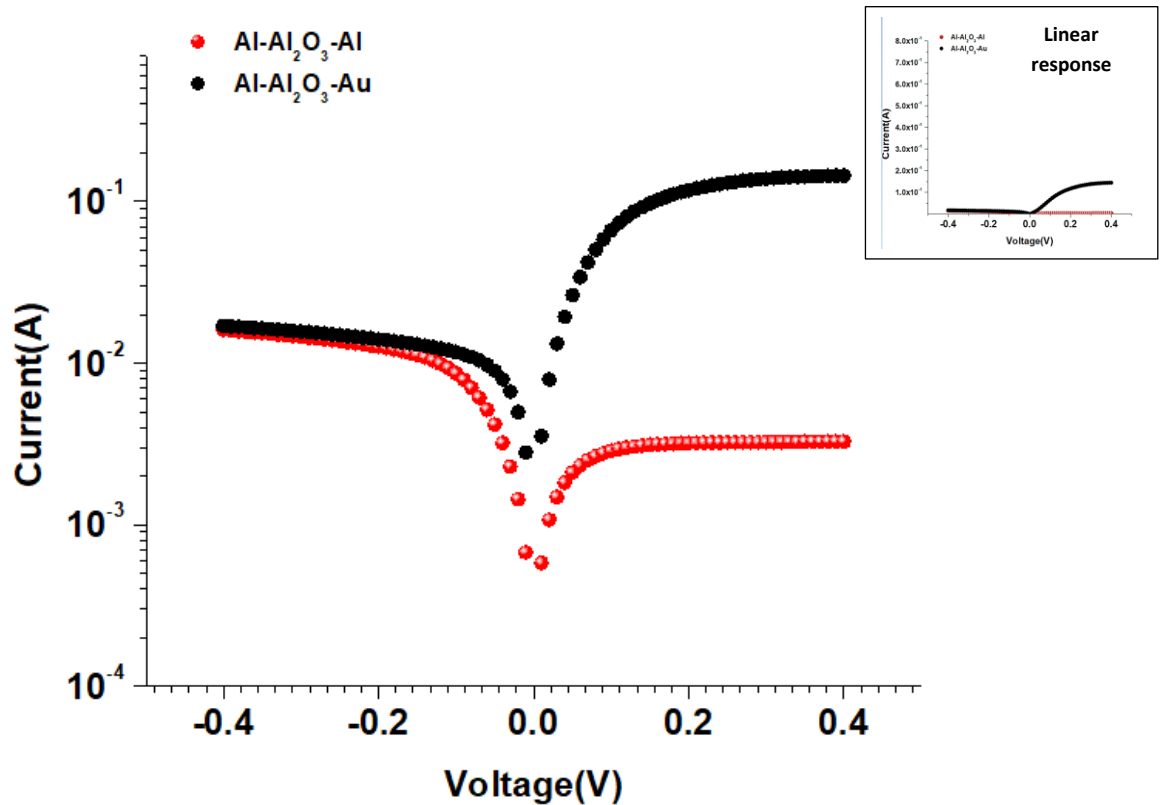


Figure (4.2) I-V characteristics curve for symmetric (Al-Al₂O₃-Al) and asymmetric (Al-Al₂O₃-Au) MIM diode

For rectification, a diode's asymmetry value needs to be higher than 1. The asymmetry value of the Al-Al₂O₃-Al structure is dropped steadily from 1 to approach 0 at biasing voltage equal to 0.25 V, which is undesirable for a diode, as shown in Figure 4.3(a). The asymmetry value of the Al-Al₂O₃-Au structure does, however, approach 9 at +0.25 V. Thus, it is demonstrated that the varied work functions of the metals have a significant impact on the asymmetry of MIM diodes. Figure 4.3(b) shows the f_{NL} for MIM structures that are summarized in Table (4.1). This Figure exhibits the nonlinearity. It can be seen that the nonlinearity values decrease for the two structures reach to 0.4 at 0.25 V for Al-Al₂O₃-Au while reaching 0 for Al-Al₂O₃-Al respectively. It can be seen that the MIM structure both of similar and dissimilar structures produces a weak nonlinearity. Since the nonlinearity of the diode defines the sensitivity of the MIM diode. The sensitivity of the MIM structure with electrodes' dissimilarity and similarity under the condition shown in Figure 4.3 (b) is weak, which decreased when the bias voltage increased. Figures 4.3 (c) and (d) show, respectively, the resistivity, and responsivity, for the symmetric and asymmetric structures. It can be noticed that the resistivity is almost stable and has a low value for the asymmetric MIM diode, whereas it increases in the symmetric MIM diode. In contrast, the responsivity is increased for Al-Al₂O₃-Au MIM diode reaching to 10 A/W at zero volts, and decreases in Al-Al₂O₃-Al and show negative response. From these results it can be conclude that the figures of merit (FOM) reveals a higher performance of the (Al-Al₂O₃-Au) MIM diode structure compared with the (Al-Al₂O₃-Al) MIM diode as summarized in Table (4.2). These results indicated that the structure (Al-Al₂O₃-Au) may be useful in the rectification purposes.

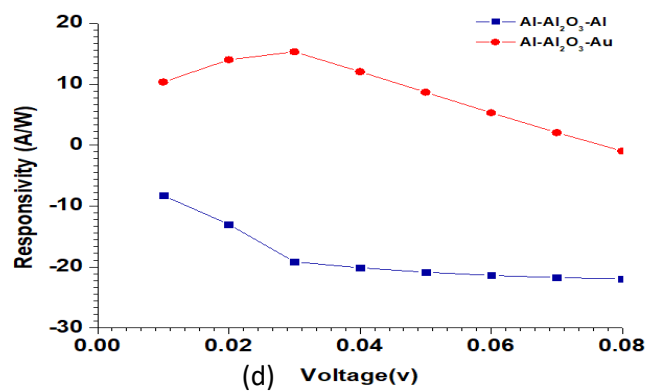
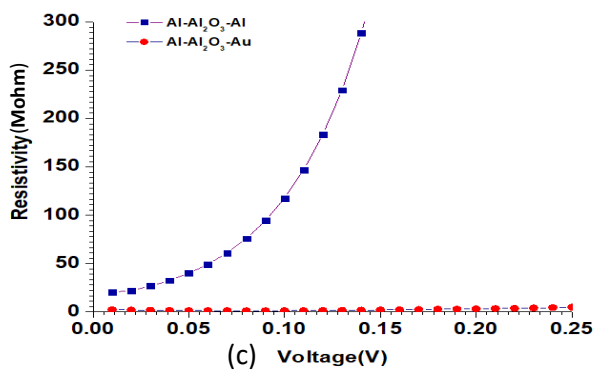
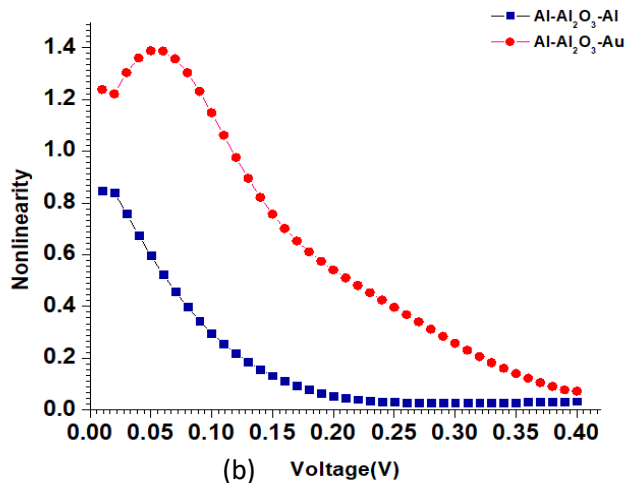
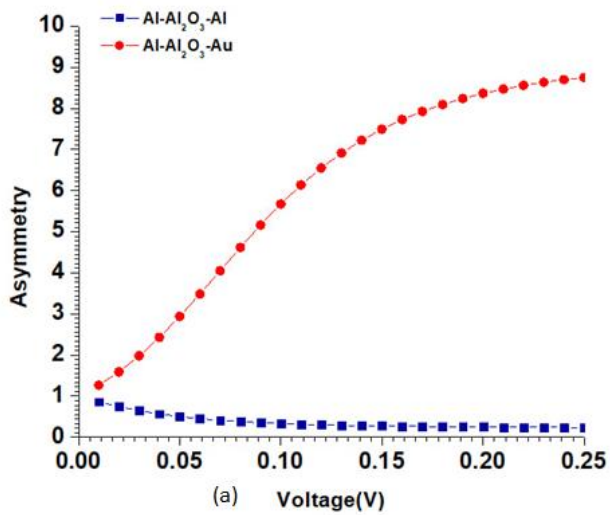


Figure (4.3) a) Asymmetry, b) Nonlinearity, c) Resistivity and d) Responsivity of symmetric and asymmetric MIM diode

4.3 Influence the Barrier Heights on the Performance of MIM diode for Dissimilar Electrodes:

In this section, the asymmetric MIM diode was simulated, at standard conditions, with different structures to investigate the impact of barrier height on the electrical properties of the MIM diode. These structures are categorized as follows:

4.3.1 Impact the Barrier Heights variation from the anode side:

The structure involved setting a fixed insulator material and a metal on one side cathode of the MIM structure. Aluminum oxide (Al_2O_3) with an electron affinity of 1.35 eV was used as an insulator layer. The thickness of this layer was fixed at 2 nm. To achieve the electrode's dissimilarity, one metal (aluminum with a work function of 4.06 eV) was used as a reference cathode on the left side of the MIM structure. This metal will produce a constant barrier height with an insulator with $\phi_c=2.71$ eV. At the right side of the MIM structure, different metals were employed individually as anodes with diverse work functions. These metals are Cd, Ag, Co, Au, and Pt with work functions 4.08, 4.65, 5.0, 5.31, and 5.65 eV, respectively. As shown in figure (4.4), the asymmetric barrier heights between the metals at the sides of the MIM structure allow tuning electrode dissimilarity. Table (4.3) summarizes the parameters of the aforementioned structures.

Table (4.3) The structures of MIM diodes with fixed cathode metal [74,75]

Structures	φ_C eV	φ_A eV	$\Delta\varphi_m$ eV
Al-Al ₂ O ₃ -Cd	4.06	4.08	0.02
Al-Al ₂ O ₃ -Ag	4.06	4.65	0.59
Al-Al ₂ O ₃ -Co	4.06	5.0	0.94
Al-Al ₂ O ₃ -Au	4.06	5.31	1.25
Al-Al ₂ O ₃ -Pt	4.06	5.65	1.59

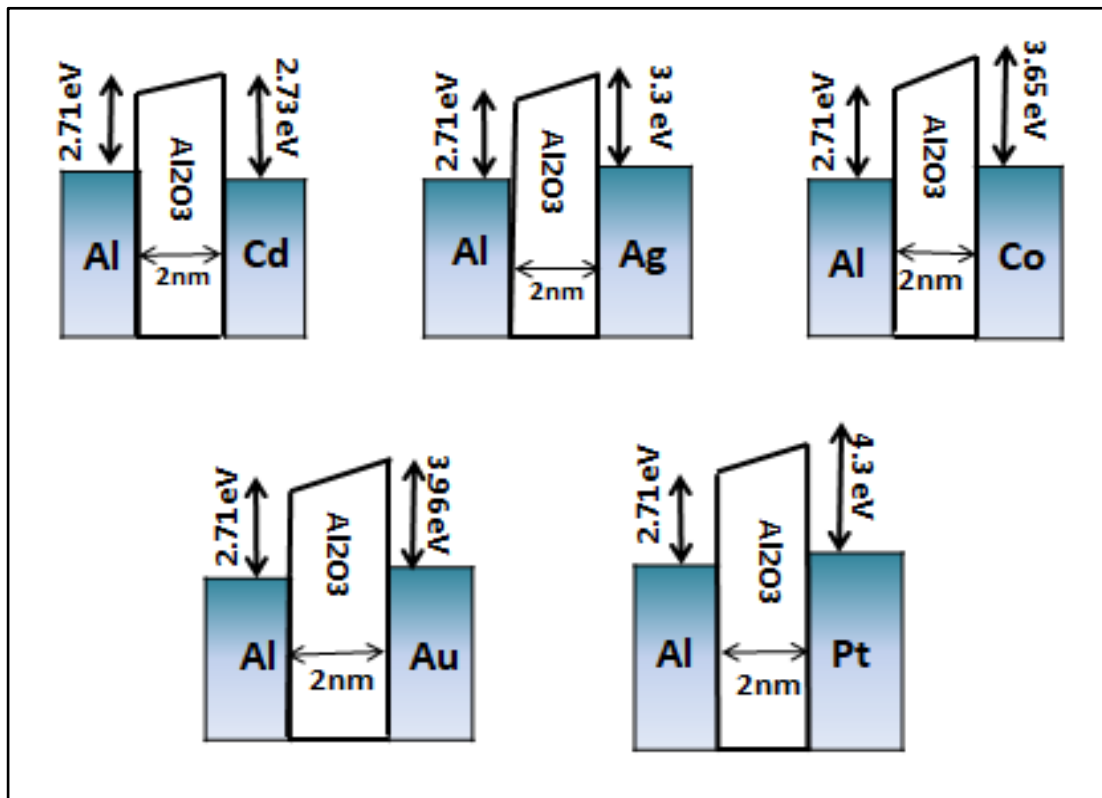


Figure (4.4) Energy band diagram for fixed cathode metal MIM diode

Figure (4.5) presents a set of I-V curves for the structures that produce electrode dissimilarity with a fixed cathode metal and different anode metals. The electrodes dissimilarity varied from 0.02 eV to 1.59 eV as illustrated in Table (4.3). Figure (4.5) reveals the asymmetric in the diode current due to the asymmetry in the MIM potential. It can be seen that the change in the work function of the anode by using different metals does not produce much difference in the tunneling current. This can be attributed to the fact that in the case of dissimilar metals, the current-voltage characteristics depend not only on the bias voltage but also on the polarity of the voltage. Conventionally, if the metal with the lower work function is positively biased and the metal with the higher work function is negatively biased, the MIM junction is said to be forward-biased. When the lower work function metal is negatively biased it is reverse biased [76]. Figure (4.5) also reveals that all the devices have a low turn-on voltage of around <0.1 V with a noteworthy asymmetric and nonlinear response under positive bias.

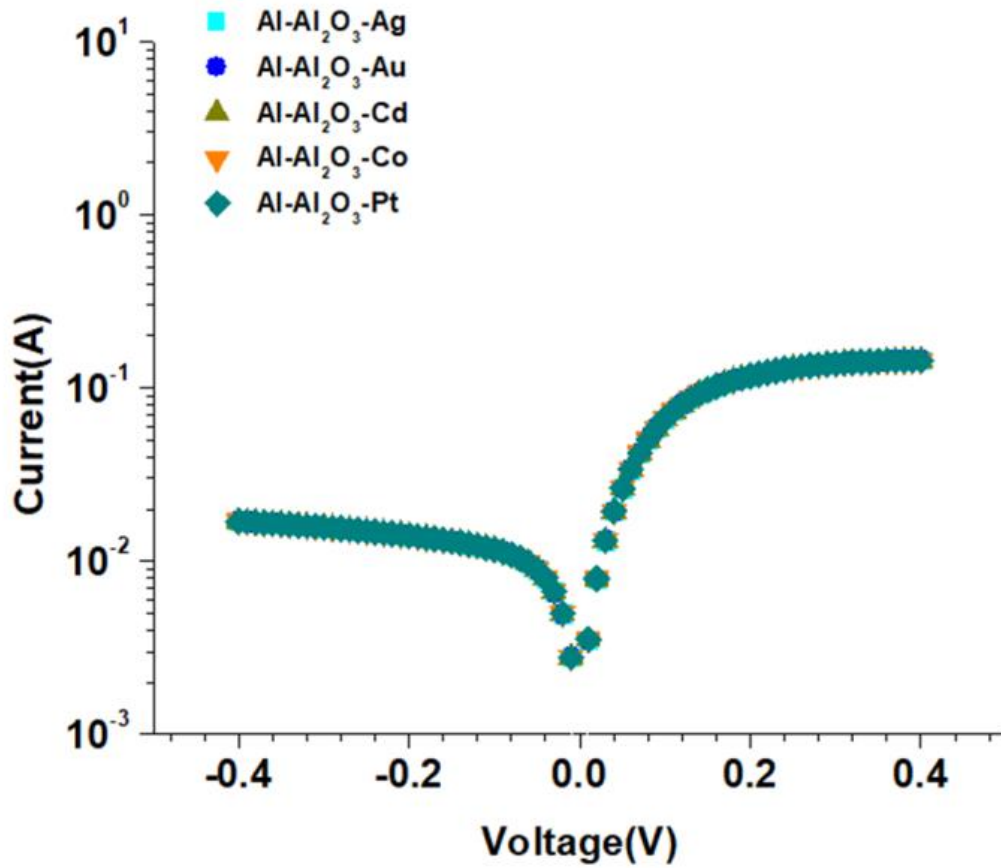


Figure (4.5) I-V characteristics curve for fixed cathode metal MIM diode

Table (4.4) Parameters Extracted at Zero Bias of MIM diode:

Parameters	Higher Difference for electrodes (Al-Al ₂ O ₃ -Pt)	Lower Difference for electrodes(Al-Al ₂ O ₃ -Cd)
Asymmetry ($\eta=I_F/I_R$)	2	2
Nonlinearity ($\frac{dI/dV}{I/V}$)	1.3	1.3
$R_D [M\Omega]$	2	2
Responsivity (A/W)	10	10
Figures of Merit (FOM)	13	13

Figure (4.6) (a) and (b) show respectively the f_{ASYM} and f_{NL} for MIM structures that are summarized in Table (4.3). These figures exhibit asymmetry and nonlinearity values of ~ 8 A/W and ~ 1.5 , respectively. It can be seen that the MIM structure with electrodes dissimilar and fixed cathode produces a good asymmetry with poor nonlinearity. Since the nonlinearity of the diode defines the sensitivity of the MIM diode, the sensitivity of the MIM structure with electrodes' dissimilarity under the condition shown in Figure 4.6(b) is weak. Whereas the responsivity and the resistivity reach 10A/W, and 2 M Ω respectively at zero volts, as shown in Figure 4.6 (c) and (d), after theoretical calculations for Figures of merit (FOM) have been illustrated, reached 13 for all structures as shown in Table (4.4).

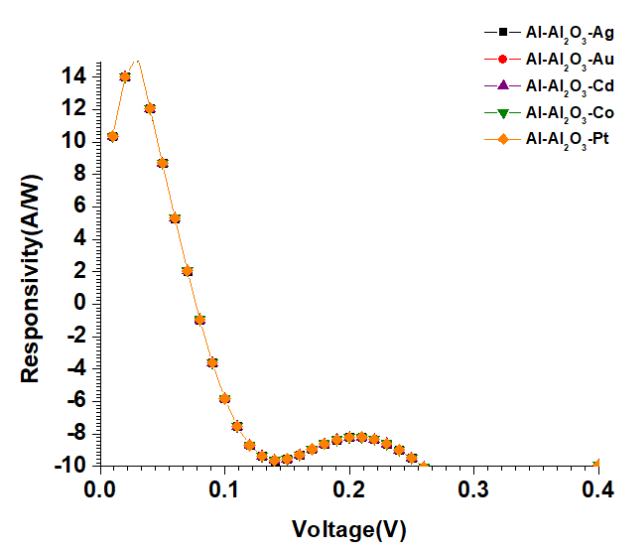
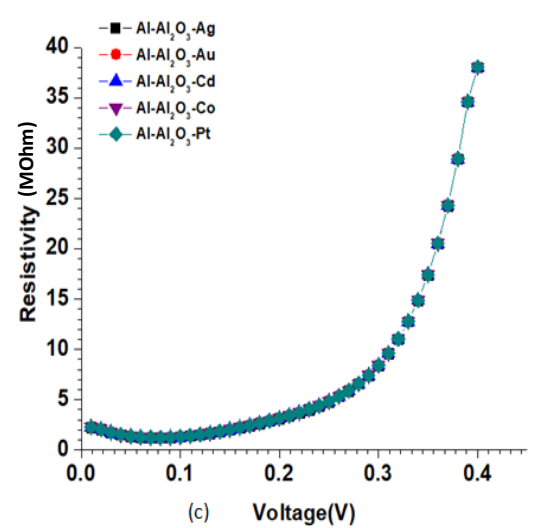
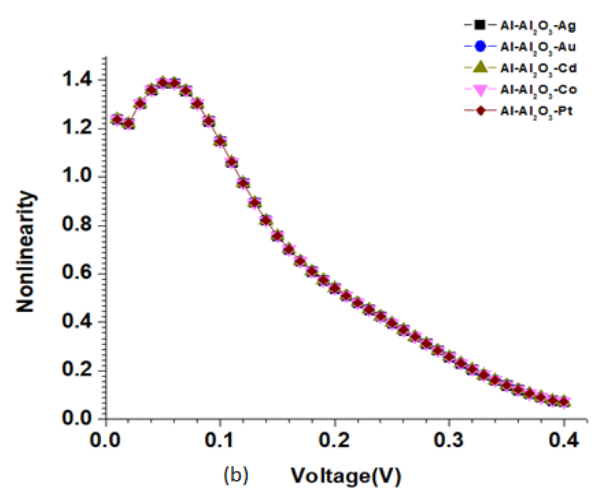
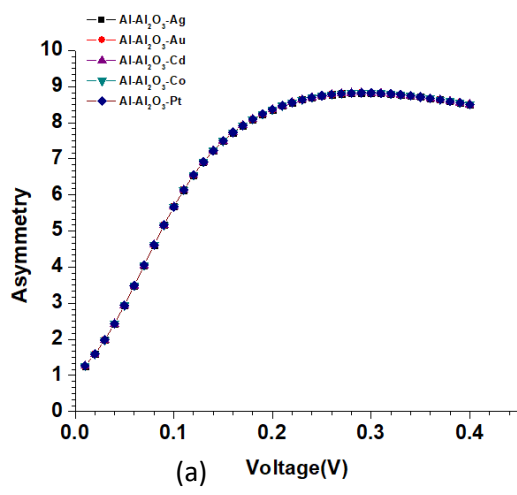


Figure (4.6) a) Asymmetry, b) Nonlinearity c) Resistivity, and, d) Responsivity for fixed cathode metal MIM diode

4.3.2 Impact the Barrier Heights variation from the cathode side:

The following structures of the MIM diode which are shown in figure (4.7) comprised setting a fixed insulator material of the previous case and metal on one side (anode) of the MIM structure. In contrast, the metal on the other side (cathode) was individually changed to achieve the electrode's dissimilarity. In this case, Ni with a work function of 5.22 eV was used as the anode while the cathode materials were Ba, Ta, La, Zn, and Nb with a work function of 2.52, 3, 3.5, 3.63, and 3.95 eV respectively. The Ni produces a constant barrier height with an insulator with $\phi_A=3.87$ eV. Table (4.5) summarizes the parameters of these structures.

Table (4.5) The structures of MIM diodes with fixed anode metal [74,75]

<i>Structures</i>	<i>ϕ_C eV</i>	<i>ϕ_A eV</i>	<i>$\Delta\phi_m$ eV</i>
Ba-Al ₂ O ₃ -Ni	2.52	5.22	2.7
Ta-Al ₂ O ₃ -Ni	3.0	5.22	2.22
La-Al ₂ O ₃ -Ni	3.5	5.22	1.72
Zn-Al ₂ O ₃ -Ni	3.63	5.22	1.59
Nb-Al ₂ O ₃ -Ni	3.95	5.22	1.27

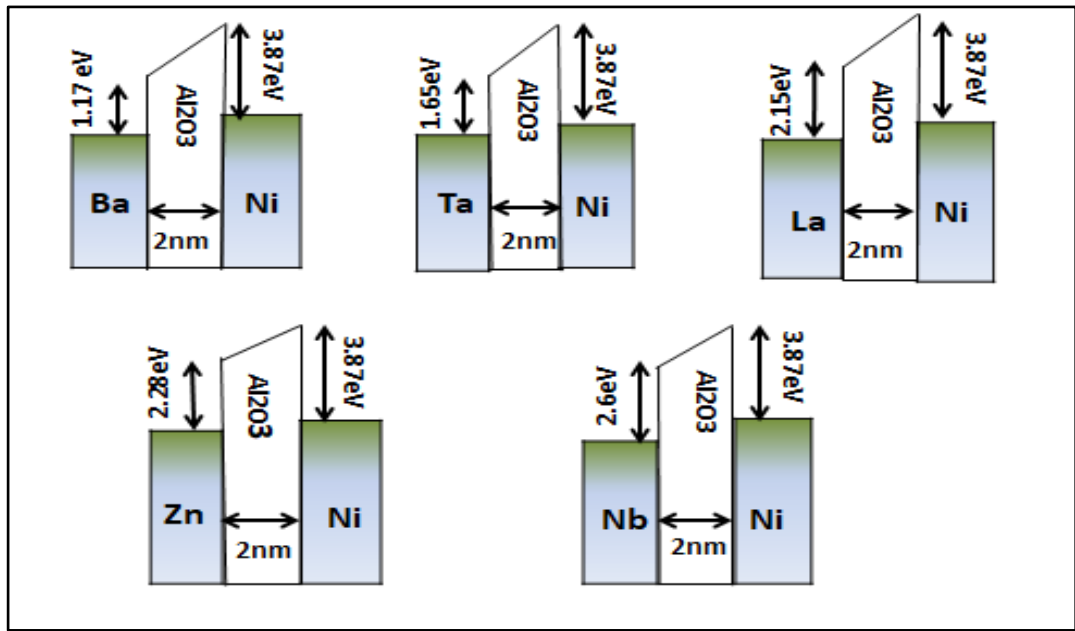


Figure (4.7) energy band diagram for fixed anode metal MIM diode

Figure (4.8) shows a set of I-V curves for the structures that are summarized in Table (4.5). At first glance, it seems that the I-V curve depends strongly on the work function difference of the metals of the MIM structure, i.e., $\Delta\phi = (\phi_C - \phi_A)$, where the structures that have a large difference between the left and right work functions produce a large forward current with a lower low turn-on voltage. It can be noticed in Figure (4.8) that the forward current increases ~ 20 times when $\Delta\phi$ increases from 1.27 to 2.7 eV while the reversed biased current is almost unaffected with $\Delta\phi$ variation. By comparing these results with the results of the previous case it can be deduced that the MIM diode forward current is strongly dependent on the barrier height at the interface between the cathode and insulator. The Nb/Al₂O₃ and Al₂O₃/Ni interfaces have high barrier heights that limit electron transit until a bias voltage on the order of the barrier height is applied. Such bias voltage resulting an electric field across the insulator enough to breakdown the insulator as reported in [77].

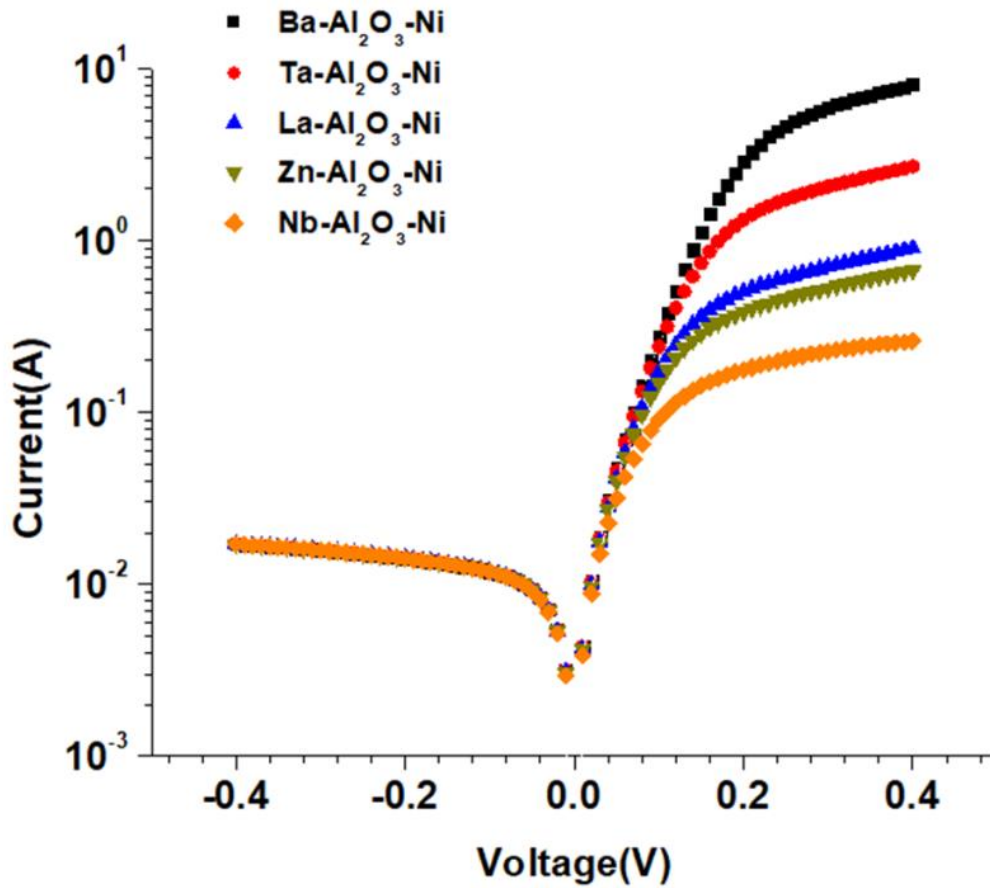


Figure (4.8) I-V characteristics for fixed anode metal MIM diode

Table (4.6) Parameters Extracted at Zero Bias of MIM diode:

Parameters	Ba-Al ₂ O ₃ -Ni	Ta-Al ₂ O ₃ -Ni	La-Al ₂ O ₃ -Ni	Zn-Al ₂ O ₃ -Ni	Nb-Al ₂ O ₃ -Ni
Asymmetry ($\eta = \frac{I_F}{I_R}$)	1.39	1.37	1.36	1.35	1.2
Nonlinearity ($\frac{dI/dV}{I/V}$)	1.5	1.4	1.35	1.33	1.25
$R_D [M\Omega]$	1.7	1.7	1.8	1.8	2.1
Responsivity (A/W)	19.6	19.1	17.4	17	13
Figures of Merit(FOM)	24.03	21.54	17.7	16.9	9.3

Figures (4.9) (a), (b),(c), and (d) show, respectively the responses of the MIM diode structure that are given in Table (4.5). It can be seen that the Ba-Al₂O₃-Ni diode exhibits maximum asymmetry and non-linearity. These findings agree with the hypothesis that states the minimum turn-on voltage and maximum asymmetry and non-linearity are achieved when the electron affinity of the insulator would be close to one of the metal work function values to produce a low barrier height [78]. It can also be noticed that the nonlinearity has been enhanced for the Ba-Al₂O₃-Ni MIM diode, where this structure gives higher responsivity with lower resistivity, since these features, made it suitable more than other structures for MIM diode design. To compare the figures of merit for two structures (Ba-Al₂O₃-Ni) and (Nb-Al₂O₃-Ni) that have higher and lower difference in work functions between anode and cathode metals as shown in Table (4.6), results of the figures of merit indicated that the structure(Ba-Al₂O₃-Ni) have large difference between the anode and cathode metals gives higher figures of merit. Since this structure has efficient performance, it can be more suitable for MIM diode design than other structures.

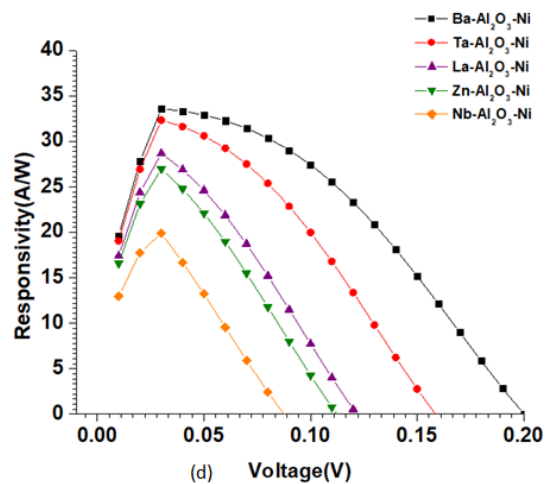
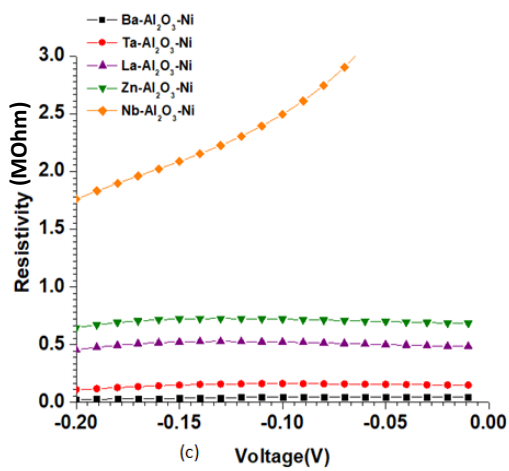
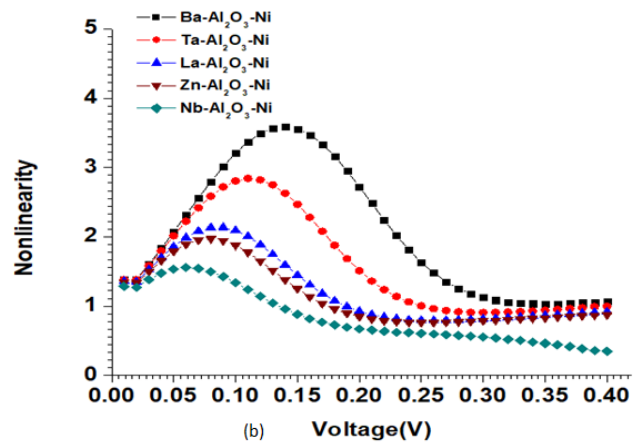
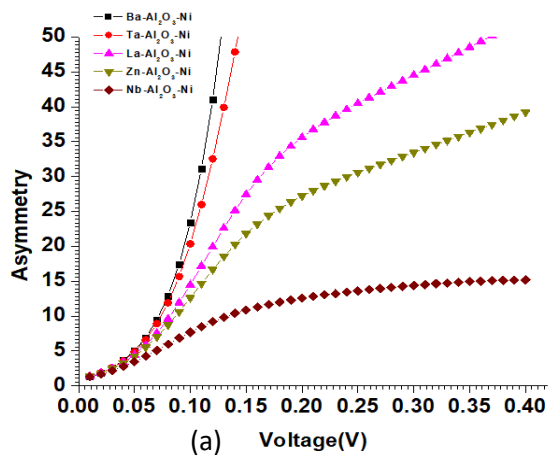


Figure (4.9) a) Asymmetry, b) Nonlinearity, c) Resistivity, and d) Responsivity for fixed anode metal MIM diode

- **Impact the difference in work functions on the Performance of MIM diode**

This section shows the simulation results for the impact of the work function difference on the MIM diode performance, as shown in Figure (4.10) (a), (b), (c) , and (d) ; Hashem et al [79] demonstrated that metal work function difference has a positive influence on the diode FOM. Deposited structures as shown in Table (4.5) with respect to work functions were simulated, effectively sweeping the work function difference between the two contacts($\varphi_C - \varphi_A$), from 1.27 eV to 2.7 eV. The results of the simulation illustrate that the asymmetry is unaffected with increasing the work functions difference, whereas the nonlinearity increased when the work functions difference increase as shown in the Figure (4.10) (a) and (b). Same parameters as shown in Table (4.5), the differential resistance shows the decreases as the ($\varphi_C - \varphi_A$) is work functions difference increased. This is strongly required to make the matching possible. The responsivity will also be increased when the work function difference increased as shown in Figure (4.10) (c). This led to concluded enhancing the figures of merit by increasing the work functions difference between anode and cathode metals for MIM diodes design. It is worth mentioning here that it is recommended to use metals that have large work functions difference to lead to an enhancement of the MIM diode performance.

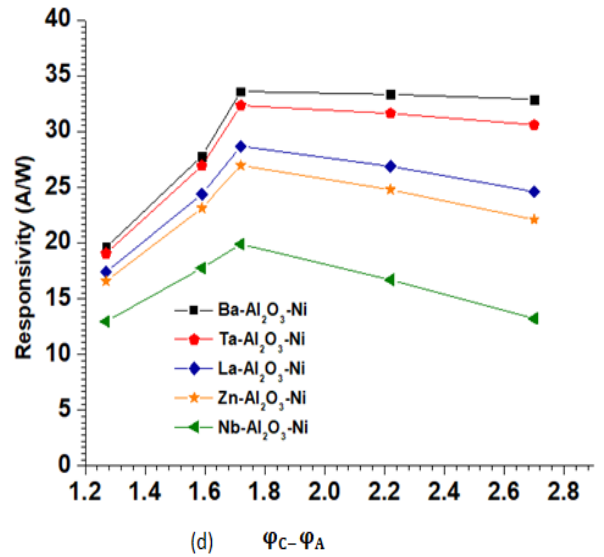
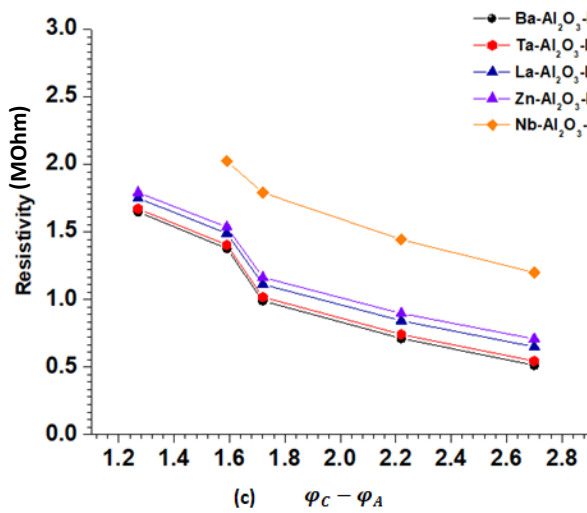
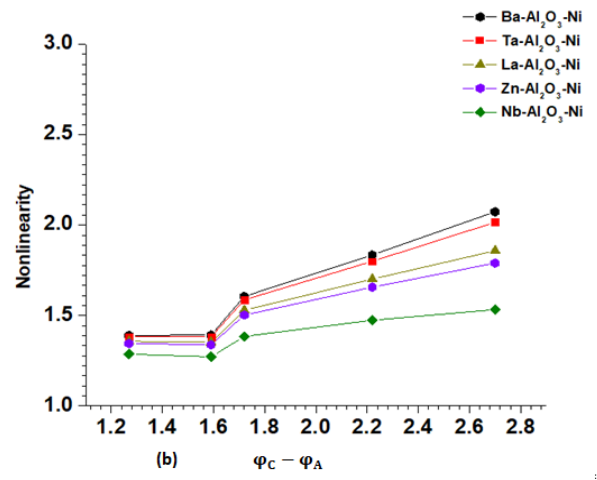
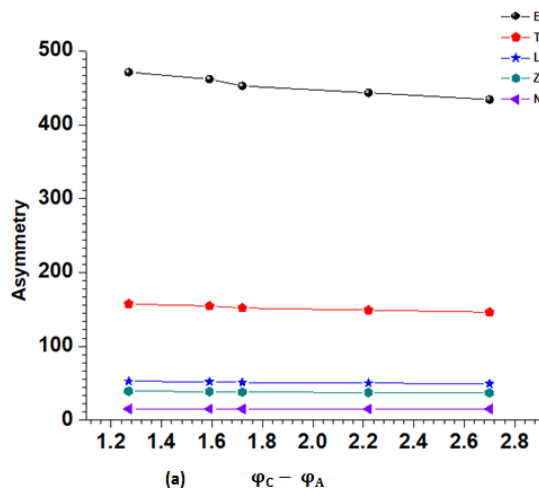


Figure (4.10) a) Asymmetry b) Nonlinearity c) Resistivity and d) Responsivity as a function of increasing work functions difference ($\phi_c - \phi_A$)

4.3.3 Impact the Barrier Heights variation with a fixed barrier difference:

To investigate the impact of the barrier height variation on the MIM performance using Al_2O_3 as an insulator, different metals, with constant work function differences $\Delta\phi$, were chosen on the both sides of the MIM diode as shown in Figure (4.11). In this case, the individual metal pairs used on both sides of the Al_2O_3 insulator material are (Ba and Ag), (Ta and Cu), (La and Pt), (Zn and Ir), and (Nb and Pt). These metals provide a constant barrier potential $\Delta\phi_m=2.1$ eV with different barrier heights. Table (4.7) summarized the parameters of these structures.

Table (4.7) The structures of MIM diodes with constant barrier potential [74,75]

<i>Structures</i>	<i>ϕ_C eV</i>	<i>ϕ_A eV</i>	<i>$\Delta\phi_m$ eV</i>
Ba- Al_2O_3 -Ag	2.5	4.6	2.1
Ta- Al_2O_3 -Cu	3.0	5.1	2.1
La- Al_2O_3 -Pt	3.5	5.6	2.1
Zn- Al_2O_3 -Ir	3.6	5.7	2.1
Nb- Al_2O_3 -Pt	3.9	5.99	2.1

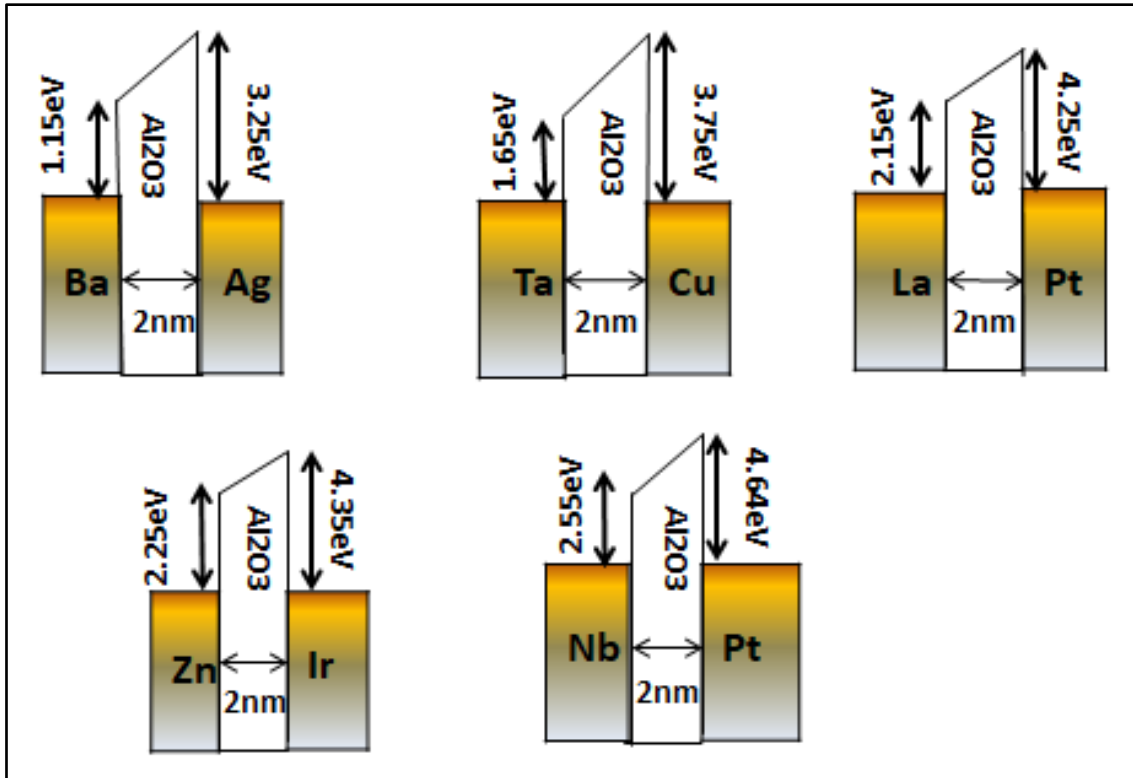


Figure (4.11) energy band diagram for constant barrier potential MIM diode

The set of the chosen metals produces a work function difference between each metal pairs of 2.1 eV. The used metals as cathode, individually, are Ba, Ta, La, Zn, and Nb which produce barrier heights of 1.15, 1.65, 2.15, 2.25, and 2.55 eV, respectively. At the same time, the corresponding anode metals are Ag, Cu, Pt, Ir, and Pt, producing barrier height from the anode interface side of 3.25, 3.75, 4.25, 4.35, and 4.64 eV respectively. Band diagrams of these MIM structures are shown in Figure (4.11) and are based on the properties of the materials tabulated in Table (4.7). Figure (4.12) shows the I-V curves of the aforementioned MIM structures. Although these structures produce a fixed work function difference but Figure (4.12) reveals that the I-V responses of the diodes are qualitatively related to the barrier height. The smaller barrier height, the larger the current response and the lower turn on voltage. This can be explained by the fact that the electrodes' low energy barriers enable thermally activated conduction

mechanisms such as Schottky emission (SE) to be effective at room temperature [80].

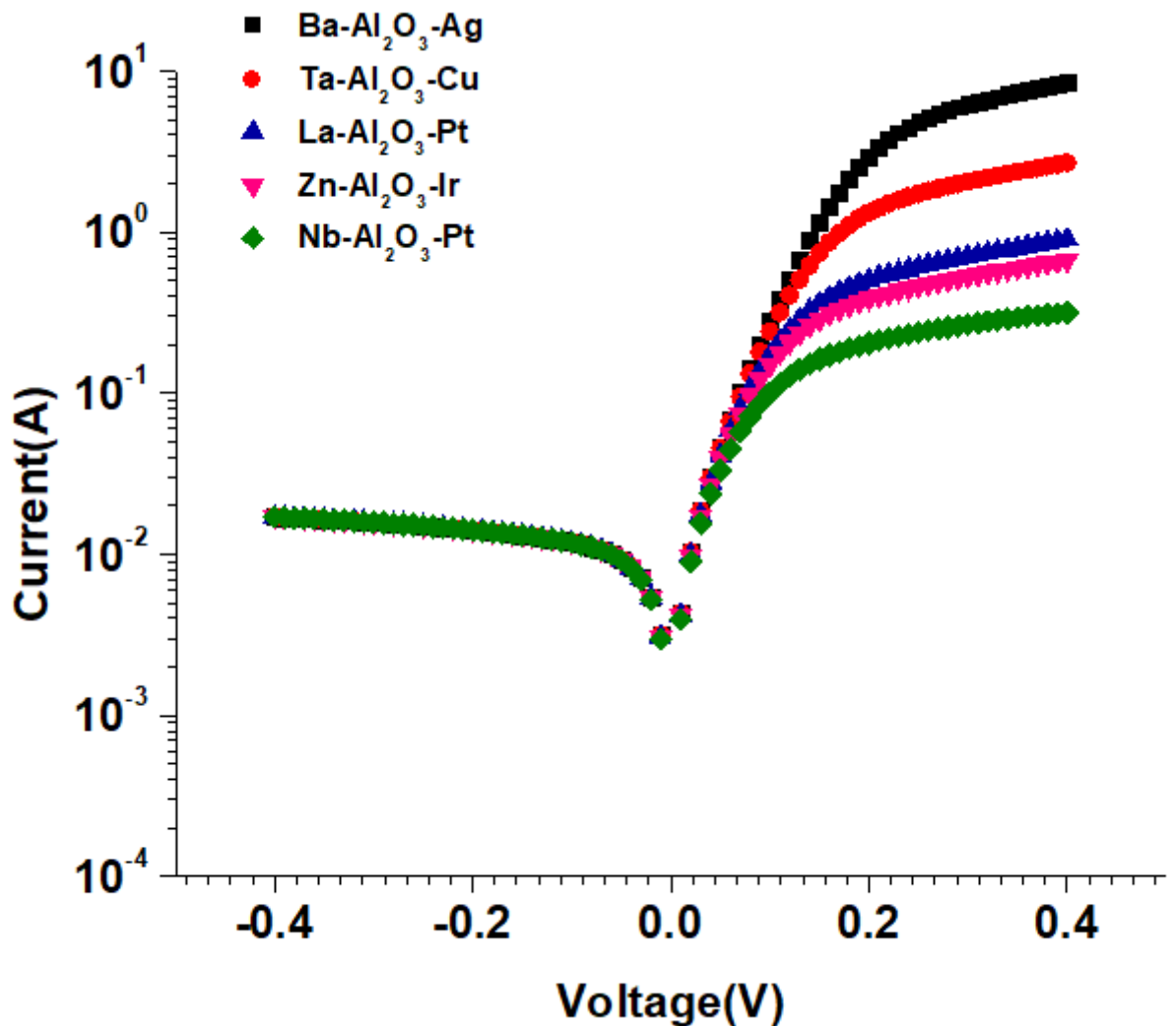


Figure (4.12) I-V characteristics curve for constant barrier potential MIM diode

Figure (4.13) (a) and (b) show, respectively the Asymmetry and the Nonlinearity of the MIM diode structures that are given in Table (4.7). The Ba-Al₂O₃-Ag diode which has a minimum barrier potential exhibits the maximum asymmetry and non-linearity. These results support the concept that a low barrier height is produced when the electron affinity of the

insulator approaches one of the metal work function values, resulting in highest levels of asymmetry and nonlinearity [81]. Figure (4.13) (c) and (d) show Resistivity and Responsivity, at zero bias. It can be noticed that the responsivity for Ba-Al₂O₃-Ag reached 20A/W, and resistivity decreases for this structure. This result makes Ba-Al₂O₃-Ag MIM diode superior over other structures.

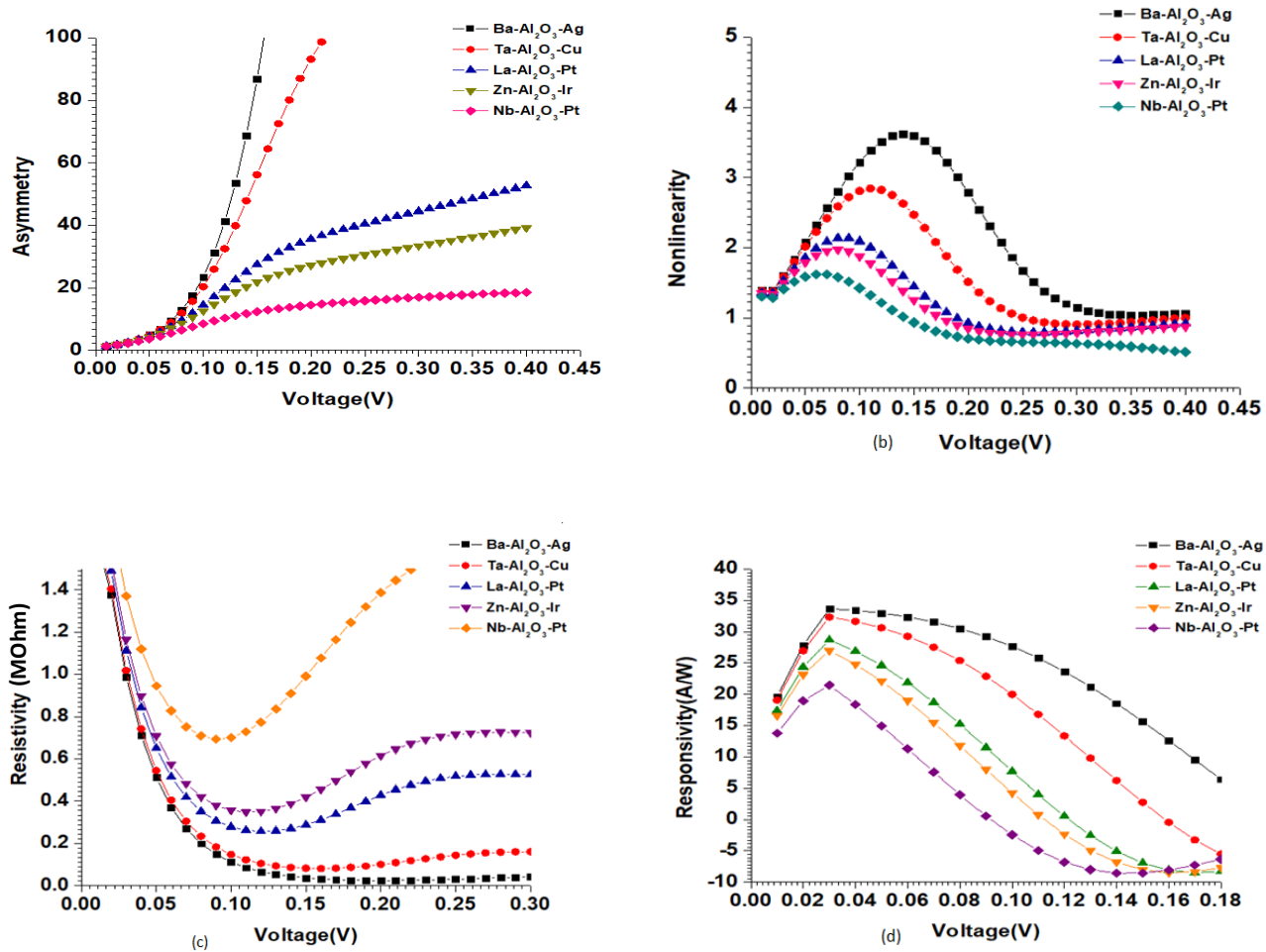


Figure (4.13) a) Asymmetry, b) Nonlinearity c) Resistivity, and d) Responsivity for constant barrier potential MIM diode

4.4 Influence of insulator thickness on the performance of MIM diode:

The physical properties of the insulator layer govern the performance of the MIM diode. Hence, the thickness of the insulator layer plays a vital role in controlling the characteristics of the I-V curves where the tunneling probability is affected by insulator thickness. Decreasing the thickness of the insulator layer makes higher tunneling probability possible at lower voltages. The turn-on voltage can be close to zero volts in MIM diodes with a very thin insulator layer [82,83]. From the previous paragraph (4.3.3), it can be seen that the (Ba-Al₂O₃-Ag) gives the highest levels of asymmetry and nonlinearity. So, in this section, this structure is selected to study the impact of the thicknesses of the insulator layer on the MIM diode performance. Simulations are launched from 1.0 nm insulator thickness to 3.0 nm insulator thickness with steps of 0.5 nm. The simulation results in Figure (4.15) reveal that the increase in the insulator thickness reduces the forward current, thus it can be noted that the asymmetrical in (I-V) curves decrease with the increase of the thickness. Asymmetrical current-voltage characteristics lead to enhancing extracted Figures of merit (f_{ASYM} and f_{NL}). The results of simulated (asymmetry and nonlinearity) at low voltage reach 25 A/W and 4 respectively at 1nm thickness of insulator as shown in Figure (4.16). These results proved tunneling phenomena happening at the lowest thickness of insulators.

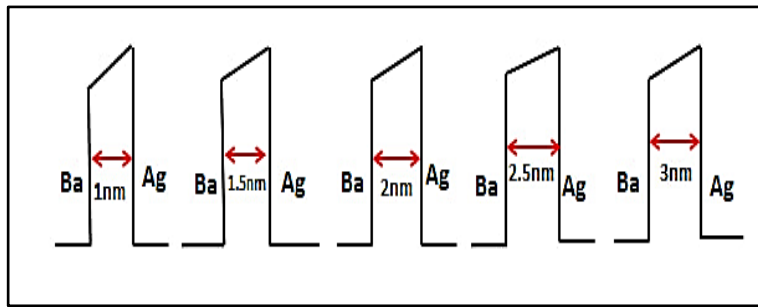


Figure (4.14) energy band diagram of MIM diode with different thicknesses of insulator

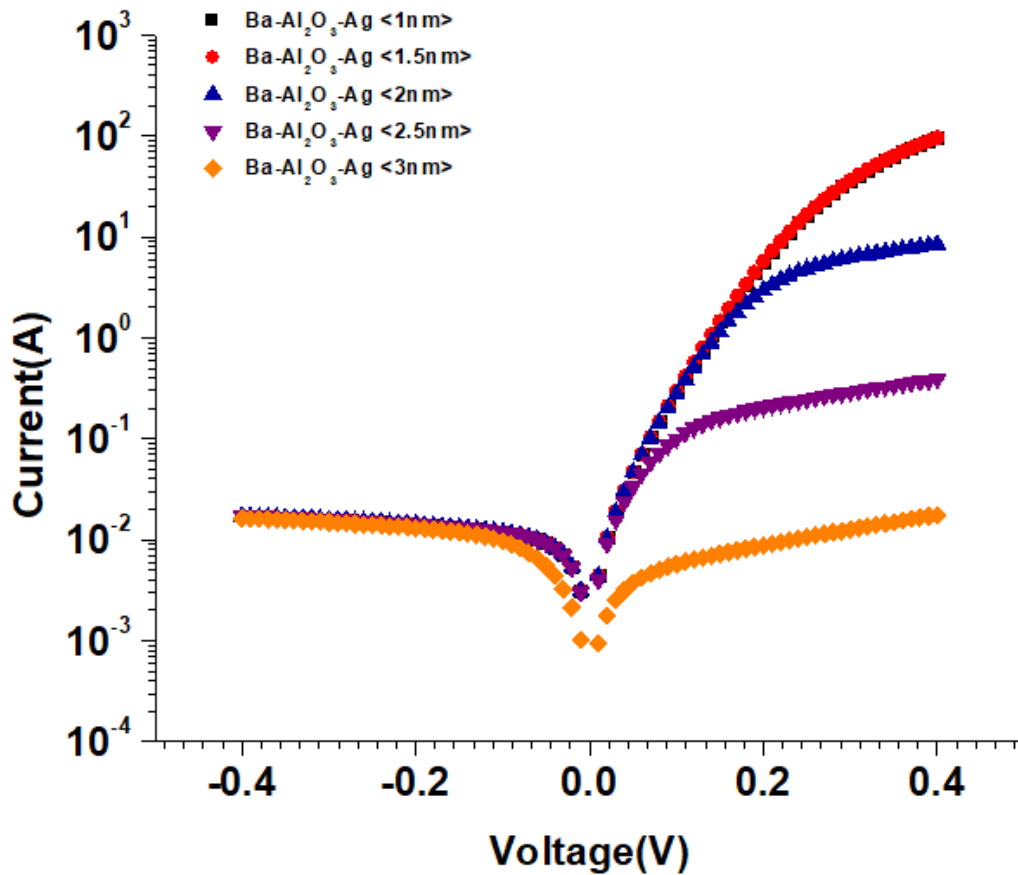


Figure (4.15) I-V characteristics curve with various Thicknesses for MIM diode

The differential resistance and responsiveness of the diode are the properties that often need to be adjusted. As previously mentioned, maintaining low barrier heights allows for the efficient coupling of the diode to the antenna, which requires a low resistance. Effective square-law (small signal) rectification requires high responsiveness. Here, these qualities at zero bias were examined, which simplifies the comparison of the resistance and responsiveness of various diodes. The resistance and responsiveness against the bias voltage for a single type of insulator with various thicknesses were plotted in Figure (4.16) (c), (d). It is observed that the resistivity increased as the insulator's thickness increased, which is undesirable order for designing the MIM diode, as indicated in the figure. On the other hand, the responsivity gave a stronger response at a lower thickness of the insulator 1nm reaching ~20 at 0.01 V. These results of simulator show a reasonable matching with the results represented by the researcher hashim et al [79].

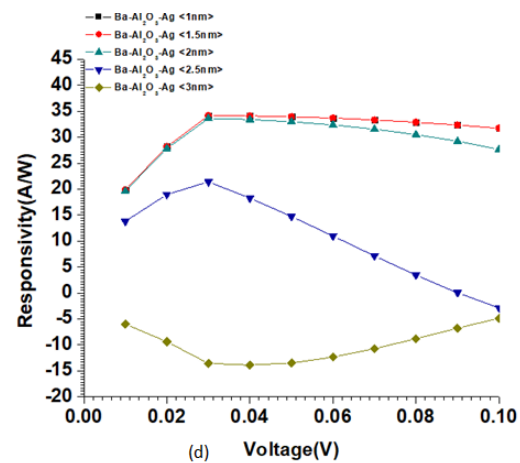
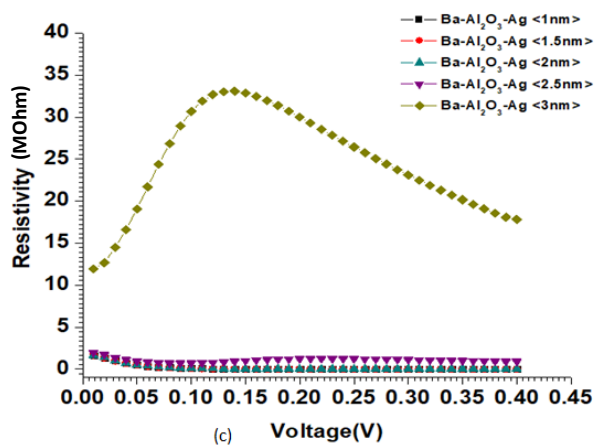
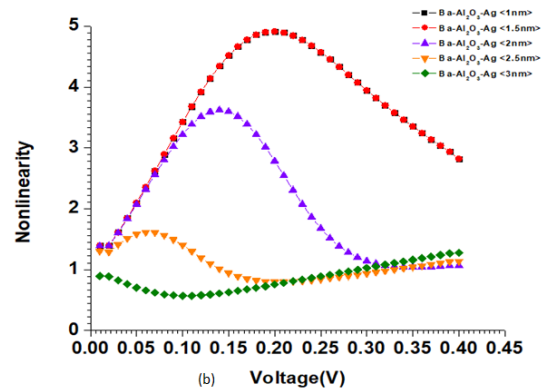
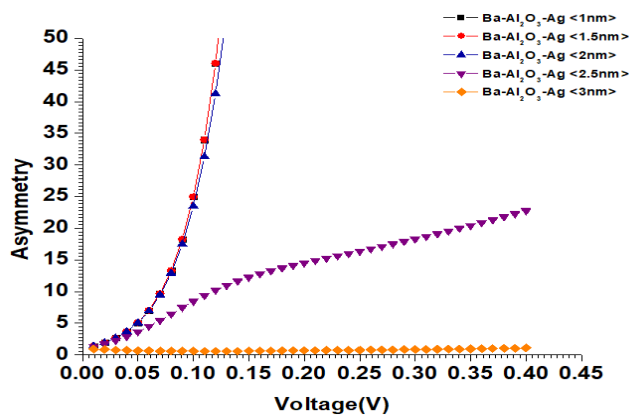


Figure (4.16) a) Asymmetry b) Nonlinearity c) Resistivity and, d) Responsivity for various thicknesses MIM diode

4.5 Impact of the insulator Electron Affinity on the Performance of MIM Diode:

The Metal-Insulator-Metal (MIM) diode was simulated at standard conditions to investigate the effect of using different insulators on the electrical properties of the MIM diode. Different insulators oxides are used including: silicon oxide (SiO_2) with an electron affinity of 0.9 eV, Aluminum oxide (Al_2O_3) with electron affinity of 1.35 eV, Hafnium oxide (HfO_2) with electron affinity of 2.25 eV, and Zirconium oxide (ZrO_2) with electron affinity 2.75 eV. The band gap EG of the aforementioned insulators are 8.8eV, 6.4eV, 5.6eV and, 5.4 eV respectively. The thickness of each insulator layers was fixed at 2 nm for each structure. Table (4.8) summarized the parameters of each structure under investigation.

Table (4.8) The structures of MIM diodes with different insulators [74,75]

<i>Structures</i>	<i>φ_C eV</i>	<i>φ_A eV</i>	<i>EA eV</i>	<i>EG eV</i>
Al-SiO ₂ -Zr	4.2	4.8	0.9	8.8
Al-Al ₂ O ₃ -Zr	4.2	4.8	1.35	6.4
Al-HfO ₂ -Zr	4.2	4.8	2.25	5.6
Al-ZrO ₂ -Zr	4.2	4.8	2.75	5.4

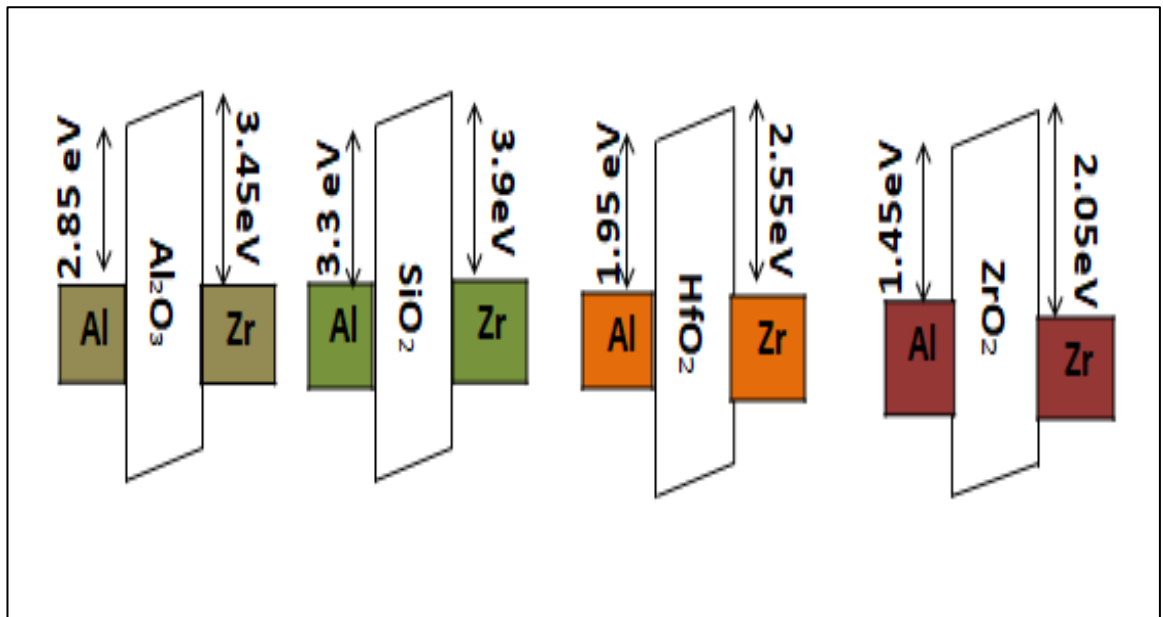


Figure (4.17) barrier heights of MIM diodes with different insulators

In the MIM diode, the height of the barrier potential is affected by the insulator electron affinity. Therefore, decreasing the barrier is anticipated to stimulate greater electron flow and subsequently reduce the diode resistance [84-89]. Aluminum was chosen as the cathode electrode, and Zirconium was chosen as the anode electrode. These electrodes are fixed in the design of all MIM structures with different insulators individually to achieve barrier heights asymmetrically. As illustrated in Figure (4.18), the simulation results demonstrate that the insulator Al₂O₃ with a band-gap of 6.4 eV produces larger asymmetry in the (I-V) curves. These results are consistent with the results obtained by Nasir Alimardani et al 2014[72]. SiO₂ is an insulator with a higher band gap (8.8eV), yet it exhibits less (I-V) curve asymmetry than Al₂O₃. It is found that Al₂O₃ and SiO₂ based on Fowler-Nordheim tunneling when the thermal energy delivered to the electrons was sufficient. They were able to cross the energy barrier at the metal-dielectric interface and transition to the dielectric through a very thin insulator layer [72]. The image force may reduce the height of the energy barrier at the metal-dielectric interaction. The Schottky effect is the name

for the barrier-lowering result of the image force, which caused the forward current to increase at low voltage bias. At high biases, it is revealed that Frenkel-Poole emission dominates ZrO_2 -based diodes, which also have the lowest asymmetry when compared to other structures. The faults that predominate Frenkel-Poole conduction's predicted trap energy levels electrically. It is discovered that conduction in HfO_2 involves a combination of Frenkel-Poole emission and trap-assisted tunneling. According to classical physics, when the energy of the incident electrons is less than the barrier potential, part of these electrons is reflected. This makes the reverse current increase, while in contrast the forward current will decrease.

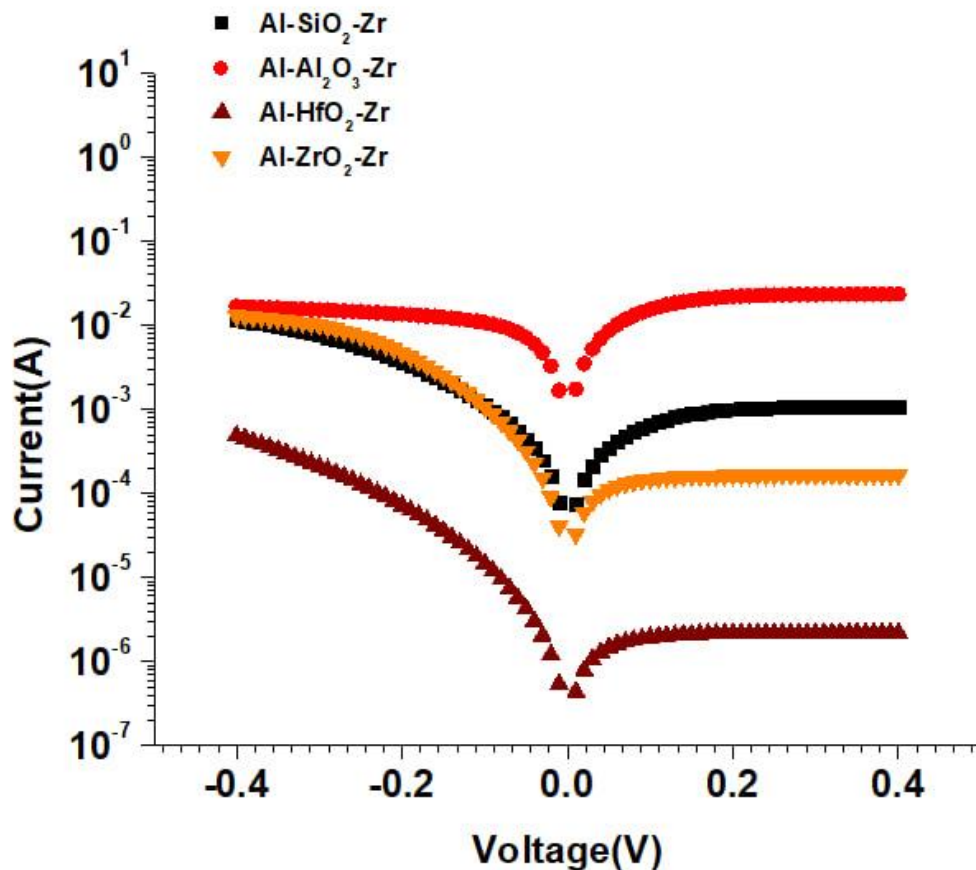


Figure (4.18) I-V characteristics curve with different insulators for MIM diode

Figures (4.19) (a),(b),(c), and (d) show the asymmetry, resistivity, nonlinearity, and responsivity respectively versus the bias voltage of the MIM diode structures shown in Table(4.8). Experimentally, this can be achieved by changing the insulator materials between the metals while keeping the metal on the left fixed and the metal on the right fixed. The results of the simulation show that the insulator Al_2O_3 has large Asymmetry, Nonlinearity, and Responsivity, asymmetry increases with small increases in the turn-on voltage (TOV) to reach ~ 2 . This indicates that insulator Al_2O_3 with electron affinity 1.35eV can be a promising candidate used for rectification performance in energy harvesting applications [72]. The insulator SiO_2 showed that asymmetry decreases gradually down to 0.2. On the other hand, we noted that the insulators (HfO_2 and ZrO_2) started to collapse and reach 0 at 0.2 v as shown in Figure (4.19) which also gives the worst case for nonlinearity as shown in Figure (4.19) (b) decreasing gradually to 0. It can be attributed to having lower band-gaps compared with Al_2O_3 and SiO_2 . Also it gave higher resistivity as a result of the worst case in the asymmetrical (I-V) curve. An improvement in responsivity is obtained for Al- Al_2O_3 -Zr MIM, and Al- SiO_2 -Zr MIM, while the worst response in Al- ZrO_2 -Zr and Al- HfO_2 -Zr respectively in contrast to the resistivity increasing for the last two structures (Al- ZrO_2 - Zr and Al- HfO_2 -Zr) this makes these structures undesirable for matching with antenna and using for rectification purposes. When the responsivity, asymmetry, and nonlinearity increases with a small voltage bias, the resistance decreases. In a rectenna, when the impedance match between the antenna and the diode becomes worse, this means structures have higher resistivity. It can be proved that the structure (Al- Al_2O_3 -Zr) with the insulator layer Al_2O_3 has a better FOM than other structures.

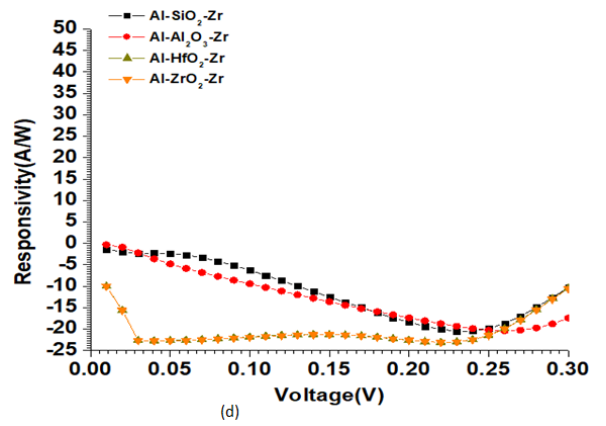
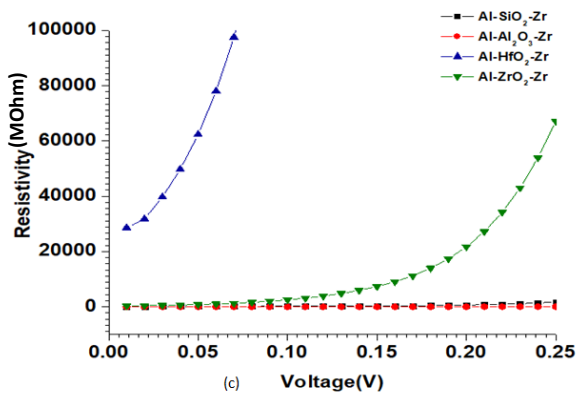
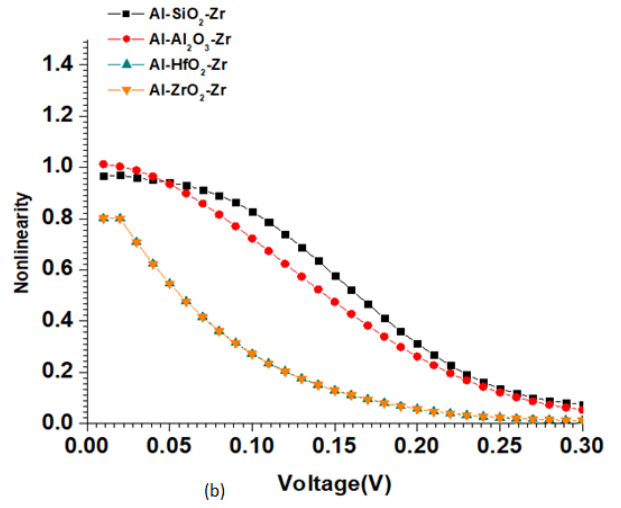
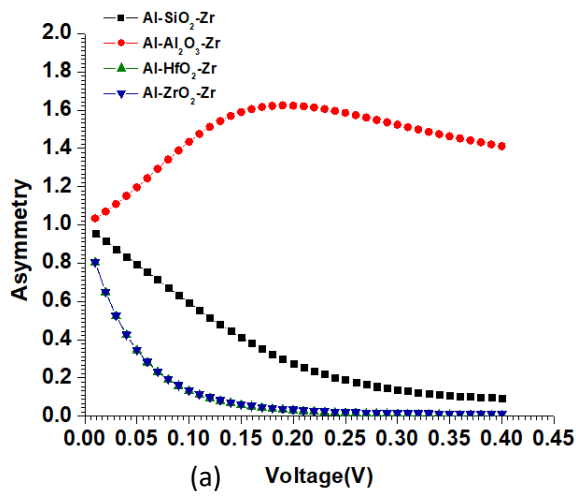


Figure (4.19) a) Asymmetry, b) Nonlinearity, c) Resistivity, and d) Responsivity for different insulators MIM diode

4.6 RF Characterization

The rectenna consists of an antenna and a rectifying circuitry to transform RF energy into dc power and it is a crucial part of RF technology. The dc power required for dependable device functioning is often generated using a number of rectenna devices. To convert the entering RF signal into a usable dc signal, a rectifier made of a diode is necessary. These seemingly low ambient RF power levels indicate the need for a rectifier with a low or zero operating bias for RF energy harvesting. Zero bias operation is the common name for a diode's operation when it requires no power. The tunnel rectifier diode needs to meet a number of requirements to be more efficient. These are: low resistance at zero bias and significant asymmetries in the current-voltage curve. Based on observed RF performance between 10 MHz and 1 THz.

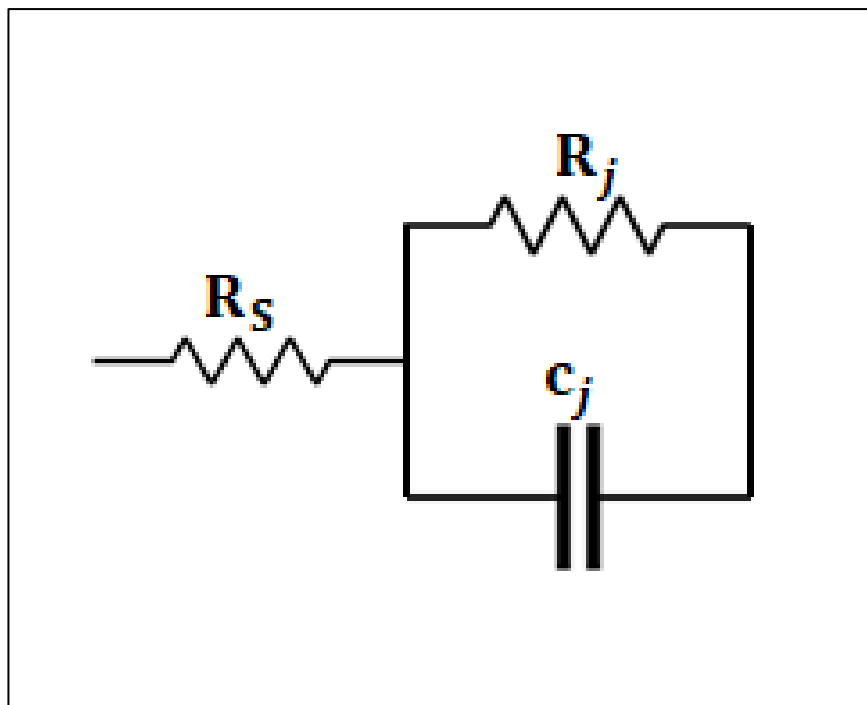


Figure (4.20) Equivalent circuit of MIM diode [89]

The equivalent circuit of the MIM diode comprises both voltage-dependent and independent parts. The bias voltage can have an impact on the band diagram and related I-V responses. This implies that voltage affects the diode's junction resistance. In contrast, the diode's capacitance is proportional to the thickness of the insulator between its metal electrodes. As a result, junction capacitance remains constant and unaffected by the bias voltage. As already established, the equivalent circuit of the diode junction is depicted in Figure (4.20), where $R_j(V_j)$ denotes the voltage-dependent nonlinear junction resistance of the diode, R_s denotes the series resistance, and C_j is the diode shunt junction capacitance.

4.6.1 MIM Diode Characterization

- **Representation the MIM diodes have different insulators in ADS**

To fully comprehend the complex impedance behavior of MIM diodes, the DC and RF characterizations of these devices are performed as a simple preliminary research. Al-Al₂O₃-Zr and Al-SiO₂-Zr MIM diodes are two different types of insulators that we used. More information is mentioned in the preceding subsection (4.5) for these insulators. The diodes' scattering properties (S-Parameter) are obtained. The RF characterization is performed using the I-V extracted from Silvaco as shown in Figure (4.21)

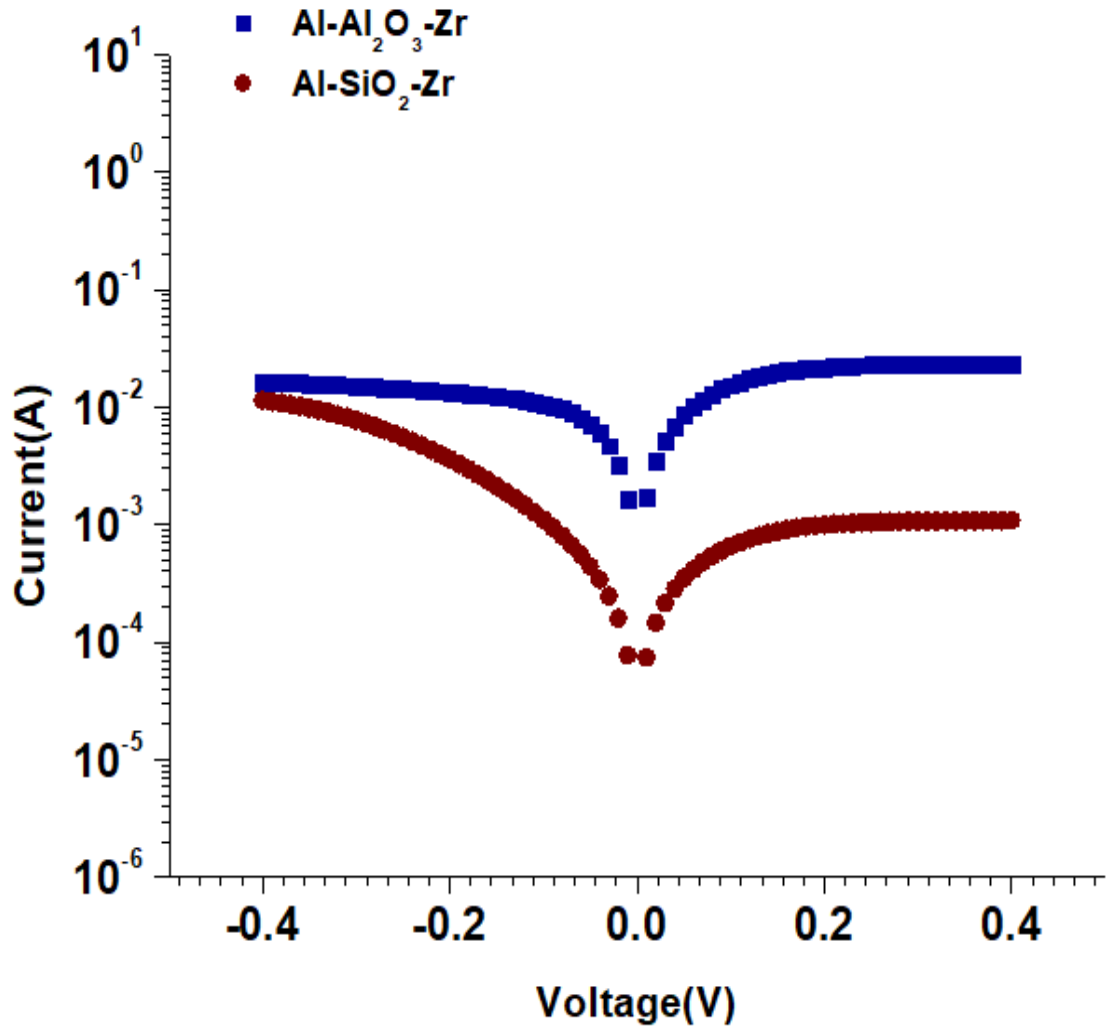


Figure (4.21) I-V characteristics curve of MIM diode have different insulators

The procedure included: Measuring the current (I) vs. voltage (V) and observing the diode's first performance. The (I-V) data was also used to determine the diode's differential resistance at zero bias voltage:

$$R_j = \frac{dV}{dI} \quad (4.2)$$

The diode's cutoff frequency was calculated using its RC time constant, which is given as:

$$f_c = \frac{1}{2 * \pi * R_j * C_j} \quad (4.3)$$

where $C_j = \epsilon A/d$, (A) is the junction area, (d) is the junction tunnel layer thickness, and (ϵ) is the dielectric constant of the junction tunnel material. Al-Al₂O₃-Zr (with Al₂O₃ that is 2 nm thick) and Al-SiO₂-Zr (with SiO₂ that is 2 nm thick) were the MIM diodes used in the modeling procedure. It is assumed that the value of series resistance $R_s = 50\Omega$. As illustrated in Figure (4.22), parameters were retrieved and tested using an equivalent circuit model of MIM created in the Advanced Design System (ADS) tool. The antenna is replaced with an equivalent power source that has an internal resistance of 50 Ω . The simulation is run with frequency steps of 1GHz from 10MHz to 1THz and bias voltage steps of 0.1V from -0.4 to 0.4. According to the illustration in Figure (4.23), the rectifier has excellent matching characteristics most effectively at 1 THz, where S_{11} for an Al-Al₂O₃-Zr diode is -27 dB, and -20 dB for the Al-SiO₂-Zr MIM diode. The Al-Al₂O₃-Zr diode has better reflection characteristics because it has lower resistance (closer to the antenna 50 Ω resistance). Furthermore, the delivered power from the antenna to the rectifier is very small at 0.1THz. It is also noticed that when the frequencies are raised, the reflection coefficient will be decreasing, allowing these structures to be utilized for terahertz frequencies applications (rectifiers and detectors). It is generally accepted that when the S_{11} value goes below -10 dB the delivered power to the rectifier is accepted where minimum reflection is obtained. Thus, by looking at Figure (4.23), it can be observed that the operating frequency of the Al-Al₂O₃-Zr diode starts from 0.14 THz, whereas the operating frequency of the Al-SiO₂-Zr MIM diode is around 0.28 THz. This makes the Al-Al₂O₃-Zr MIM diode is preferable in such applications.

Table (4.9) Theoretical and simulation parameters extracted at zero bias:

Parameters	Al-Al ₂ O ₃ -Zr	Al-SiO ₂ -Zr
C _j [fF]	33.63	17.7
R _j [MΩ]	5.7	139
R _s [Ω]	50	50

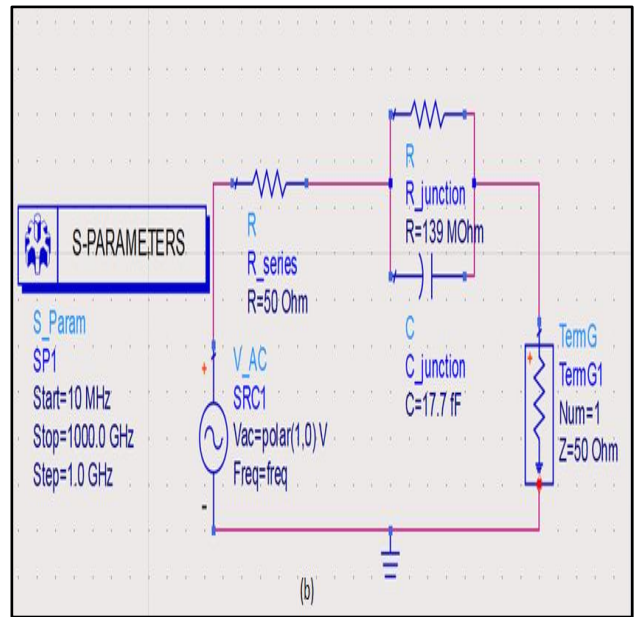
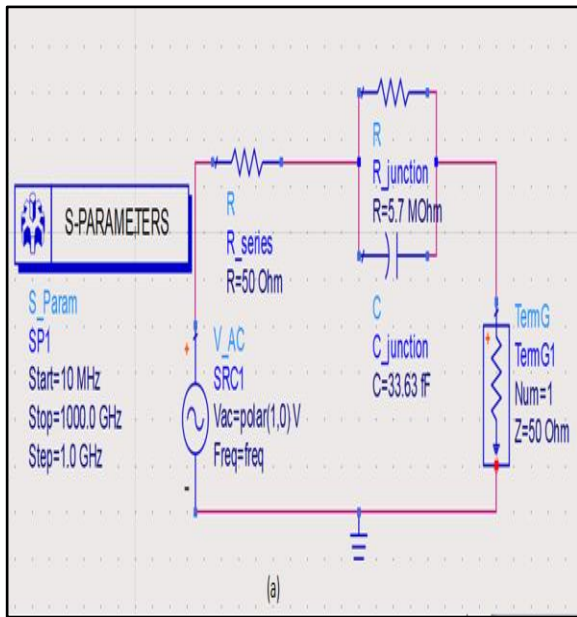
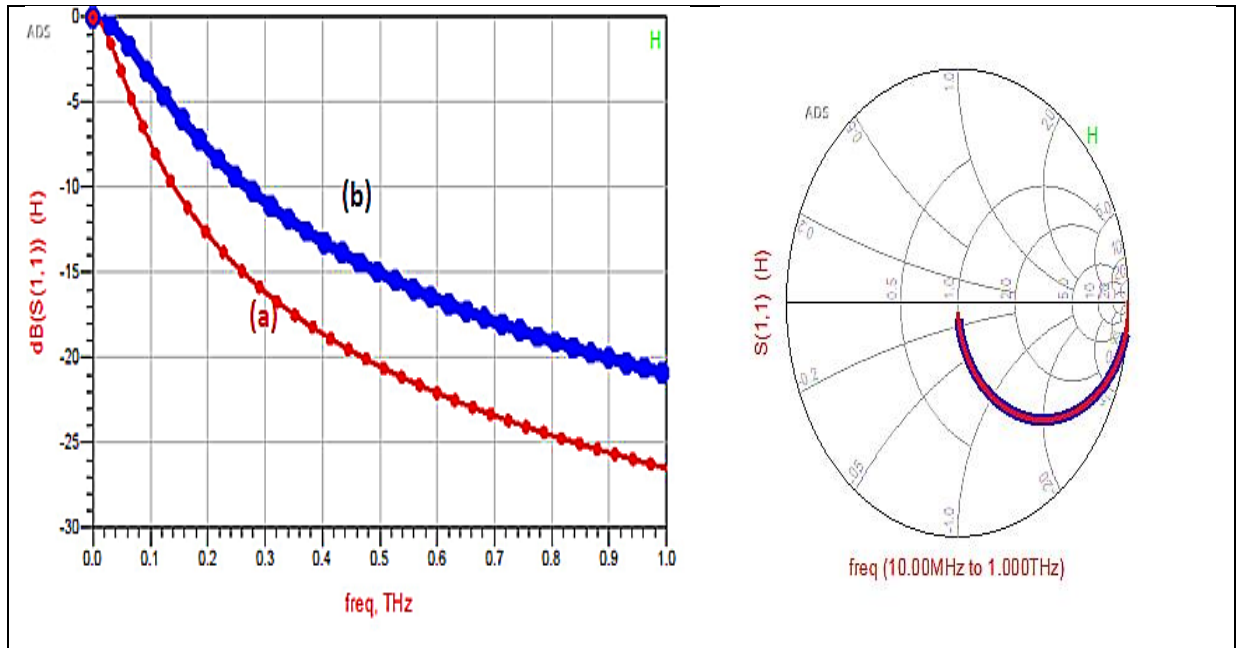


Figure (4.22) the equivalent circuit model of proposed MIM diodes in ADS: a) Al-Al₂O₃-Zr diode b) Al-SiO₂-Zr diode



**Figure (4.23) S-Parameter of the proposed MIM diode
(a)Al-Al₂O₃-Zr, (b) Al-SiO₂-Zr**

- **Representation the MIM diode that have different insulator thickness in ADS**

The physical properties of the insulator layer govern the performance of the MIM diode. Hence, the thickness of the insulator layer plays a vital role in controlling the characteristics of the I-V curves where the tunneling probability is affected by insulator thickness. Decreasing the thickness of the insulator layer makes higher tunneling probability possible as mentioned previously. (Ba-Al₂O₃-Ag) MIM diode has been simulated in Silvaco Atlas to represent the I-V curve. Simulations were launched from 1.0 nm insulator thickness to 3.0 nm insulator thickness with steps of 0.5 nm. The simulation results in Figure (4.24) reveal that the increase in the insulator thickness reduces the forward current; this affected the parameters dependent on the I-V curve extracted from

Silvaco. It is noted that the thickness of the insulator has a large impact on the junction capacitance (C_j). Again it is assumed that the series resistance is 50Ω , so the capacitance is calculated theoretically and extracted at zero bias. Table (4.10) shows these parameters and their values. As is known, increasing the diode responsivity will increase the matching efficiency. To improve the diode efficiency, a parametric study on the effect of insulator thickness on the diode performance was presented. From the frequency responses of the MIM diode, it is noted that decreasing the thickness of the insulator led to a decrease in the resistivity and vice versa. As a result for this, the scattering parameters will be increased as shown in Figure (4.25), where it reached -28dB at 500 GHz for a lower thickness of insulator (1nm). When sweeping the insulator thickness from 1nm to 3nm , it was observed that the resistivity varied from $1.63\text{ M}\Omega$ to $11.9\text{ M}\Omega$. It is also noted that increasing the insulator thickness will increase the acceptable value of operating frequency. At 1nm thickness, the operating frequency starts from 60 GHz and above. In contrast, at 3nm thickness, the operating frequency of the rectifier circuit starts from 160 GHz , which means that the rectifier does not work at frequencies lower than 160 GHz due to poor matching between the antenna and the rectifier circuit (i.e MIM diode). This led to recommend using thinner thickness for insulators to get a lower resistivity to achieve efficient matching.

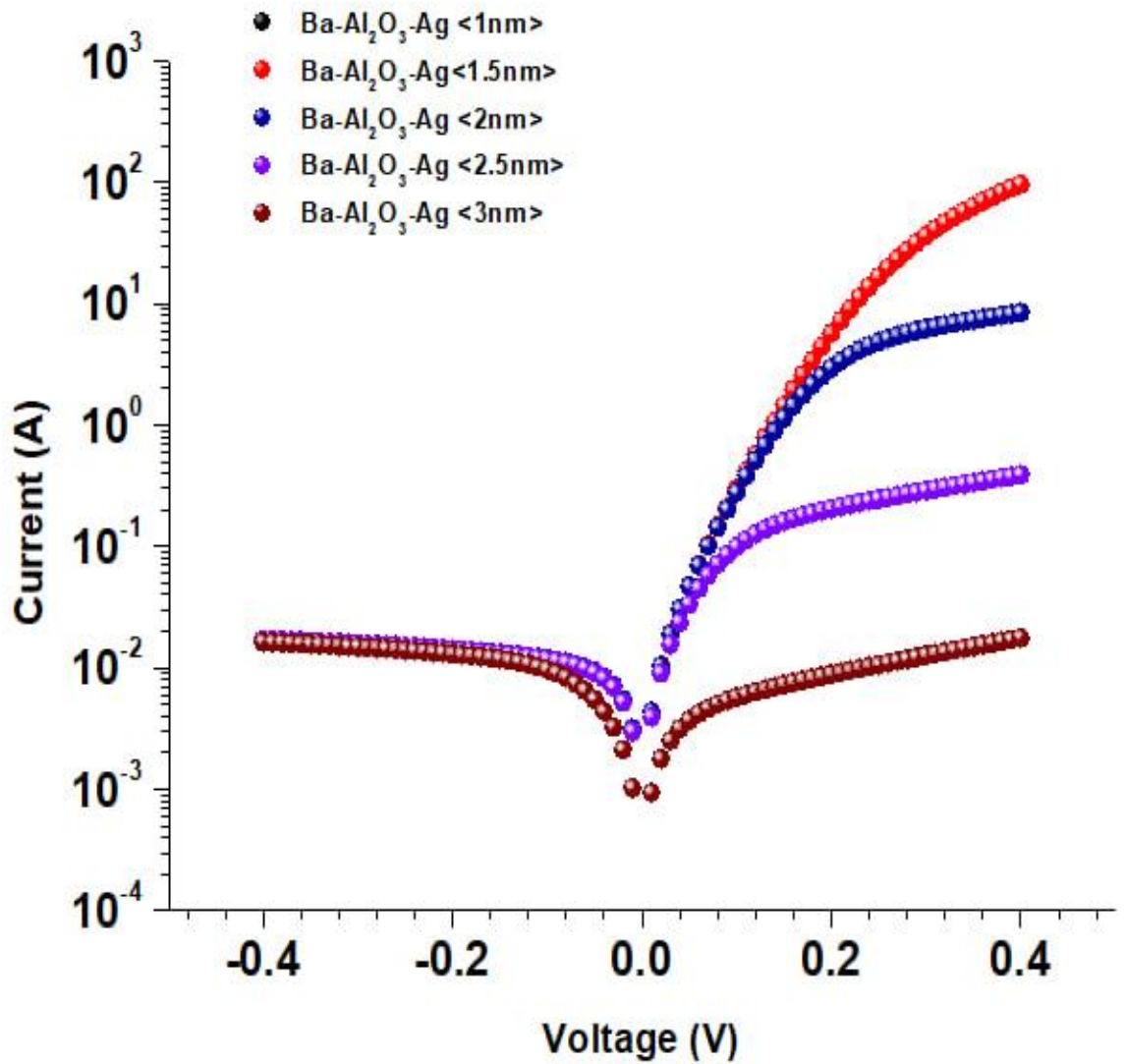


Figure (4.24) I-V curve of MIM diode with variable thickness of insulators

Table (4.10) Theoretical and simulation parameters extracted at zero bias

Thickness of insulator[nm]	C_j [fF]	R_j [M Ω]	R_s [Ω]
1	79.6	1.63	50
1.5	53.1	1.63	50
2	39.8	1.64	50
2.5	31.8	1.95	50
3	26.5	11.9	50

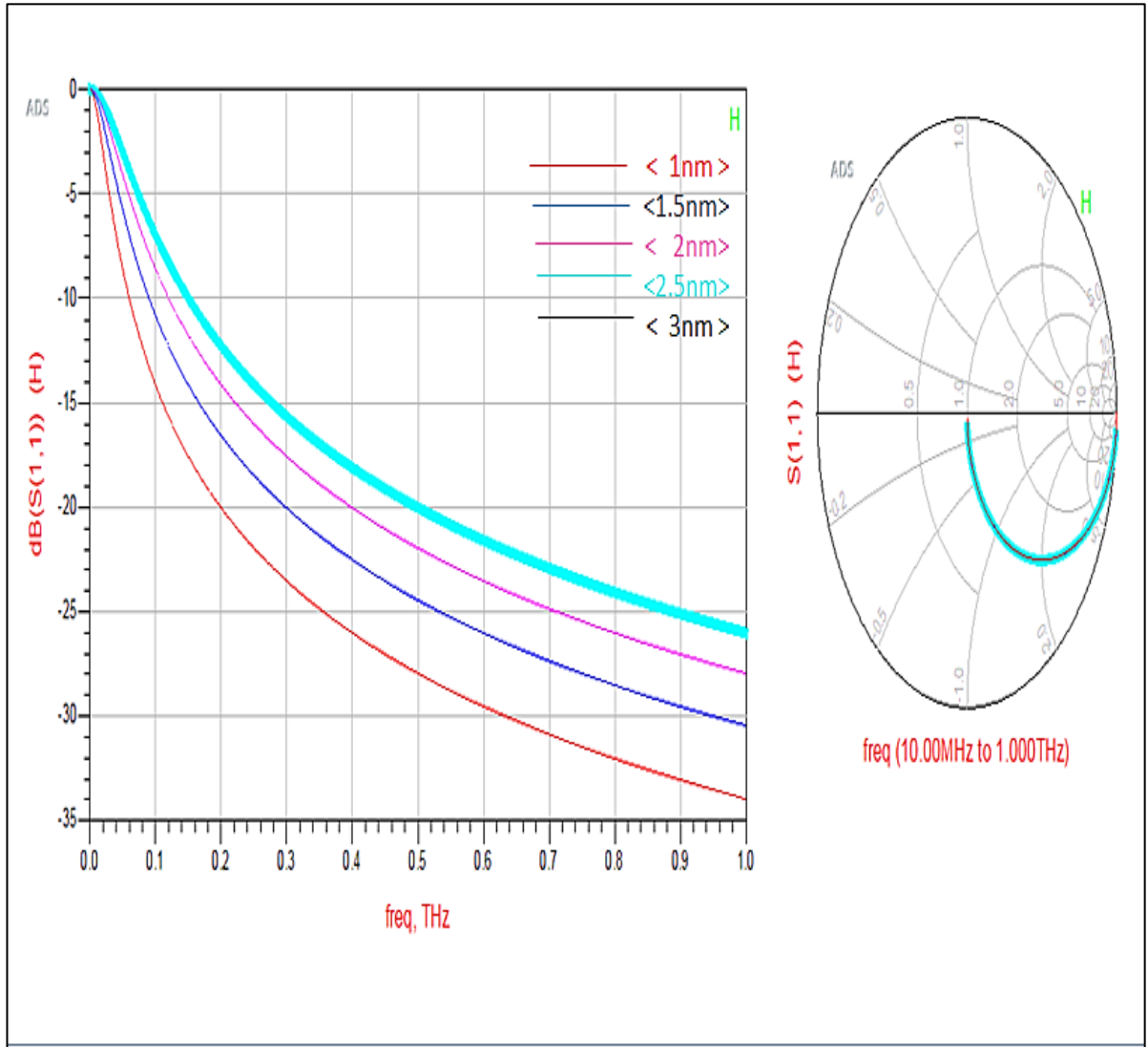
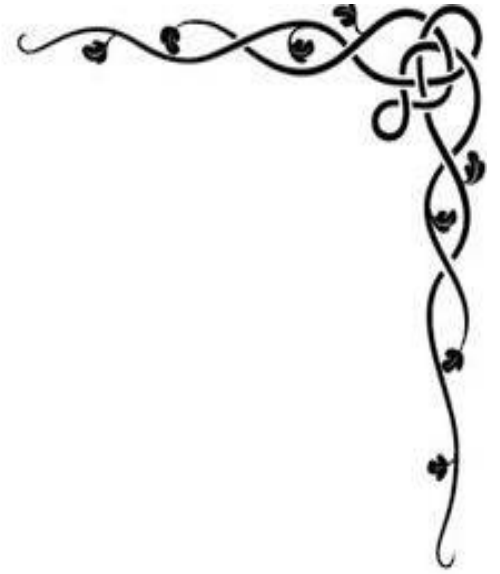


Figure (4.25) S-Parameter of the MIM diode



CHAPTER FIVE
CONCLUSIONS AND SUGGESTIONS FOR
FUTURE WORK



CHAPTER FIVE

CONCLUSIONS AND SUGGESTIONS for FUTURE WORKS

5.1 CONCLUSIONS

According to classical physics, if a particle's energy is lower than the potential barrier, it cannot pass behind it. A particle in quantum mechanics has a chance of tunneling through the potential barrier. This chance is known as the tunneling probability. Quantum physics mechanism has been explained of MIM diodes in chapter 2. The probability of tunneling is determined by the thickness of the insulators and the metal barrier heights . Before creating a MIM diode, some factors including the insulator layer's material and thickness need to be taken into consideration. The present work involved the study of impact the physical parameters on the electrical characteristics of the metal-insulator-metal (MIM) tunnel diode. The proposed work included a study of several main factors, the most important of which are: the effect of changing the barrier heights, influence of using same and different materials on the both side of electrodes and thickness of dielectric films.

- The simulation results reveal that using different metals in the MIM diode structure is necessary to obtain the tunneling diode phenomenon and hence the asymmetry in the (I-V) characteristic curve. Since the structures that have a difference between the left and right work functions produce a large forward current with lower turn-on voltage (TOV). It is demonstrated that the varied work functions of the metals have a significant impact on the asymmetry, nonlinearity, and responsivity of MIM diodes.
- The obtained results show that using different materials electrodes that have large difference work functions metals on the electrodes sides' gives higher rectification current, at the same time we also get high FOM.

The conclusions of the parametric studies:

- The simulation results show that decreasing in the thickness of insulator leads to an increase in the tunnel phenomenon. It was also noted that higher figures of merit are obtained at a lower thickness of insulator, where a higher asymmetry, nonlinearity, and responsivity at 1nm. And high resistivity.
- Different insulators have been used which are: Al_2O_3 , SiO_2 , ZrO_2 and HfO_2 . The results of simulation show Al_2O_3 has best feature as high asymmetrical (I-V) curve, and better results in FOM for this insulator than other insulators
- The equivalent circuit of the MIM tunnel diode was represented in ADS software based on the results of the Silvaco to study the scattering parameters at higher frequencies. Selected the structures that have different insulators thicknesses and represented it in ADS. The obtained results reveal a low value for S_{11} reaching to -28 dB for structure that has less insulator thickness. This result indicated that junction capacitance has high effect on S-Parameter (S_{11}).

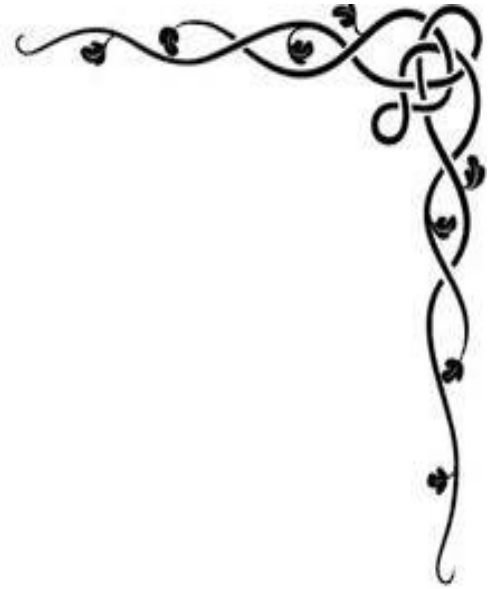
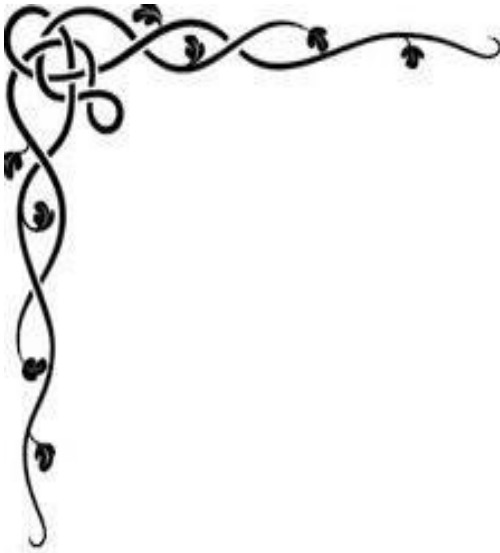
5.2 SUGGESTIONS for FUTURE WORKS

1-The possibility of using the multiple dielectric films (MI2M and MI3M) between the metals, and integrating them with antennas to achieve better efficiency than MIM single insulator layers.

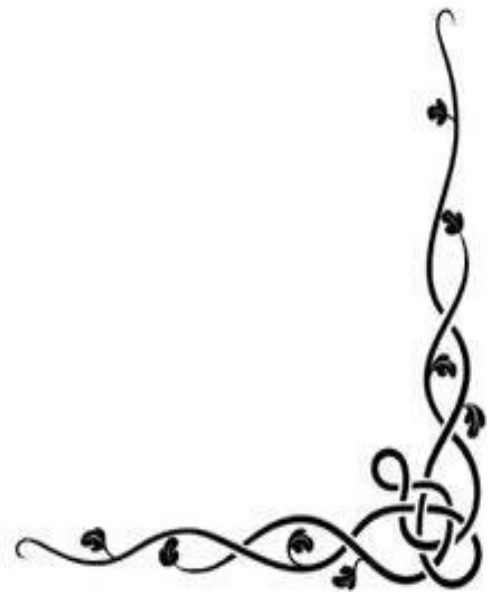
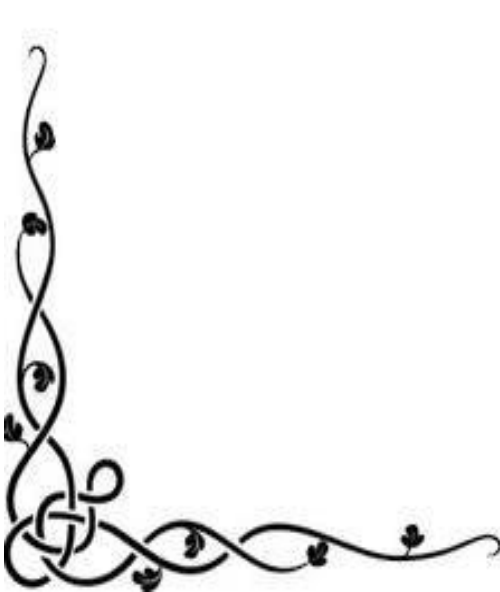
2-The RF circuit topology discussed in Chapter4 can be easily extended to test all structures of MIM tunnel diode have been simulated in this thesis to design and characterize a rectifying antenna(i.e.,rectenna)for terahertz frequency applications.

3- Study the influence of changing the temperature on the performance of the MIM tunnel diodes.

4- Impact of the high K dielectrics materials on the FOM for the MIM diode.



REFERENCES



References

- [1] Nunzi, J. M. "Requirements for a rectifying antenna solar cell technology." SPIE Photonics Europe. International Society for Optics and Photonics, 2010.
- [2] Gadalla, M. N., Abdel-Rahman, M. & Shamim, A. Design, Optimization and Fabrication of a 28.3 THz NanoRectenna for Infrared Detection and Rectification. *Sci. Rep.* 4, 79–85 (2014).
- [3] Donchev, E., Pang, J. S., Gammon, P. M., Centeno, A., Xie, F., Petrov, P. K., Breeze, J. D., Ryan, M. P., Alford, N. M. The rectenna device: From theory to practice (a review). *MRS Energy Sustain.* 1, E1.Riley, D. J (2014).
- [4] Bhatt, K. & Tripathi, C. C. Comparative analysis of efficient diode design for terahertz wireless power transmission system. *Indian J. Pure Appl. Phys.* 53, 827–836 (2015).
- [5] K. Bhatt and C. C. Tripathi, "Comparative analysis of efficient diode design for terahertz wireless power transmission system," *Ind. J. Pure Appl. Phys.* 53, 827–836 (2015).
- [6] K. Choi, M. Dagenais, F. Yesilkoy, A. N. Chryssis, and M. C. Peckerar "Solar spectrum rectification using nano-antenna and tunneling diodes". *Proc. SPIE*, vol. 7605, pp. 1–12, Feb. (2010).
- [7] S. Grover and G. Moddel, "Applicability of metal/insulator/metal (MIM) diodes to solar rectennas," *IEEE J. Photovoltaics*, vol. 1, no. 1, pp. 78 Jul. (2011).
- [8] Heiblum, Mordehai. "Tunneling hot electron transfer amplifiers (THETA): Amplifiers operating up to the infrared." *Solid-State Electronics* 24.4 (1981): 343-366.
- [9] Fumeaux, C., et al. "Nanometer thin-film Ni–NiO–Ni diodes for detection and mixing of 30THz radiation." *Infrared physics & technology* 39.3(1998):123-183.
- [10] Gustafson, T. K. Coherent conversion of the sunlight spectrum. Final Report, 28 July April 1982. No. N-8325026; NASA-CR-170185. California Univ., Berkeley(USA),1982,30-1980.
- [11] Donchev, E., Pang, J. S., Gammon, P. M., Centeno, A., Xie, F., Petrov, P. K., Breeze, J. D., Ryan, M. P., Riley, D. J Alford, N. M. The rectenna device: From theory to practice (a review). *MRS Energy Sustain.* 1, E1(2014).
- [12] Eliasson, Blake J. "Metal-insulator-metal diodes for solar energy conversion." Ph.D. diss -University of Colorado, 2001.
- [13] Kotter, Dale K., et al. "Solar antenna electromagnetic collectors." *Proc. Int'l Conf Energy Sust.* No. 43208.2008.
- [14] Bareiß, Mario, et al. "High-yield transfer printing of metal–insulator–metal nanodiodes." *ACS nano* 6.3 (2012): 2853-2859.

- [15] Nagae, Moichiro. "Response time of metal-insulator-metal tunnel junctions." *Japanese Journal of Applied Physics* 11 (1972): 1611-1621.
- [16] Subramanian, k, Elias Stefanos, and Shekhar Bhansali, "Effects of dielectric thickness and contact area on current-voltage characteristics of thin film metal-insulator-metal diodes", " *science Direct*", 516(2007)2244-2250.
- [17] K.Choi, Filiz. Y, and, Geunmin. R, "AFocused asymmetrical-Insulator-Metal Tunneling Diode" *IEEE Transactions on electron devices*, Vol,58, No,10, October(2011).
- [18] Prakash. P, Joseph. J, A.Dameron, David.S, "Fabrication and characterization of Metal-Insulator-Metal diodes based on Nb/Nb₂O₅ Via Rapid screening technique", *Adv, Mater*, 2011, 23.3080.3085.
- [19] F. Aydinoglu, M. Alhazmi, S. Algarni, B. Cui, O. M. Ramahi, M. Yavuz, 24th Canadian Congress of Applied Mechanics, "Design and fabrication of (Pt-Al₂O₃-Al)MIM Diode," 2013, Saskatoon, Saskatchewan, Canada.
- [20] Sachit. G, and Garrett.M, "Metal single-insulator and multi-insulator diodes for Rectenna Solar cells", Springer Science, Bussiness Media New York(2013).
- [21] Aparajita.S, Rudraskandan.R, SK.rishnan, Y.Emirov, "Niox-Zno based MIIM tunnel diode fabrication and current-voltage characteristics", 2014.Elsevier.
- [22] SHILPI.SH, and, C.C.TRIPATHI, "Metal-Insulator-Metal diodes; A potential High-frequency rectifier for rectenna application"; 2018.the Minerals, Metals, and Material society.
- [23] Su Jin Heo. MIM tunnel diode with various materials and structural designs for rectifying effect. Department of Information and Communication Engineering. 2018. 54p.
- [24] Daisuke.M, Makoto.SH, and, H.Yugami, "High-current density and High-asymmetry MIIM diode based on oxygen-non-stoichiometry controlled homointer face structure for optical rectenna", (2019); 9:19639.
- [25] S.B.Taken, A.D.Weerakkody, N.Sedghi, S.hall, and, P.R.chalker, "Single and triple insulator Metal-Insulator-Metal diodes for infrared rectenna"; *Solid-State-Electronics*: 185(2021)108096.
- [26] Abdullah.Alodhayb, A.Meredov, and, Parul.D, "A Simulation Study of multi-junction insulator tunnel diode for solar energy harvesting app"; *Mater, Res, Express* 8(2021)095509.
- [27] S. Abrar, M. Bilal, and, Abdelaziz.S, "Synthesis and characterization of Nano-structured Multi-layer Cr-SnO₂-NiO-Cr, coating prepared Via E-Beam Evaporation technique for MIIM diode, *Materials* 2022, 15, 3906.

- [28] Fatima M. AbdelHamied, K. Mahmoud, M. Hussein, Salah. S.A; "Design and analysis of a nano-rectenna based on double-insulator tunnel barrier for solar energy harvesting", *Optical and Quantum Electronics* (2022)54:144.
- [29] Shamil.H.Hussein, and, Khalid Mohammed, The article is titled "Physical Modeling of the Quantum Well Asymmetric Spacer Tunnel Layer Diodes for High Frequency Applications."; *PRZEGLAND ELEKTROTECHNICZNY*, ISSN 0033-2097, R99NR,5/2023.
- [30] L. Esaki, "Long journey into tunneling," *Science*, vol. 183, pp. 1149-1155, 1974.
- [31] B. R. Pamplin, Prefix *Molecular beam epitaxy in Molecular beam epitaxy: Elsevier*2017.
- [32] F. Capasso, "Band-gap engineering: from physics and materials to new semiconductor devices," *Science*, vol. 235, pp. 172-176, 1987.
- [33] S.J.heo "Metal-Insulator-Metal tunnel diode with various materials and structural designs for rectifying effect"; Department of information and communication Engineering,(2018).
- [34] Jeong Hee Shin, "Metal-Insulator-Metal Diodes for High-Frequency Application" Master.
- [35] Marwah,"Study and design of high efficiency multilayer solar cells"; *Electronic Engineering*,2021.
- [36] Krishnan Subramanian, "Design, fabrication, and characterization of thin-film M-I-M diodes for rectenna array", Master's Thesis, University of South Florida, USA, 2004, 84 p.
- [37] Thesis Daegu Gyeongbuk Institute of Science and Technology, Daegu, Republic of Korea (2013).
- [38] https://en.wikipedia.org/wiki/Schottky_barrier.
- [39] A. Ramesh, Prefix; "Tunneling based quantum functional devices and circuits for low power VLSI design", The Ohio State University, 2012.
- [40] T. Kuphaldt, "Lessons In Electric Circuits: Volume III: Semiconductor: Chapter, Solid-state Device Theory," ed: Transistor as a switch", Design Science License2009.
- [41] M. J. Kelly, Prefix *Low-dimensional semiconductors: materials, physics, technology devices in Low-dimensional semiconductors: materials, physics, technology, devices* vol. 3: Clarendon Press, 1995.
- [42] Khairul. N.Z.A,"Physical modeling of tunnel diodes for terahertz frequency applications"; School of Electrical and Electronic Engineering, (2018).

- [43] Su Jin Heo, Metal-Insulator-Metal tunnel diode with various materials and structural designs for rectifying effect. Department of information and communication Engineering .2018.54P.
- [44] S. M. Sze and K. K. Ng, Prefix Physics of Semiconductor Devices in Physics of Semiconductor Devices: John Wiley & Sons, 2006.
- [45] Martin, Suzanne, et al. "Fabrication of 200 to 2700 GHz multiplier devices using GaAs and metal membranes." Microwave Symposium Digest, 2001 IEEE MTT-S International. Vol. 3. IEEE, 2001.
- [46] Subramanian, Krishnan, "Design, fabrication and characterization of thin-film M-I-M diodes for rectenna array", Master. Thesis, University of South Florida, USA. 2004, 84 pages.
- [47] J. G. Simmons, in Handbook of Thin Film Technology (Eds: L. Maissel, R. Glang) McGraw-Hill 1970, 14.
- [48] Islam E.Hashem,Nadia H.Rafat and Ezzeldin A.Soliman,"Theoretical study of Metal-Insulator-Metal Tunneling Diode Figures of Merit", IEEE JOURNAL OF QUANTUM ELECTRONICS, VOL. 49, NO. 1, JANUARY 2013.
- [49] F. Aydinoglu, M. Alhazmi, S. Algarni, B. Cui, O. M. Ramahi, M. Yavuz, "Design and fabrication of Pt-Al₂O₃-Al Metal-Insulator-Metal Diode", 24th Canadian Congress of Applied Mechanics, 2013, Saskatoon, SK: Canada.
- [50] D. R. Lamb, Electrical Conduction Mechanisms in Thin Insulating Films, Methuen, London, UK, 1967.
- [51] M. A. Lambert and P. Mark, Current Injection in Solids, Academic Press, New York, NY, USA, 1970.
- [52] J. G. Simmons, "Electronic conduction through thin insulating. films," in Handbook of Thin Film Technology, L. Maissel and R Glang, Eds., chapter 14, McGraw-Hill, New York, NY, USA.
- [53] J. J. O'Dwyer, The Theory of Electrical Conduction and Breakdown in Solid Dielectrics, Clarendon Press, Oxford, UK, 1973.
- [54] N. F. Mott and E. A. Davis, Electronic Processes in Non-Crystalline Materials, OxfordUniversity Press, Oxford, UK, 1979.
- [55] K. C. Kao and W. Hwang, Electrical Transport in Solids, Pergamon Press, New York, NY, USA, 1981.
- [56] P. Hesto, "The nature of electronic conduction in thin insulating films," in Instabilitiesin Silicon Devices: Silicon Passivation and Related Instabilities, G. Barbottin and A. Vapaille, Eds., Elsevier Science, North Holland, Amsterdam, The Netherlands, 1st edition, 1986.
- [57] C. Hamann, H. Burghardt, and T. Frauenheim, Electrical Conduction Mechanisms in Solids, VEB Deutscher Verlag der Wissenschaften, Berlin, Germany, 1988.

- [58] K. C. Kao, *Dielectric Phenomena in Solids*, Academic Press, New York, NY, USA, 2004.
- [59] J. Y. M. Lee, F. C. Chiu, and P. C. Juan, "The application of high dielectric-constant and ferroelectric thin films in integrated circuit technology," in *Handbook of Nanoceramics and Their Based Nanodevices*, T. Y. Tseng and H. S. Nalwa, Eds., vol. 4 American Scientific Publishers, Stevenson Ranch, Calif, USA, 2009.
- [60] Fu-Chien Chiu, "A Review on Conduction Mechanisms in Dielectric Films", *Advances in Materials in Science and Engineering*, 2014(2014), 18 pages.
- [61] W.-C. Lee and C. Hu, "Modeling CMOS tunneling currents through ultrathin gate oxide due to conduction-and valence-band electron and hole tunneling," *IEEE Transactions on Electron Devices*, vol. 48, no. 7, pp. 1366–1373, 2001.
- [62] Su Jin Heo, Metal-Insulator-Metal tunnel diode with various materials and structural designs for rectifying effect. Department of information and communication Engineering .2018.54P.
- [63] Donchev, Evgeniy, et al., "The rectenna device: From theory to practice (a review)", *Journal 1, MRS Energy Sustainability* 2014.
- [64] Hashem, Islam E., Nadia H. Rafat, and Ezzeldin A. Soliman. "A Theoretical Study of Metal Insulator Metal Tunneling Diode Figures of Merit.", *IEEE Journal of Quantum Electronics*, VOL.49,NO,january (2013).
- [65] Edgar Briones, Javier Alda, and Fabrication Javier.G;"Conversion efficiency broad-band rectennas for solar energy harvesting applications", *Applied Optics Complutense Group, University Complutense of Madrid Faculty of Optics and Optometry, Ave.Arcos de Jalón, 118, 28037 Madrid, Spain*.
- [66] I. Silvaco, "ATLAS user's manual device simulation software," St. Clara, CA, 2010.
- [67] M. Hermle, G. Le'tay, S. P. Philipps and A. W. Bett, "Numerical Simulation of Tunnel82 Diodes for Multi-junction Solar Cells," *Photovoltaics Res. Appl.*, vol.16, pp. 409-418.
- [68] S. Narasimha, A. Rohatgi, and A. W. Weeber, "An optimized rapid aluminum back surface field technique for silicon solar cells," *IEEE Trans. Electron Devices*, vol. 46, no. 7, pp. 1363-1370, 1999.
- [69] <https://www.everythingrf.com/products/rf-software/agilent-technologies/679-23-advanced-design-system>.
- [70] F. Aydinoglu, M. Alhazmi, S. Algarni, B. Cui, O. M. Ramahi, M. Yavuz, "Design and Fabrication of Pt-Al₂O₃-Al Metal-Insulator-Metal Diode", *24th Canadian Congress of Applied Mechanics*, 2013, Saskatoon, SK: Canada.
- [71] Nasir Alimardani, Sean W.king, Benjamin L.french and et al," Investigation of the impact of insulator material on the performance of dissimilar electrode metal-

insulator-metal diodes”, *Journal of Applied Physics* 116, 024508 (2014); doi: 10.1063/1.4889798.

[72] Su Jin Heo, Metal-Insulator-Metal tunnel diode with various materials and structural designs for rectifying effect. Department of information and communication Engineering .2018.54P.

[73] Holzl, J., and Schulte, F. K., Work Function of Metals, in solid surface physics, Hohler, G., Editor, Springer-Verlag, Berlin, 1979.

[74] Riviere, J.C., Work Function: Measurements and Results, in solid state surface science, Vol.1, Green, M., Editor, Decker, New York, 1969.

[75] Simmons J.G. *Journal of Applied Physics*, 34 (1963), No. 9, 2581-2590.

[76] Singh A., Pratap R., *Thin Solid Films* 87 (1982), No.87, 147–150

[77] Prakash P., Harvey L. Guthrey, Aziz I. Abdulagatov, Paul F. Ndione, Joseph J. Berry, David S. Ginley, Steven M. George, Philip A. Parilla, Ryan P. O'Hayre, *Adv. Materials*. 25 (2013), 1301–1308.

[78] I. E. Hashem, N. H. Rafat, and E. A. Soliman, " Theoretical study of metal-insulator-metal tunneling diode figures of merit," *IEEE J. Quantum Electron* .49, 72-79(2013).

[79] Fu-Chien Chiu, *Advances in Materials Science and Engineering* (2014), 578168.

[80] Kissan Mistry, Mustafa Yavuz, and Kevin P. Musselman, *Journal of Applied Physics* 121, 184504 (2017); doi: 10.1063/1.4983256.

[81] Michaelson, H.B., *J. Appl. Phys.*, 48, 4729, 1977.

[82] F. Aydinoglu, M. Alhazmi, S. Algarni, B. Cui, O. M. Ramahi, M. Yavuz, "Design and Fabrication of Pt-Al₂O₃-Al Metal-Insulator-Metal Diode", 24th Canadian Congress of Applied Mechanics, 2013, Saskatoon, SK: Canada.

[83] Y. Nakano, S. Saeki, and T. Morikawa, "Optical bandgap widening of p-type Cu₂O films by nitrogen doping," *Appl. Phys. Lett.* 94, 22111 (2009).

[84] L. Gupta, A. Mansingh, and P. K. Srivastava, "Band gap narrowing and the band structure of tin-doped indium oxide films," *Thin Solid Films* 176, 33–44 (1989).

[85] R. K. Gupta, F. Yakuphanoglu, and F. M. Amanullah, "Band gap engineering of nanostructure Cu doped CdO films," *Physica E* 43, 1666–1668 (2011).

[86] Nasir Alimardani, , Sean W. King, Benjamin L. French, : *Journal of Applied Physics* 116, 024508 (2014); doi: 10.1063/1.4889798

- [87] S. Monaghan, P. K. Hurley, K. Cherkaoui, M. A. Negara, and A. Schenk Solid-State Electron. 53(4), 438 (2009).
- [88] O. A. Ajayi, "DC and RF Characterization of high Frequency ALD Enhanced Nanostructured Metal-Insulator-Metal Diodes, "2014.
- [89] Ch.Wenger, Hans-joachim.N , Mindaugas.L and, G.Ruhi; "Influence of the electrode material on HFO₂ metal-insulator-metal capacitors" 2009, American vacuum society [DOI:10.11163].

الطلب المتزايد على الأجهزة الإلكترونية التي تعمل بتردد عالٍ للغاية في مجالات الاتصالات وحصاد الطاقة والفضاء يدفع الباحثين إلى تطوير أجهزة تعمل بسرعات استجابة عالية. الصمام الثنائي النفق هو مرشح مناسب للعمل في منطقة التردد العالي (تيرا هيرتز). مع هيكل معدني عازل، النفق ضروري لإنتاج عملية عالية السرعة، وذلك باستخدام أنواع مختلفة من هذه الأجهزة. الهدف الرئيسي من هذه الأطروحة هو التحقيق في تأثير بعض الخصائص الفيزيائية، مثل ارتفاعات الحاجز، وتقارب الإلكترون، والدراسات البارامترية الأخرى مثل سمك الحاجز المحتمل (سمك العازل) وأنواع المواد، على الخصائص الكهربائية للصمام الثنائي للنفق. تم محاكاة هذه المعلمات باستخدام برنامج سيلفاكو. الألومنيوم-أكسيد الألومنيوم-ألومنيوم. تم محاكاة الثنائيات (معدن-عازل-معدن) لدراسة تأثير استخدام أقطاب مماثلة ومختلفة على منحني الجهد - التيار للصمام الثنائي (معدن-عازل-معدن). وكشفت النتائج أن الصمام الثنائي الألومنيوم-أكسيد الألومنيوم-ألومنيوم، لا يسلك سلوك الصمام ثنائي نفق، أشارت نتائج هذا إلى أن هذا الهيكل يعمل كدائرة مفتوحة. في حين أن الألومنيوم-أكسيد الألومنيوم-الذهب لديه منحني جهد-تيار غير متناظرة جداً ولها أيضاً أرقام جدارة عالية مقارنة بالتركيب الأول، حيث تشير أرقام الجدارة إلى تميز أداء التركيب المعدني غير المتماثل. تمت محاكاة تأثير ارتفاعات الحاجز للأقطاب الكهربائية غير المتشابهة باستخدام سيناريوهين؛ أحدهما عن طريق تغيير ارتفاع الحاجز من جانب الأنود والآخر عن طريق تغيير ارتفاع الحاجز من جانب الكاثود. تم تثبيت الألومنيوم كمعدن الكاثود الثابتة وتغيير المعدن على الجانب الآخر، لاحظنا أن التغيير في وظيفة العمل من الأنود لا تنتج الكثير من الفرق في نفق الحالي. ثانياً، تمت دراسة تأثير اختلاف ارتفاع الحاجز من جانب الكاثود. كان النيكل ثابت الجانب الأنود والمعادن المختلفة على الجانب الكاثود. كشفت النتائج أن منحني الجهد الحالي يعتمد بشدة على وظيفة عمل المعدن، حيث يكون للهيكل فرق كبير بين وظائف العمل اليسرى واليمينية مما ينتج عنه تيار أمامي كبير بجهد تشغيل أقل. في الجزء الثالث من العمل الحالي، تم التحقيق في تأثير اختلاف ارتفاع الحاجز مع ثبوت الفرق بين وظائف العمل، باستخدام معادن مختلفة على كلا الجانبين. على الرغم من أن هذه الهياكل تنتج فرقاً ثابتاً في وظيفة العمل، إلا أن النتيجة تكشف أن استجابات منحني تيار-فولتية من الثنائيات مرتبطة نوعياً بارتفاع الحاجز. تمت دراسة تأثير سمك العازل على أداء الصمام الثنائي (معدن-عازل-معدن)، حيث تم أخذ قيمة سمك العازل من 1 نانومتر إلى 3 نانومتر بخطوات 0.5 نانومتر. تظهر نتائج المحاكاة أن الانخفاض في سمك العازل يؤدي إلى زيادة ظاهرة النفق، كما لوحظ أن الأرقام الجدارة هي الأعلى عند سمك أقل للعازل، حيث يتم الحصول على عدم تناسق أعلى، وعدم خطية، واستجابة عند 1 نانومتر. نظراً لأن تقارب الإلكترون هو معلمة فيزيائية مهمة للمواد، فقد تضمنت الدراسة الحالية تأثيره على الخصائص الكهربائية للصمام الثنائي (معدن-عازل-معدن). حيث استخدمنا مجموعة من العوازل المختلفة، مع تقارب الإلكترون مختلفة، مثل أكسيد الألومنيوم، وأكسيد السليكون، وأكسيد الهافنيوم، وأكسيد الزركونيوم في هيكل (معدن-عازل-معدن)، تظهر النتائج أعلى عدم تماثل في الجهد - التيار للعازل (أكسيد الألومنيوم). بعد ذلك، تم تمثيل الدائرة المكافئة من الصمام الثنائي نفق (معدن-عازل-معدن) في برنامج نظام التصميم المتطور استناداً إلى نتائج سيلفاكو لدراسة المعلمات تشتت في ترددات أعلى. اخترنا الهياكل التي لها سمك عازل مختلفة وتمثيلها في البرنامج. تكشف النتائج التي تم الحصول عليها عن قيمة منخفضة لـ معامل الانعكاس تصل إلى -28 ديسيبل للهياكل ذات سمك عازل أقل. هذه النتيجة المشار إليها تقودنا لاستنتاج أن سعة التقاطع الصمام الثنائي لها تأثير كبير على معامل الانعكاس.

محاكاة تأثير المعلمات الفيزيائية
على الخصائص الكهربائية للصبام الثنائي النفق

رسالة في هندسة الإلكترونيك

بإشراف

البروفيسور. قيس ذنون نجم

و

الدكتور. احمد محمد سلامة



جامعة نينوى
كلية هندسة الإلكترونيات
قسم الإلكترونيك

محاكاة تأثير المعلمات الفيزيائية
على الخصائص الكهربائية للوصام الثنائي النفق

رسالة تقدمت بها

الباحثة: رفل عماد عبدالقادر

الى

مجلس كلية هندسة الإلكترونيات- جامعة نينوى

وهي جزء من متطلبات نيل شهادة الماجستير

علم في هندسة الإلكترونيك

بإشراف

البروفيسور.الدكتور قيس ذنون نجم

و

الدكتور احمد محمد سلامة